Model electrodes for electrocatalysis: Ultrathin palladium films on Pt(111)

Dissertation

zur

Erlangung des Doktorgrades (Dr. rer. nat.)

der

Mathematisch-Naturwissenschaftlichen Fakultät

der

Rheinischen Friedrich-Wilhelms-Universität Bonn

vorgelegt von

Matthias Arenz

aus Aachen

Bonn 2002

Angefertigt mit der Genehmigung der Mathematisch-Naturwissenschaftlichen Fakultät der Rheinischen Friedrich-Wilhelms-Universität Bonn

1. Referent: Professor Dr. Klaus Wandelt
2. Referent: Professor Dr. Helmut Baltruschat

Tag der Promotion: 07.06.2002

Table of Contents

Chapter 1
Introduction

Electrochemistry and heterogeneous catalysis are among the oldest fields in chemistry. The term catalyst was introduced by Berzelius [1] as early as 1835, and can be defined as a substance which enhances the *rate* of a chemical reaction without being either consumed or generated in the process. In analogy to catalysis, in electrocatalysis, i.e. the combination of electrochemistry and heterogeneous catalysis, materials are investigated which promote *electrochemical* reactions. Today, (electro-) catalytic reactions play an all important role in various aspects of chemistry and more than 80 percent of all industrial chemical processes involve in some way a catalyst.

One of the main goals in (electro-) catalysis is to a create link between the microscopic level of understanding the atomic and electronic structure of a catalyst and the macroscopic reaction rate of a process, i.e. the activity of the catalyst. For this kind of *fundamental* research the use of well-defined single crystals is essential since investigations on polycrystalline materials are often too complex and difficult to interpret. Only recently, with the advent of new preparation methods as well as modern analytical tools in electrochemistry such as in-situ STM[1], in-situ infrared spectroscopy and the rotating ring-disk electrode technique, the frequent use of well-defined surfaces has become meaningful also in electrocatalysis.

An interesting class of systems, which have received considerable attention in catalysis are bimetallic surfaces. In ultra-high-vacuum (UHV[2]) their electronic, structural, chemical and catalytic properties have been studied in some detail by a variety of experimental methods. It has been shown that upon deposition of one metal onto another one new structures can be formed which are not seen in bulk alloys. One particularly interesting

---

[1] **S**canning **T**unneling **M**icroscopy

[2] **U**ltra-**H**igh-**V**acuum

case are pseudomorphic monolayers, where the metal overlayer adopts a lattice constant which differs from its bulk crystal structure but which is in registry with the lattice of the underlying substrate. By choosing different substrates, with different electronic structures and lattice constants, the electronic and geometrical properties of the pseudomorphic monolayers can be changed. As a consequence, the reactivity of the metal overlayer towards adsorbate molecules can be significantly modified. Compared to the work performed in UHV the investigations in an electrochemical environment are, however, rather scarce.

An important *application* of such fundamental research on electrocatalysts are fuel cells. Although the basic concept of a fuel cell as a device for direct conversion of chemical energy into electric energy was described by Grove [2] well before the invention of either the internal combustion engine or the steam generator, the technological implementation has proved difficult. Consequently, at the beginning of the 20th century it was the heat engine rather than the electrochemical engine which was chosen as the main source of motive power, although the latter offers theoretically a higher efficiency for energy conversion. In the beginning of the 1960's fuel cells became technological relevant. However, as long as primary energy resources were abundant and inexpensive, the use of fuel cells has been restricted to specific areas (as for example the use of fuel cells in the NASA Apollo space program). In the last decade of the 20th century, finally, rising concern about environmental consequences of the use of fossil fuels and the increasing dependence of industrialized countries on oil have led to a resurgence of interest in the fuel cell technology. Now widespread use as flexible power generators, portable power devices and for fuel cell powered vehicles is being reconsidered [3]. The main challenges of fuel cells today are to find an alternative to platinum as the electrode material, and pure hydrogen as the only viable fuel [4]. The basic reaction of a fuel cell is the oxidation of hydrogen and the reduction of oxygen to form water. The electrodes in the fuel cell serve as a catalyst where the adsorbed molecules from the fuel can react. Consequently the development of fuel cells into commercially useful devices is strongly tied to the field of electrocatalysis.

In this work the electrocatalytic activity of a bimetallic model catalyst, a pseudomorphic monolayer of palladium supported on Pt(111), denoted hereafter as Pt(111)-Pd, is characterized. Rather than investigating one single reaction in great detail, the *aim* of this work, is the elucidation of the general catalytic properties of the Pt(111)-Pd surface by probing a *variety* of important reactions, which are related to fuel cells. The reactions investigated are the carbon monoxide oxidation reaction, the oxygen reduction reaction, the hydrogen evolution as well as the hydrogen oxidation reaction, and the oxidation

of small organic molecules. The oxidation of small organic molecules is of particular importance for the DMFC[3] where methanol is the fuel. CO oxidation is investigated, because CO_{ad} blocks the active sites of the anode catalyst, primarily platinum alloys, in low-temperature fuel cells [3]. In a PEMFC[4] CO adsorption occurs due to contaminations in the hydrogen feed gas, whereas in a DMFC the oxidation of methanol produces CO_{ad} [4]. The oxygen reduction and the hydrogen oxydation reaction, finally, are the *basic* processes in all low-temperature fuel cells.

The structure of the thesis is as follows. Before the experimental results are presented, in the first part of chapter 2 the main theoretical aspects of the analytical tools, used in this work, are introduced. The focus lies on the two main techniques used, which are the rotating ring-disk technique and the in-situ Fourier transform infrared spectroscopy. In the second part of the chapter 2 details on the experimental procedures are given. Then, in chapter 3, the preparation and the characterization of Pt(111)-Pd electrodes are introduced. The first electrochemical reaction probed on the well characterized Pt(111)-Pd surface is the adsorption and electrooxidation of CO. The experiments are described and discussed in chapter 4. In the next two sections, chapter 5 and 6, the electrocatalytic activity of Pt(111)-Pd regarding the basic anode and cathode reaction in a fuel cell, i.e. the reduction of oxygen and the oxidation of hydrogen, is investigated. In the subsequent chapter 7, the electrooxidation of formic acid is discussed and shortly compared to the electrooxidation of methanol. Finally, in the last chapter (chapter 8), a concluding discussion of the most important results and a summary is given in English as well as in German.

---

[3] **D**irect **M**ethanol **F**uel **C**ell

[4] **P**olymer **E**lectrolyte **M**embrane **F**uel **C**ell

Chapter 2

Experimental

In the following chapter the experimental details are given. The first part of the chapter deals with the theoretical background of the applied techniques. Here the focus lies on the main analytical tools used in this work, viz., the rotating (ring) disk electrode (R(R)DE) technique and the Fourier transform infrared (FTIR) spectroscopy, which are discussed in more detail. Auger electron spectroscopy, cyclic voltammetry and low energy ion scattering are only described shortly. For the interested reader, however, references are given at the end of each section.

In the second part of the chapter the experimental setup, e.g. the electrochemical cells, the UHV equipment and the FTIR spectrometer, is specified. Moreover the experimental procedure applied in this work is introduced. The UHV preparation as well as the electrochemical preparation of Pt single crystal electrodes is described and this part also includes details concerning electrolyte preparation, cleaning of the electrochemical cells, and the chemicals used.

2.1 Methods

2.1.1 Auger Electron Spectroscopy

Auger electron spectroscopy (AES) is a widely used method in order to gain information on the near-surface chemical composition of an investigated sample. In AES the surface of a probe is subjected to an electron beam of a kinetic energy of 1 keV up to 10 keV and the emitted Auger electrons are detected in a cylindrical mirror analyzer.

The underlying process of the emission of Auger electrons from the sample is the creation of core-hole excitations due to the impinging electron beam. The Auger electrons of the characteristic energies are emitted through a radiationless two-electron process as the excited atoms decay to their ground state. In order to facilitate the separation of the Auger electrons from the background the signal is commonly recorded by utilizing the Lock-In technique. Consequently the Auger spectra are depicted as the first derivative of the number of detected electrons with the energy, i.e. $dN(E)/dE$.

The kinetic energy of the Auger electrons is completely defined by the energy levels of the involved orbitals in the atom. Therefore AES is element specific and can be used for the chemical analysis of surfaces. Since electrons are detected, the application of Auger electron spectroscopy is limited to an UHV environment. The surface sensitivity of AES is a result of the very limited pathway of electrons in solid matter. The information depth of the elemental composition of the investigated surface is about 1 to 10 nm. Further information about Auger electron spectroscopy can be found in ref. [5].

2.1.2 Cyclic Voltammetry

Cyclic voltammetry (CV) usually is the technique of choice when investigating an electrochemical system for the first time. With a limited effort an "electrochemical spectrum" indicating the potentials at which processes occur can be rapidly obtained [6]. In cyclic voltammetry the potential of the working electrode (we) is periodically scanned between an upper and a lower limit with a constant sweep rate. The responding current through the working electrode is recorded as a function of the applied potential resulting in a cyclic voltammogram. The sweep rates in conventional experiments range from a few mVs^{-1} up to some Vs^{-1}. The imminent surface sensitivity of this method is due to the nature of charge transfer reactions, taking place only at the solid/liquid phase boundary.

When applying cyclic voltammetry the use of a three-electrode configuration is crucial. It consists of a variable current source to pass a current through the working and counter (ce) electrodes. Changes in the potential of the working electrode are measured versus a reference electrode (re), which carries practically no current. In this way the polarizing current flows through one circuit (which includes the working and the counter electrode) while the resulting change in potential is measured in a different circuit (consisting of the working and reference electrode), through which the current is essentially zero [7]. Since no current flows through the reference electrode, the measured change in potential (between working and reference electrode) is equal to the change of potential of the working electrode. In order to minimize the potential drop between the working and counter electrode a Luggin capillary with its tip near the working electrode is placed between reference and working electrode. As a reference electrode nonpolarizable electrodes with a high exchange current density are used, which provide a stable and reproducible potential. More detailed descriptions about cyclic voltammetry can be found in references [6, 8, 9].

2.1.3 Infrared Spectroscopy

2.1.3.1 Conventional infrared spectroscopy

Infrared reflection absorption spectroscopy (IRAS) is a powerful method for investigating adsorbed molecules at the solid/gas as well as at the solid/liquid interface.

Before dealing with the special requirements for IRAS the basic principles of infrared spectroscopy, i.e. the interaction of molecules with light, will be shortly reviewed.

Light absorption by a molecule occurs when the molecule initially in a state of energy E_1 is excited to an upper state of the energy E_2 by a photon of the energy $h\nu_0$, satisfying the Planck relation [10]:

$$h\nu_0 = \Delta E = E_2 - E_1 \tag{2.1}$$

The transition probability ω for this process can be calculated by solving the time-dependent Schrödinger equation utilizing the time-dependent perturbation method. Without going into details, it should be stated that the main task is the calculation of the matrix element, which is directly proportional to the transition probability:

$$\omega \propto \left\langle \Psi_1 \left| \vec{\mu}\vec{E} \right| \Psi_2 \right\rangle \tag{2.2}$$

Ψ_1, Ψ_2 : unperturbed quantum states of the energy E_1 and E_2

$\vec{\mu}$: electric dipole moment

$\vec{E}$: Electric field vector

For calculating the energy levels of the quantum states the Born-Oppenheimer approximation can be applied, which means that the energy of the molecule can be separated into three additive components, viz., the vibrational energy, the rotation energy and the electronic energy (the translational energy can be ignored). The energy levels involved in the infrared range are associated with the vibrational energy and can therefore be approximated by those of the harmonic oscillator. The consequences of the previous description can be summarized in the IR selection rules, which state that only those molecules are IR active having an electrical dipole moment of nonzero and for which the matrix element (2.2) is different from zero [10].

In conventional infrared spectroscopy the IR beam is directed trough a cell with the investigated molecules, commonly in the gas phase, and the remaining intensity is measured, yielding to the so-called sample spectrum. Then a second spectrum is recorded, the so-called background spectrum, by directing the IR beam through a reference cell without the molecules within. The spectrum showing the frequencies absorbed by the molecules is obtained by subtracting the background spectrum from the sample spectrum. The Fourier

transformation (FT) technique enables one to use an incident beam of a wide frequency range and to gain the frequency-intensity relationship by a mathematical backtransformation. Therefore the recording time of one spectrum is minimized and the signal to noise ratio can be improved by adding several spectra.

2.1.3.2 Infrared Reflection Absorption Spectroscopy

In contrast to conventional IR spectroscopy in IRAS the infrared beam is directed on a surface and changes in the intensities due to absorption of *adsorbed* molecules are detected in the reflected beam.
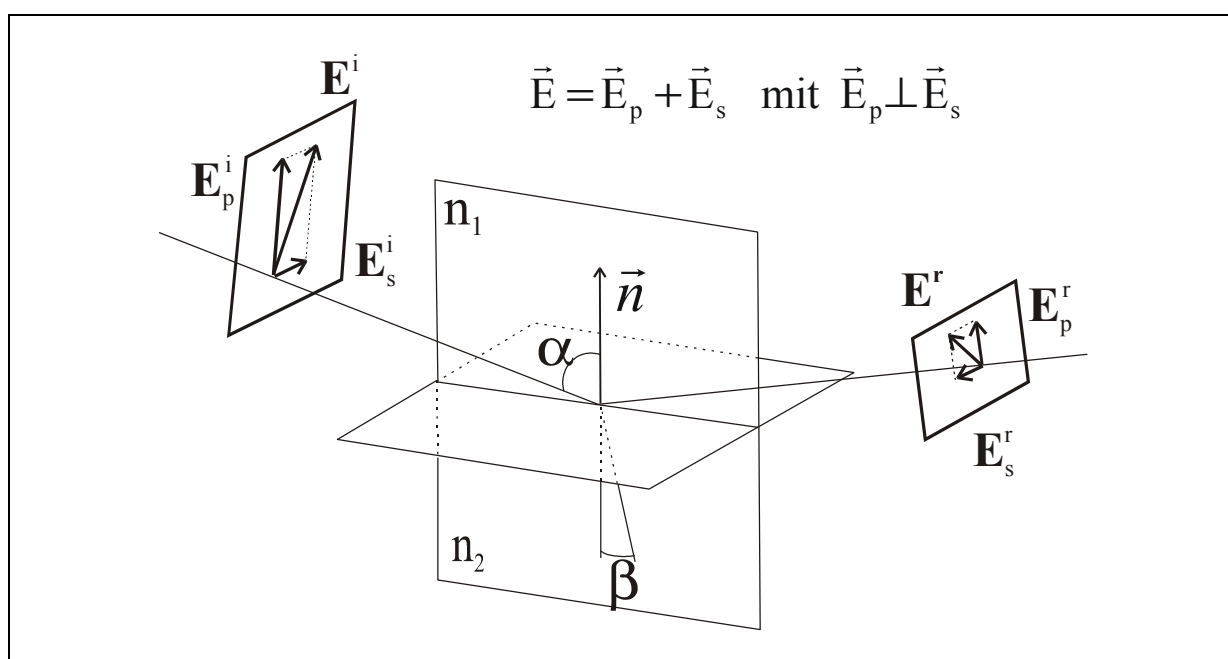
Figure 2.1: Reflection of an electromagnetic wave at the boundary between two homogenous media of different refractive index n_1 and n_2;

Regarding the nature of IRAS for a complete description it is necessary to outline the basic principles of specular refection of light. When light is reflected at the surface separating two homogenous, isotropic phases both the intensity and the state of polarization are affected [10]. The electric field vectors of the incident and the reflected light are denoted as $\vec{E}^i$ and $\vec{E}^r$, respectively (see Figure 2.1). The direction of propagation, parallel to the wave vector $\vec{k}$, and the unit vector $\vec{n}$ perpendicular to the plane of reflection, defines the plane of incidence. In order to simplify the mathematical description it is useful to separate the electric field vector of the electromagnetic wave in two perpendicular parts, $\vec{E}_p$ and $\vec{E}_s$ respectively. The former vector lies in the plane of incidence (p-polarization) whereas the latter vector is perpendicular to the plane of incidence (s-polarization) (see Figure 2.1). As a consequence,

for these two components, there is no change in the polarization state upon reflection, but only the amplitude and the phase are affected as described by Fresnel (2.3):

$$E_p^r = -E_p^i \frac{\tan(\alpha - \beta)}{\tan(\alpha + \beta)} \text{ and } E_s^r = -E_s^i \frac{\sin(\alpha - \beta)}{\sin(\alpha + \beta)} \tag{2.3}$$

The angle of incidence α and the angle of refraction β are dependent on the refractive indices n_i of the two phases and can be calculated using Snell´s law (2.4):

$$n_1 \sin \alpha = n_2 \sin \beta \tag{2.4}$$

At the phase boundary of the two phases both the incident electric field vector $\vec{E}^i$ and the reflected electric field vector $\vec{E}^r$ are simultaneously present. Moreover, as a consequence of equation 2.3 the phase angles of the p-polarized and s-polarized light are changed upon reflection. For the case of $\alpha + \beta > \pi / 2$ and $n_1 < n_2$, which is fulfilled for specular reflection on metal electrodes, the change in the phase angles of $\vec{E}_p$ and $\vec{E}_s$ are 0 and π, respectively. This, in turn, means that the incident and reflected waves tend to cancel out for s-polarization, whereas for p-polarization both waves add in phase.

Therefore, the interaction with the adsorbed molecules will only be important for molecules having their electric dipole moment perpendicular to the surface. This restriction constitutes the so-called surface selection rule [10]. Another consequence is that the maximum absorption of the infrared beam occurs when using p-polarized light and therefore a polarizer for the incident beam is used when applying IRAS.

Since in this work FTIR spectroscopy was applied at the solid/liquid interface we will focus in the following on this technique, e.g. in-situ IRAS, and its special requirements. The most obvious obstacle applying IR in an solution is the strong absorption of the IR beam by the solvent, i.e. generally water. This difficulty has only recently been overcome with the introduction of the thin layer configuration [11]. Using this configuration the pathway of the IR beam through the electrolyte is minimized by pressing the electrode surface on an IR transmitting prism, commonly a CaF_2 prism (see Figure 2.2). One major drawback, however, is that no diffusion of the electrolyte in the thin layer can take place. The thin layer behaves more or less as a closed system. This, however, limits in some cases where irreversible adsorption occurs the ability to investigate surface reactions by IRAS. In these cases it is appropriate to apply internal reflection (with its own limitations, for example the use of conventional single crystals is not possible in internal reflection). Furthermore, it is important to note that the thickness of the thin layer can not be calibrated in such a defined way which

would meet the demands of controlling the IR intensity. Therefore the sample and background spectra, from which the ratio is calculated, must be recorded in one set of spectra, e.g. using the same thin layer. No lifting of the electrode during the measuring of a set of spectra is allowed. The background spectrum therefore is usually recorded at a potential at which adsorption of the investigated molecule did not yet take place or where the molecule is already oxidized.

There are two factors which influence the absorption frequency of an adsorbed molecule. First the electric field due to the applied electrode potential, the so-called electrochemical Stark effect [12, 13], and secondly the surface coverage of the molecules due to dipole-dipole coupling. There are two equivalent explanations for these effects. From a chemical viewpoint the electric field at the interface is shifting the Fermi energy of the metal, and hence the molecular orbitals of the adsorbed molecules and the chemical bonding are influenced. From a physics point of view an interaction energy of the dipole and the electric field (due to the applied electrode potential) has to be added to the matrix element in equation 2.2. Independent from the point of view, the reason for this effect is the fact that the electric field is effective only in a very small range of the interface, the double layer, leading to enormous field strength of up to 10^7 V/cm [14].

For the interested reader detailed reviews of IRAS and its application in electrochemistry are given in the references [10, 15, 16].
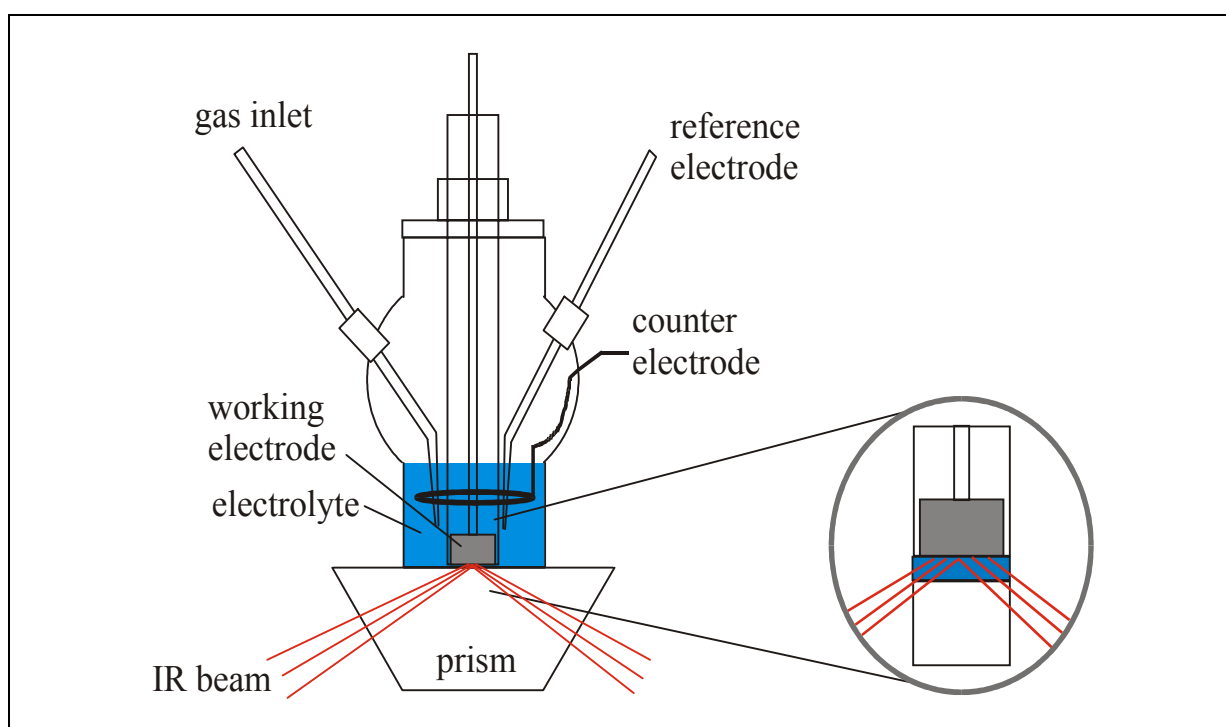
Figure 2.2: Sketch of the thin layer configuration in IRAS cell

2.1.4 Rotating Ring-Disk Electrode

For kinetic studies of electrochemical reactions a defined mass transport is crucial. One possibility to carry out electrochemical measurements under defined mass-transport conditions is the use of rotating electrodes, such as the rotating ring-disk electrode (RRDE). The rotation induces a forced convective mass-flow of the electrolyte, and hence of the reactants being dissolved within, to the working electrode. As discussed below the mass flow to the electrode can easily be controlled by the rotation rate. From the recorded current-potential relationship at different rotation rates, the kinetic parameters of a reaction at the investigated electrocatalysts can be extracted.

For the determination of the solution flow profiles (and hence the mass flow of electroactive species to the electrode) as a function of rotation rate, solution viscosity and density, the hydrodynamic problem has to be solved for the used type of electrode (e.g. disk, ring or cylinder). Here only the (ring) disk electrode, schematically shown in Figure 2.3, will be discussed.
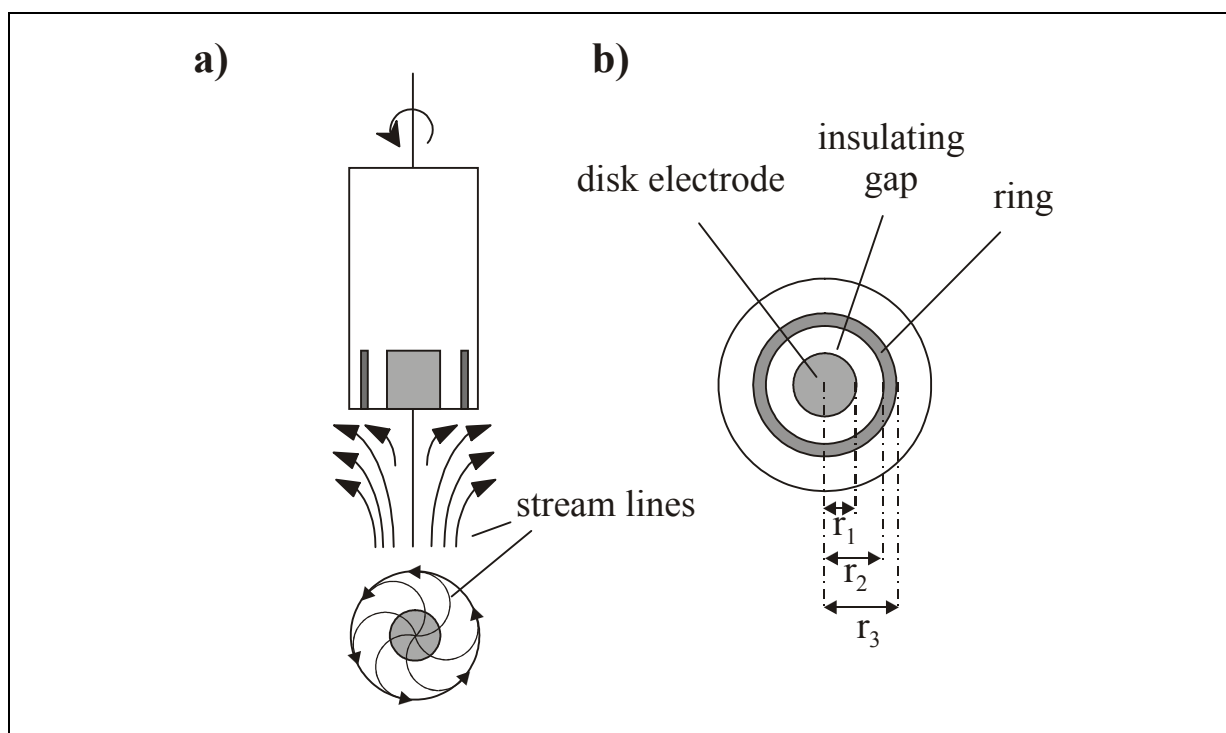
Figure 2.3: Sketch of a rotating ring-disk electrode; a) top and side view with schematical streamlines; b) top view with ring, disk and insulating separator

Before coming to utilization of the ring electrode in the RRDE, the description is focused on the RDE. The RDE consists of a smooth circular electrode embedded in an insulator, where the central surface normal defines the rotation axis. Due to the rotation the electrolyte is sucked to its surface and propelled outwards as sketched in Figure 2.3a. In a theoretical treatise introduced by Levich, it is assumed that the mass transport of the electrolyte to the surface is up to a small diffusion layer convective and diffusion takes part afterwards. The diffusion layer thickness δ_{RDE} is given by [17]:

$$\delta_{RDE} = 1.61\, D^{1/3} v^{1/6} \omega^{-1/2} \qquad (2.5)$$

where D, v and ω denote the kinematic viscosity of the electrolyte, the diffusion coefficient of the reactant in the electrolyte, and the rotation rate (in rad/s) of the electrode. Note that in contrast to a stationary electrode according to equation (2.5) for the RDE the diffusion layer thickness is not time dependent, but for a given system only dependent on the rotation rate. Assuming Fick´s law the current density measured at the disk electrode can be expressed in terms of the concentration of the reactants in the bulk of the electrolyte c_0 and at the electrode surface c_σ by:

$$I = nF \frac{D}{\delta}\left(c_0 - c_\sigma\right) \qquad (2.6)$$

with n, F being the number of transferred electrons in the reaction and the Faraday constant, respectively.

If the reaction rate at the electrode is much larger than the diffusion of the reactant to the electrode, i.e. the reactant reacts "immediately" when reaching the surface, the surface concentration of the reactant is essentially zero and the current is called diffusion limited. The diffusion limited current density I_d can be calculated by:

$$I_d = nF\, c_0 \frac{D}{\delta} \qquad (2.7)$$

By combining the equation (2.5) and (2.7) one obtains the Levich-equation for the diffusion limited current density on a RDE $I_{d,\,RDE}$:

$$I_{d,RDE} = 0.62\, nFD^{2/3} v^{-1/6} c_0 \omega^{1/2} = B\omega^{1/2} \qquad (2.8)$$

where B denotes the so-called Levich constant. Note, that in the literature the notation of B is not consistent. Sometimes the Levich constant is defined without the bulk concentration of the reactant in the electrolyte c_0. Here, however, c_0 is included in the Levich constant B.

When working with low reactant concentrations (e.g., dissolved gases in aqueous electrolytes with typically $c_0 \approx 10^{-3}$ M), the time-independent small diffusion layer thickness on a RDE results in increased and constant current densities compared to stationary electrodes. Summarizing, the advantage of the RDE is a controlled, time independent mass flow of the electroactive species to the electrode. The mass flow can be conveniently regulated by varying the rotation rate.

A suitable method to study multi-step electrode reactions or adsorption processed is the rotating ring-disk electrode, first described and theoretically treated by A.N. Frumkin et al. in 1959 [18]. The RRDE consists of two concentric electrodes: the disk electrode with radius r_1 and the ring electrode with inner and outer radius r_2 and r_3, respectively (see Figure 2.3b). The disc and ring electrode are separated by an insulating gap (usually Teflon). Analogous to the RDE the limiting current of the ring electrode is given by:

$$I_{d,Ring} = \beta^{2/3} B \omega^{1/2} \tag{2.9}$$

where β is a constant based on the ring and disk radii ($\beta = r_3^3/r_1^3 - r_2^3/r_1^3$). Although two types of RRDE experiments can be distinguished [18], here only measurements in the *collection* mode will be discussed.

In the collection mode, species which are generated on the disk electrode are detected (collected) under pure convective-diffusion control on the independently potentiostated ring electrode. In this work the collection mode is applied when investigating the oxygen reduction reaction. The ring electrode is potentiostated at a positive potential sufficient to oxidize the peroxide which is formed in one reaction pathway of the ORR on the disk electrode. For details see Chapter 5.

Detailed descriptions of the R(R)DE method can be found in references [6, 17-20].

2.1.5 Low Energy Ion Scattering

The most reliable method for determining the composition of a bimetallic surface is by low energy ion scattering (LEIS) using an inert gas like helium or neon [21]. In LEIS a beam of noble gas ions with an energy between 0.1 and 10 keV is scattered from the surface atoms of an investigated crystal and the kinetic energy of the scattered ions is detected. As described below, the kinetic energy of the scattered ions depends on the mass of the target atom on the surface and hence an analysis of the recorded spectra allows one to determine the surface composition.

The inherent surface sensitivity of this method lies in the large neutralization cross section of the incident ions by the metal. For example, 1 keV He[+] ions have a neutralization probability of about 99% in passing through one layer of substrate atoms [22]. Hence, the majority of ions that reach the detector must have scattered from the outermost surface layer. The sputtering effect of the surface depends on the choice of the inert gas. Helium ensures at a short recording time only a negligible alteration of the surface.

Since the de Broglie wave length of the impinging ions is short in comparison to the interatomic distance of the crystal, the scattering process can be described by the classical theory. The ratio of the final and initial kinetic energy, E_f and E_i respectively, of the elastically scattered ions is given in (2.10). It can be seen that the ratio depends only on the masses of the incident ion (m_i) and the target atom (m_t) as well as the scattering angle θ.

$$\frac{E_f}{E_i} = \left(\frac{\cos\theta + \sqrt{(m_t/m_i)^2 - \sin^2\theta}}{1 + (m_t/m_i)} \right)^2 \qquad (2.10)$$

In Figure 2.4 the resulting ratios E_f/E_i for helium ions scattered at an angle of 127 degree are plotted against the mass of the target surface atom. The masses of the, for this work interesting, target atoms palladium and platinum are indicated. The resulting ratios for palladium and platinum are 0.886 and 0.936 respectively.
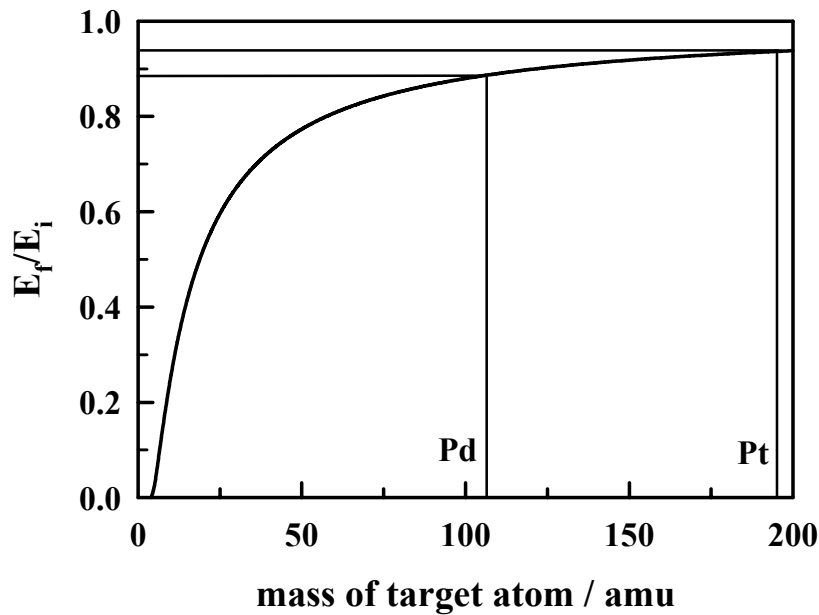

Figure 2.4: Relative energy of scattered He^{+}-ion vs. the mass of target atom; $\theta = 127°$

As shown in the Results section this difference in the energy between ions scattered on palladium and platinum atoms, respectively, can be easily resolved. A detailed review of the principles and applications of LEIS is given by Niehus et al. [23].

2.2 Experimental Details

The measurements discussed in this work were conducted on bare Pt(hkl)-electrodes and on thin Pd films supported on Pt(hkl)-electrodes. For the single crystals (*MaTeck, Jülich*), all having the same surface area of 0.283 cm^2, a miscut of $\leq 0.5°$ was determined by using X-ray diffraction. The preparation and characterization of thin palladium films on a Pt(111) electrode was performed in UHV as well as in an electrochemical cell. In the following section the experimental details of the preparation and characterization in UHV are described. Subsequently the electrochemical preparation of the thin palladium films is introduced.

2.2.1 UHV Measurements

The cleaning of the crystal, the Pd deposition and the characterization of the surfaces were performed in a UHV system equipped with an angular-resolving double pass cylindrical mirror analyzer (PHI-DPCMA Φ15-255GAR) under a base pressure of $2 \cdot 10^{-10}$ mbar. The sample cleaning was done by Ar$^+$ sputtering with an ion energy of 600 eV, subsequent annealing at 1200 K and the removal of carbon by heating the sample in an oxygen atmosphere at 800 K. This procedure was repeated until no contamination with carbon (or other elements) could be determined by means of AES anymore. The Auger spectra were recorded in the derivative mode using an electron beam of 3 keV energy, 3 eV$_{p-p}$ modulation and 5 µA beam current, in a range from 140 to 900 eV. Different amounts of palladium onto the clean Pt(111) surface were deposited using a UHV evaporator Omicron/Focus model EFM3/4, equipped with an integrated flux monitor. The deposition of Pd was followed simultaneously recording the AE signal for Pt at 64 eV in a range of ± 10 eV. After deposition of a submonolayer film the total coverage of Pd was also determined by low energy ion scattering. The LEIS spectra were recorded using a He$^+$ ion beam with an energy of 1 keV and a current (measured at the sample) between 5 to 100 nA, in order to minimize the sputtering rate by the ion beam. The incidence angle was 45° and the scattering angle was 127°. The ion beam was rastered over an area of 3×3 mm^2 and the time of recording one spectrum was 60 s.

2.2.2 Electrochemical Measurements

The preparation procedure of the Pt single crystals and the subsequent mounting in the RDE or thin layer configuration strictly followed the method described by Markovic et al. [24]. Before each measurement, the single crystal was annealed in a hydrogen flame [25], and subsequently cooled down to room temperature in a mild stream of Argon [26]. Then the crystal was protected against contamination from the atmosphere by a droplet of ultrapure, triply-pyrodistilled water and subsequently mounted into the disk position of an insertable disk electrode assembly (*Pine Instruments*) or in the electrode position of the spectroelectrochemical cell. Afterwards the electrode was transferred into the respective electrochemical cell and emersed into Argon saturated electrolyte.

For the electrochemical deposition of palladium the clean, flame annealed sample was subjected to a potential cycling between $0.05 < E < 0.9$ V in a 0.05 M $H_2SO_4 + 5 \cdot 10^{-6}$ M Pd^{2+} solution with a sweep rate of 50 mV/s. The amount of Pd deposited was controlled by monitoring the continuous change of the voltammetric features, from those characteristic of bare Pt(111) to those characteristic of a monolayer of palladium on Pt(111). Afterwards the electrode was rinsed with ultra pure water and transferred either into the *in-situ* FTIR cell or to a standard three compartment electrochemical cell for kinetic measurements. The electrochemical cell (see Figure 2.5) was a thermostated standard three compartment cell equipped with a water jacket. A circulating constant temperature bath (Fischer Isotemp Circulator) maintained the temperature of the electrolyte within ± 0.5 K. The reference electrode was a saturated calomel electrode (SCE) separated by a closed electrolyte bridge from the working electrode compartment in order to avoid chloride contamination. All measurements were conducted nonisothermally, *i.e.*, keeping the temperature of the reference electrode constant (≈ 298 K) while that of the working electrode was varied. All potentials shown in the text, however, refer to the reversible hydrogen electrode in the same solution, calibrated from the reversible potential for the hydrogen evolution/oxidation reaction. The counter electrode was a platinum mesh of high surface area, which was flame annealed before each measurement.
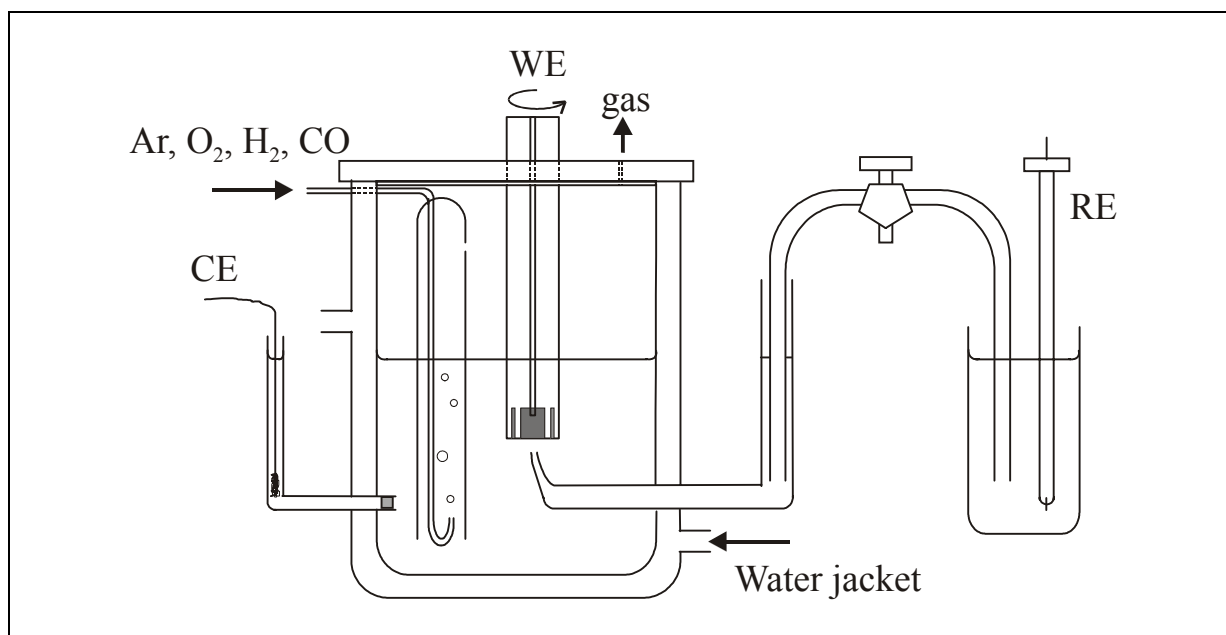
Figure 2.5: Standard three compartment electrochemical cell

Sulfuric acid, perchloric acid and formic acid solutions were prepared from concentrated acid (*Baker Ultrex*, *EM Science suprapure* and *EM Science research grade*). Methanol solution was prepared from concentrated solution (*EM Science research grade*), whereas potassium hydroxide solution was prepared from pellets (*Aldrich Semiconductor Grade*). All solutions were diluted using triply-pyrodistilled water. Before the use all glassware was cleaned by applying the following procedure. First, the glassware was put in concentrated KOH solution (5 M) for several hours and subsequently thoroughly rinsed with deionized water. Then the glassware was put for several hours in a mixture of concentrated nitric and sulfuric acid (1:1) and in the last step repeatedly boiled in ultrapure water. Prior to each experiment the electrolyte was deaerated by purging with argon (Air Products 5N5 purity). The CO, H_2, and O_2 (Spectra Gases N4.5) measurements were carried out in saturated electrolytes. The RDE measurements were performed under a continuous gas flux. The adsorption procedures are described in detail in the corresponding sections.

2.2.3   In-situ FTIR Measurements

For the in situ FTIR measurements a Nicolet Nexus 670 spectrometer was available with a liquid nitrogen cooled MCT[5] detector. All IR measurements were performed in a spectroelectrochemical glass cell designed for an external reflection mode in a thin layer configuration (see Figure 2.2). The cell is coupled at its bottom with a CaF_2 prism beveled at

---

[5] **M**ercury **C**admium **T**elluride

60° from the surface normal. All spectra were recorded with a resolution of 8 cm^{-1} using p-polarized light. Absorbance spectra were calculated as the ratio $-\log(R/R_0)$ where R and R_0 are the reflectance values corresponding to the sample and reference spectra, respectively. The reference potential in the spectroelectrochemical cell was controlled by a reversible hydrogen electrode (RHE). Prior to each measurement a cyclic voltammogram was recorded in order to check the cleanliness. All FTIR measurements were carried out non thermostated at room temperature (T≈298 K).

Chapter 3

Preparation and characterization of Pt(111)-Pd electrodes

Bimetallic surfaces can be classified in two categories, bulk alloys and pure metal surfaces modified by the deposition of a second metal. Metal deposition can be performed in UHV by physical vapor deposition, or electrochemically (usually by underpotential deposition). Electrodeposition methods have the advantage of not requiring any additional equipment for the preparation of the surface, other then an electrochemical cell and a potentiostat being used in typical electrochemical measurements. Electrodeposition is also a fast method of preparation and is particular advantageous for screening the reactivity of candidate bimetallic catalysts [21]. For fundamental studies of reactions on bimetallic surfaces the electrodeposition method of preparation, however, has the major drawback of creating an unknown surface. Efforts to characterize the surface *in-situ* in an electrochemical cell are considerably less strict than a characterization by UHV methods. The reasons for this are the limited range of characterization tools as well as the fact that in an electrochemical cell no such thing as an uncovered free surface exists, instead the surface is in constant interaction with at least the supporting electrolyte. In contrast, the *preparation* and *characterization* of bimetallic surfaces in UHV is well established. Therefore it presents a much more complicated problem to characterize the surface in-situ than ex-situ. In electrocatalysis this so-called ex-situ approach, i.e. the preparation of electrodes in UHV with the subsequent transfer to an electrochemical cell, enables one to utilize the full range of modern methods of both bulk and surface sensitive analysis that is essential for developing a molecular level understanding of the reactivity of surfaces [27].

The chemical and electronic properties of bimetallic surfaces are particularly relevant to the field of (electro)catalysis where changes in the catalytic activity can be attributed to structure (or morphological) effects, ensemble effects and electronic (or ligand) effects. Electronic effects have their origin in the fact that the electronic structure of the surface atoms is modified due to the interaction of the components of the bimetallic system. This modified electronic structure, in turn, leads to a different interaction of adsorbed molecules with the surface. The influence of the distribution and composition of reaction sites, e.g. bridge and

three-fold hollow adsorption sites, is denoted as ensemble effect. Structure effects arise due to changes in the local bond geometry of surface atoms [28]. Furthermore, a bifunctional effect is given if the second component of the metal surface is providing the necessary reactive intermediates for a catalyzed reaction. However, these different effects are difficult to separate and generally a *combination* of them is operative.

In the first part of this chapter the physical properties of palladium and platiunum are introduced and the basic conceptions of surface science are given. Subsequently the previous work related to the subject of catalysis on thin metal films is summarized. There, also a short overview over previous investigations concerning the electrochemical preparation of thin palladium films supported on Pt(111) is given. Then, in the second part of the chapter, the method of *electrochemical* Pd deposition on Pt(111) used in this work is introduced. The behavior of a Pt(111) electrode in contact with $0.05 \, M \, H_2SO_4 + 5 \cdot 10^{-6} \, M \, Pd^{2+}$ solution is depicted and the surface morphology of the electrodeposited films is probed by using FTIR spectroscopy. The experimental results are discussed in the light of the previous work. In this context difficulties in the determination of the Pd coverage, solely based on in-situ measurements, are specified and the *combined* ex-situ/in-situ approach, used in this work, is introduced.

In the following part of the chapter the preparation and characterization of Pd films evaporated on Pt(111) in ultra high vacuum as well as the voltammetric behavior of these *UHV prepared* Pt(111)-xPd surfaces in sulfuric acid solution is described. Based on these results, in the last section, the properties of the UHV prepared electrodes and the properties of the electrochemical deposited films are discussed and a correlation between UHV-prepared (and –characterized) and electrodeposited Pd films is developed.

3.1 Details: Single crystals

3.1.1 Properties of Pt and Pd single crystals

Both metals, Pd and Pt, are crystallizing in an fcc structure[6] and the surface structure can be characterized by the so-called Miller indices (hkl) [29].

---

[6] **f**ace **c**entered **c**ubic
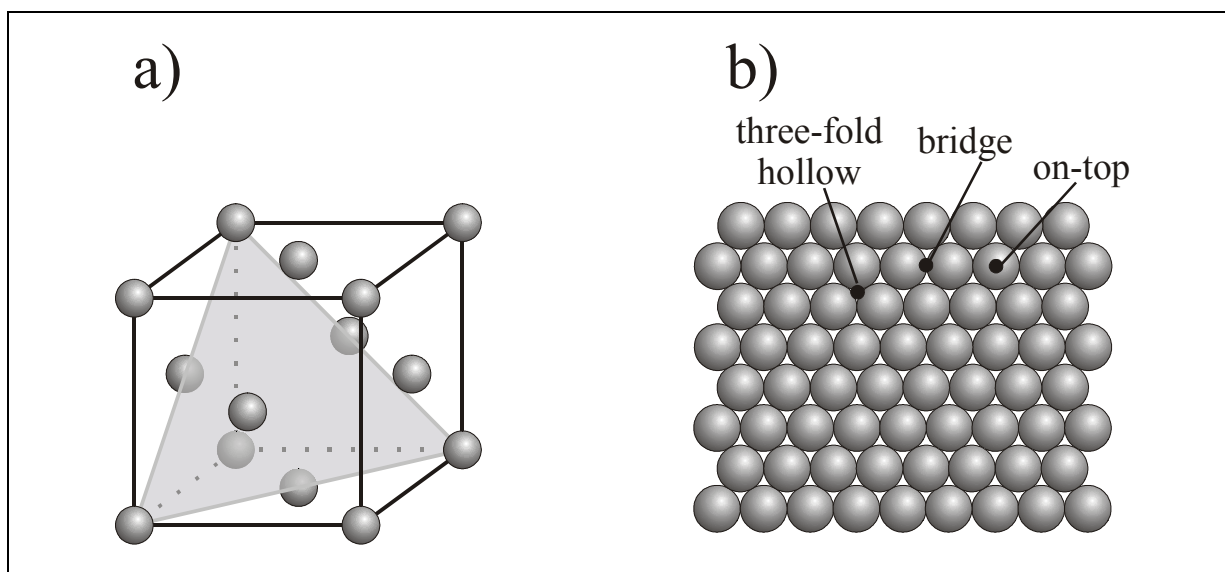
Figure 3.1: The (111) surface of an fcc single crystal; a) side view b) front view

Without going into details the (111) surface of an fcc metal has a hexagonal structure, as shown in Figure 3.1. As depicted, three different simple adsorption sites for small molecules can be distinguished on the (111) surface, namely on-top, bridge and three-fold hollow sites, respectively. For the sake of completeness, it should be noted that the three-fold hollow sites can be further distinguished in fcc and hcp[7] sites depending on the site in the second layer under the adsorption site being also a hollow site or a metal site, respectively (not shown in Figure 3.1).

	Pt	Pd
bulk lattice constant /nm	0.392	0.389
Nearest neighbor /nm	0.277	0.275
work function (111) /eV	6.0	5.6
standard electrode potential for Me/Me^{2+} couple /V$_{RHE}$	1.23	0.83

Table 1: Basic physical and electrochemical properties of palladium and platinum; data taken from [17, 30]

The basic physical and electrochemical properties such as the bulk lattice constants and the standard electrode potential of the redox couple of both metals are listed in Table 1. It

---

[7] **h**exagonal **c**lose **p**acked

can be seen that the lattice constant of both metals are almost the same and consequently there is not much strain produced in the pseudomorphic palladium monolayer on Pt(111).

3.1.2 Literature

3.1.2.1 Thin metal films

By using modern surface characterization techniques applied under UHV conditions Goodman et al. showed in their work that thin metal films supported on a foreign metal substrate provide a means for modifying the chemical and electronic properties of surfaces [31, 32]. The influence of this modified chemical composition and electronic structure on the catalytic properties was probed by investigating several surface reactions. It has been shown that upon deposition of one metal onto another one new structures can be formed which are not seen in bulk alloys. One particularly interesting class of systems are pseudomorphic monolayers, where the metal overlayer adopts a lattice constant which differs from the corresponding bulk crystal structure but which is in registry with the lattice of the underlying substrate. By choosing different substrates the electronic and geometrical properties of the pseudomorphic monolayers, and hence their reactivity towards adsorbate molecules can be significantly modified. Two main reasons can be related to these modified properties of pseudomorphic monolayers, first, the electronic interaction between the substrate atoms and the adlayer, and second, the strain induced by the substrate lattice on the geometry of the thin metal film [31-37].

The experimental work has been supported and motivated by theoretical calculations in which a strong correlation was found between the molecular chemisorption energy and the energy position of the d-band center of the surface metal atoms [38-41]. Only shortly after the successful UHV studies, the adsorption and catalytic properties of pseudomorphic metal films supported on single crystal metal surfaces has also received considerable attention in the field of surface electrochemistry [42-47]. In electrochemistry one of the main driving forces for the investigation of thin palladium films was the difficult in-situ preparation of Pd(hkl) electrodes. Consequently, for the electrochemical measurements, thin metal films were prepared either in UHV (ex-situ) by evaporation or in solution (in-situ) by (electro)chemical methods. Electrodeposition proved to be a particularly reliable method of preparing palladium films on platinum [45-49] and gold [50-55] single crystals.

3.1.2.2 Thin palladium films supported on Pt(111)

UHV investigations of palladium films deposited by physical vapor deposition on Pt(111) were performed by Attard and co-workers using AES and LEED[8] [42, 44]. The AES

---

[8] **L**ow **E**nergy **E**lectron **D**iffraction

and LEED measurements indicated that palladium grows layer by layer on Pt(111) and no evidence for any other ordered phases were observed.

Besides vacuum-deposition, the so-called "forced-deposition" chemical method and a pure electrochemical method were also developed for creating well-ordered thin palladium films on Pt(hkl) [43, 45, 46, 56-58]. The structure of the obtained films is different depending on the preparation methods. Employing for example the so-called forced deposition method, i.e. the reduction of the metal oxide solution in a stream of hydrogen (without applied potential) [59], leads to a three dimensional island growth [43, 56, 57, 60]. In contrast, with continuous cycling in sulfuric acid, containing only small amounts of palladium oxide, a rather smooth palladium monolayer is formed before island growth sets in [49, 55].

As shown in table 1, the reversible Nernst potential of the couple Pd/Pd^{2+} is 0.83 V vs. RHE [17]. In electrochemical deposition, depending on the nature of the anions in the supporting electrolyte the deposition proceeds without overpotential, i.e. an underpotential deposition process takes place (in chloride containing electrolytes) or palladium is deposited only at potentials negative of the Nernst potential, i.e. in the overpotential range (in sulfuric acid) [55]. In fact, in sulfuric acid solution the deposition proceeds only slow and an overpotential of more than 50 mV is necessary for the palladium deposition.

The morphology of these palladium overlayers, deposited in sulfuric acid solution, has been recently examined by SXS[9] measurements [49]. The pseudomorphic growth mode has been verified and an enhanced stability of the palladium film towards surface roughening, compared to bare Pt(111), has been reported.

3.2 Measurements

3.2.1 Electrochemical preparation of Pt(111)-Pd electrodes

In this section the electrochemical preparation of thin Pd films supported on Pt(111) is described. Since the measurements presented in this work, are focused on the palladium coverage range of $\Theta \leq 1ML$ the palladium deposition is performed in sulfuric acid solution containing small amounts of palladium oxide. Consequently the deposition process always takes place in the overpotential range, i.e. negative of the reversible Nernst potential. The supporting electrolyte was 50 mM H_2SO_4, into which 5 x 10^{-6}M PdO was added for palladium

---

[9] **S**urface **X**-ray **S**cattering

deposition. Before dealing with the deposition procedure, at first the voltammetric response of bare Pt(111) with the pure sulfuric acid solution will be shortly discussed.
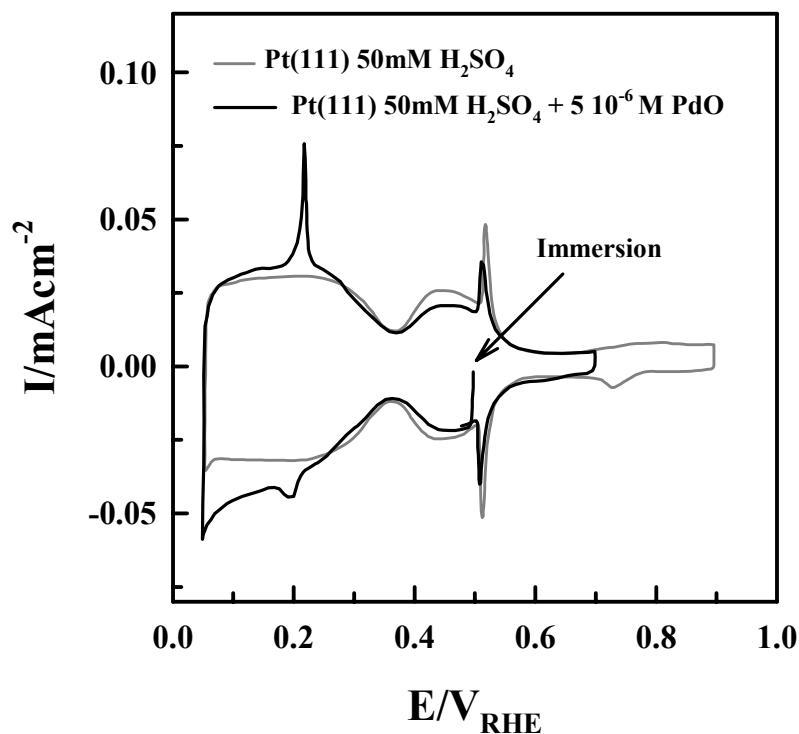
Figure 3.2: Cyclic voltammograms of Pt(111) in contact with 50mM H_2SO_4 and 50 mM $H_2SO_4 + 10^{-6}$ M PdO solution (first scan); 50 mV/s at room temperature

The well known voltammogram of a Pt(111) surface in contact with 50 mM H_2SO_4 is shown in Figure 3.2. Given the consensus in the interpretation of the voltammetric features with respect of the nature of the underlying processes [61] here only a short interpretation of the voltammogram will be presented. In the current-potential curve three potential regions can be distinguished. Starting from the negative potential limit, in the voltammogram a broad H_{upd} potential region (0.05-0.375 V) is followed first by the sulfate adsorption (0. 375-0.55 V), the so-called butterfly feature, and then by the so-called "double layer" region. A further polarization to more positive potentials (not shown) finally yields to an "irreversible" oxide formation. In the cathodic scan at a potential of about 0.75 V a small peak, the reduction of coadsorbed OH anions can be seen. It is documented that on Pt(111) the desorption of H_{upd} is not accompanied by simultaneous sulfate adsorption, rather the potential regions of these two processes are well separated from each other [62].

When introducing small amounts of PdO to the sulfuric acid solution the observed voltammogram changes immediately. Figure 3.2 displays also the first voltammogram obtained for Pt(111) in 50 mM H_2SO_4 solution containing 5×10^{-6} M PdO. After the immersion at 0.5 V the potential was scanned in a negative direction. Immediately an additional (to the voltammogram in pure sulfuric acid) small peak at 0.23 V is formed in the voltammogram. Reversing the scan direction a sharp anodic peak at the same potential, already larger than the cathodic peak, can be seen. Note also, that in the potential region of sulfate adsorption on platinum sites the current densities are decreasing.

The behavior of a Pt(111) electrode upon continuous cycling (increasing deposition time) in sulfuric acid solution containing PdO is shown in Figure 3.3. For comparison the voltammogram for pure H_2SO_4 is included as well. It can be seen that with increasing number of cycles the peak at 0.23 V is, at first, increasing. After several potential cycles a maximum in the current density at 0.23 V is reached, and subsequently a second peak at 0.28 V develops. Upon further cycling the second peak at 0.28 V is increasing while the initial peak at 0.23 V decreases. Note also that, as mentioned before, the current density in the potential region of sulfate adsorption/desorption on platinum $(0.375 - 0.55$ V) is decreasing with increasing numbers of cycles.

As discussed, the observed electrochemical behavior of Pt(111) in Pd containing sulfuric acid solution can be interpreted as the continuous pseudomorphic growth of palladium on Pt(111) [43, 49]. The appearance of the second peak located at 0.28 V is attributed to the growth of palladium in a second layer.

It is important to note, that the cyclic voltammograms shown in Figure 3.3 remain unaltered upon the transfer of the Pt(111)-xPd electrodes into a second electrochemical cell containing pure sulfuric acid without palladium oxide. Therefore the sharp peak in the voltammogram cannot be attributed to a charge transfer due to metal deposition. By utilizing IR spectroscopy it has been revealed that the sharp peak at 0.23 V is caused by the coupled desorption/adsorption of H_{upd} and sulfate molecules on palladium, respectively [48]. This finding fits well with the observation that the butterfly feature, which is caused by sulfate adsorption on bare Pt(111), is decreasing with ongoing palladium deposition. The fact that hydrogen adsorption/desorption and sulfate desorption/adsorption emerge in a single peak implies a strong interaction of the sulfate anions with the palladium surface atoms.
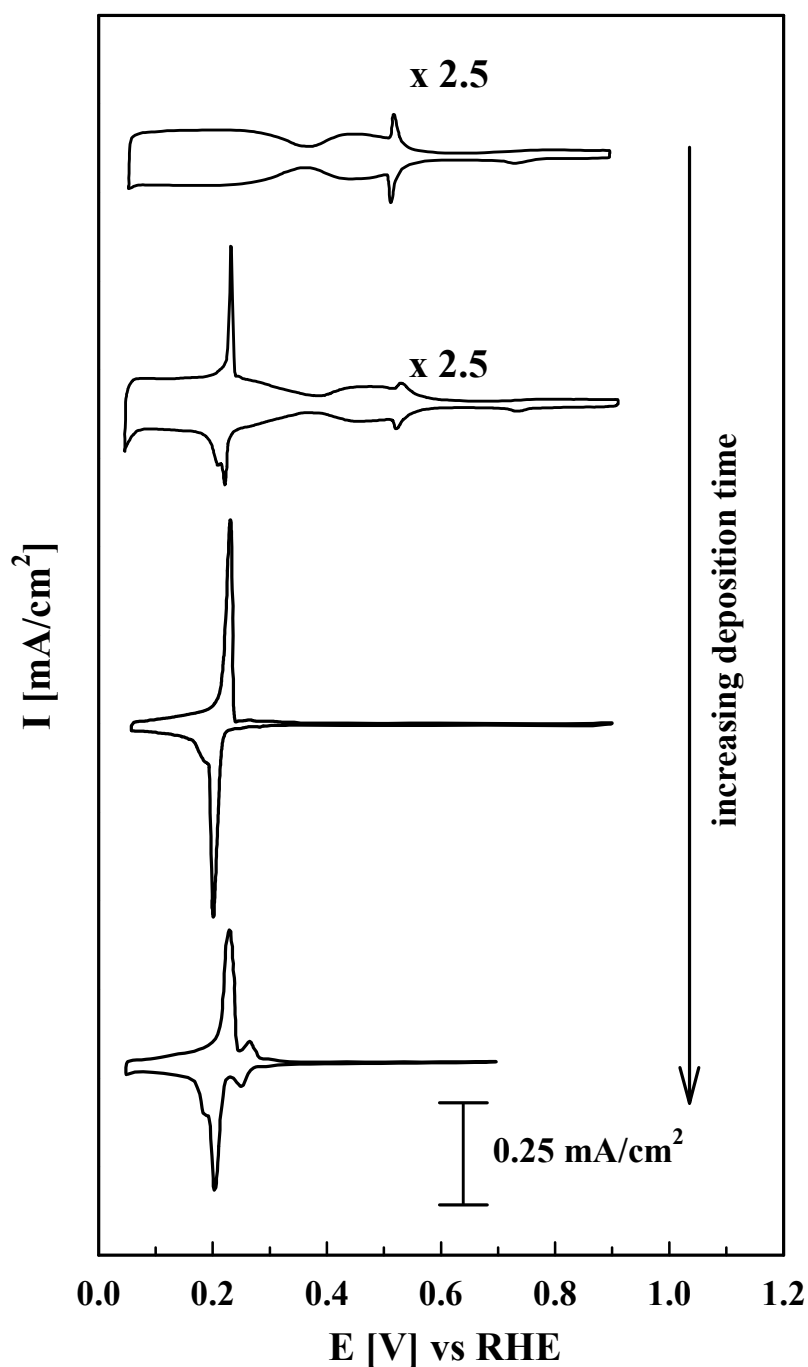
Figure 3.3: Series of cyclic voltammograms of Pt(111) in contact with 50mM H_2SO_4 solution containing $10^{-6}M$ PdO; the number of applied cycles is increasing from top to the bottom; scan rate 50 mV/s at room temperature

Whether a smooth palladium monolayer on Pt(111) is achieved, or island growth sets in before completing the first palladium layer, is strongly dependent on the deposition procedure. As mentioned in the literature review (section 3.1.2) employing the so-called forced deposition method leads to a three dimensional island growth [43, 56, 57, 60]. In

contrast, with continuous cycling in sulfuric acid, containing only small amounts of palladium oxide, a rather smooth palladium monolayer is formed before island growth sets in [49].

Unlike in UHV, the evaluation of the palladium coverage Θ_{Pd} of electrochemically deposited Pt(111)-xPd is not straightforward. There is only one study in the literature, where the palladium coverage of electrodeposited Pt(111)-xPd surfaces is systematically studied. In the work Alvarez et al. the authors reported the determination of Θ_{Pd} by the integration of the current densities in the observed cyclic voltammograms. This procedure, however, is not without drawbacks as will be discussed later.

In this work a different approach for the determination of the palladium coverage is introduced, where ex-situ analytical tools are combined with electrochemical methods.

3.2.2 Surface morphology of electrodeposited Pt(111)-Pd electrodes
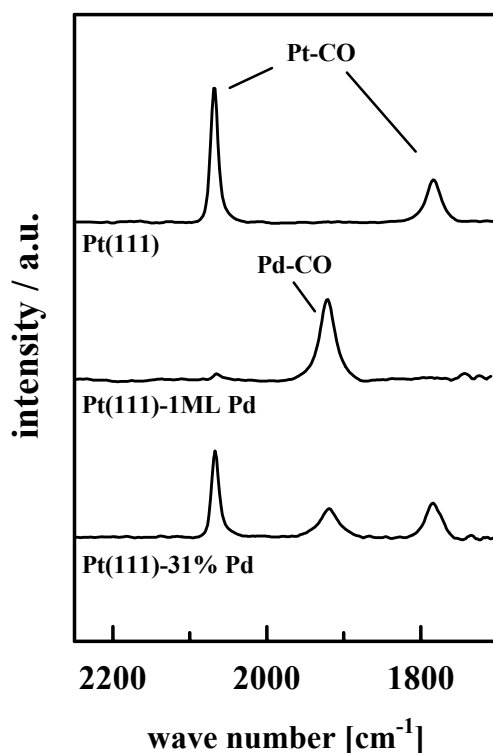
Figure 3.4: FTIR spectra obtained on different Pt(111)-xPd surfaces in CO saturated perchloric acid solution (x = 0, x = 0.31, x = 1); the applied electrode potential is 0.1 V; the background spectrum is recorded at 1 V;

Before introducing the results of the deposition of palladium on Pt(111) performed in UHV the surface morphology of the electrodeposited film is shortly discussed. In Figure 3.4 FTIR spectra for three different Pt(111)-xPd surfaces are shown. All spectra are obtained

under the same conditions. The electrolyte is CO saturated perchloric acid solution at room temperature and an electrode potential of 0.1 V is applied. The background spectrum is recorded at 1.0 V.

Without going into details (the spectra are discussed in the next chapter), on the bare Pt(111) surface two different CO absorption bands can be seen, whereas on the complete palladium film only one CO absorption band is observed. The absorption frequencies for Pt-CO and Pd-CO are well separated. The spectra of CO adsorbed on the Pd *submonolayer* reveal both the characteristic features of CO bound on Pt and CO bound on Pd, indicating that there is *no coupling* between Pt-CO$_{ad}$ and Pd-CO$_{ad}$ molecules on Pt(111)-xPd surfaces.

Moreover the CO spectra obtained on the Pd submonolayer are a *superposition* of the spectra observed for bare Pt(111) and for a full monolayer of Pd, respectively. This is an important result which allows conclusions on the film *morphology*. In a study of ruthenium deposition on Pt(111) Stimming and co-workers reported for the Pt(111)-Ru-CO system no coupling between the CO molecules adsorbed on the respective metals, whereas on a PtRu surface alloy coupling does take place [63]. Therefore, the fact that no coupling of CO$_{ad}$ for the Pt(111)-xPd surfaces takes place strongly suggests that Pd is deposited on Pt(111) in metallic islands (or patches). As mentioned, this island growth was already previously suggested by Clavilier et al. from voltammetric measurements [43] and Ito et al. from FTIR measurements [64]. Furthermore, by comparing the FTIR spectra with the data obtained for bulk Pd(111) electrodes a three dimensional growth mode, as obtained by the forced deposition method (see literature section 3.1.2), can be excluded. In the case of a high step/defect density, introduced by electropolishing the Pd(111) crystal clearly *two* CO absorption bands can be observed. Whereas one band is due to bridge bonded CO, the second absorption band can be assigned to CO bound on steps and/or defect sites.

Therefore it is important to note that in this study no second CO band was observed until the Pt(111) electrode is (almost) completely covered by the palladium film. The shown spectra demonstrate that in-situ FTIR experiments performed with CO can serve as an indirect probe for the determination of the film *morphology*. The results clearly indicate that Pd is deposited on Pt(111) in the form of metallic *islands*.

3.2.3 UHV preparation and characterization of Pt(111)-Pd electrodes

The palladium deposition on Pt(111) in UHV was performed by physical vapor deposition at room temperature varying the deposition time. The amount of palladium deposited was controlled by simultaneously recording the decrease of the AES signal for Pt at 64 eV in a range of ±10 eV. Immediately after the deposition AE spectra were measured in a

range from 130 eV to 550 eV. Figure 3.5a displays a set of five different spectra. In the first spectrum of pure Pt(111) the characteristic platinum peaks at 166, 173, 241 and 256 eV [65] can be seen. Peaks for typical impurities of platinum, such as C and O (the peaks are located at 275 eV and 510 eV, respectively) are absent.
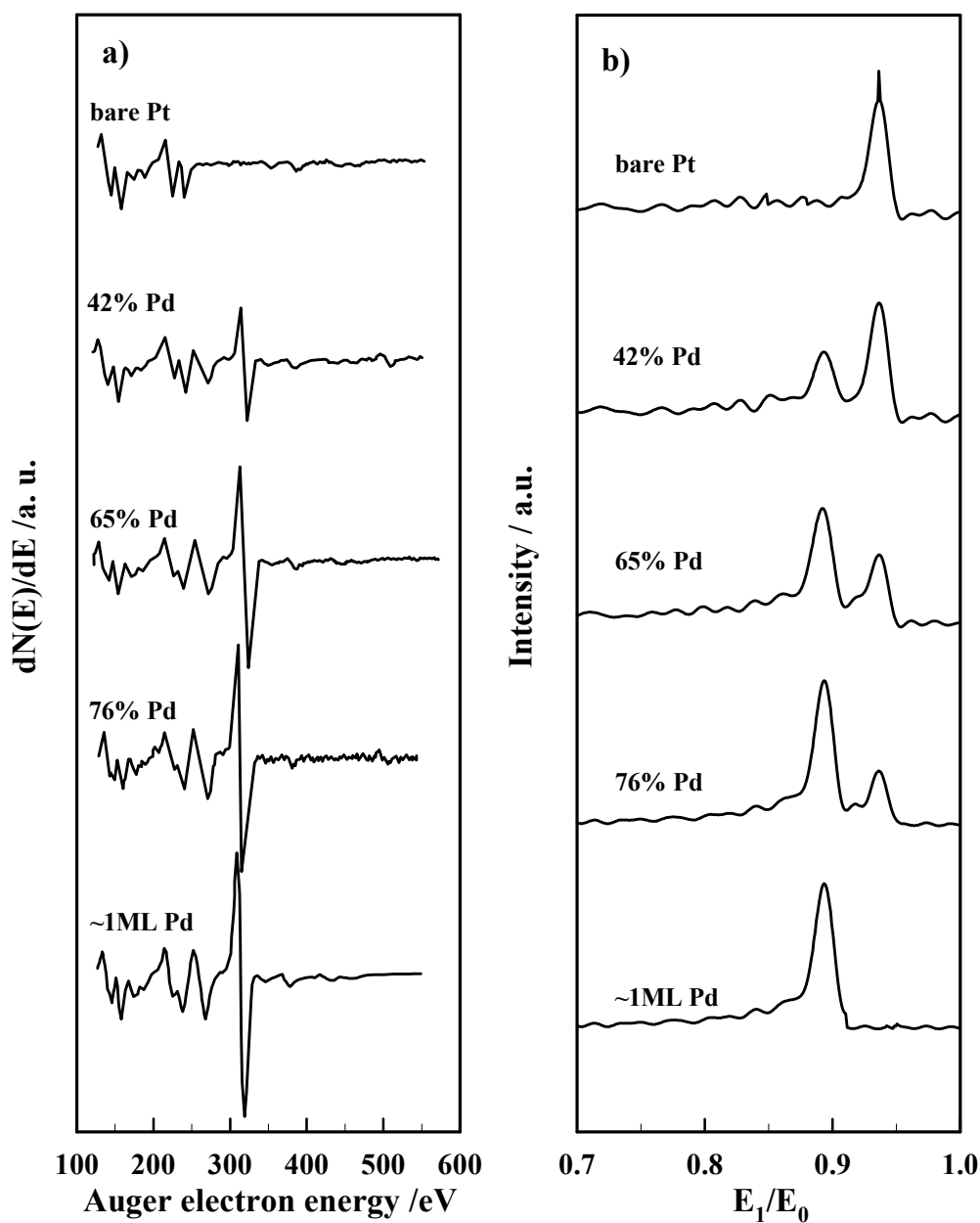

Figure 3.5: a) Auger spectra recorded after UHV palladium deposition; b) corresponding LEIS spectra; the palladium coverage calculated from the LEIS spectra is indicated

As can be seen in the following spectra of Figure 3.5a palladium deposition on Pt(111) leads to the formation of two additional peaks at 283 and 333 eV. The peak heights are clearly related to the deposition time. Since AES is not sensitive only to the first surface layer but the information depth is about 10 nm [5] the evaluation of the absolute Pd coverage by AES is difficult. In contrast LEIS is sensitive to only the topmost surface atoms [21]. Therefore additional LEIS spectra were recorded after the palladium deposition.

In Figure 3.5b the corresponding LEIS spectra are shown. In the first spectrum of unmodified Pt(111) only one peak, with a ratio of the energy of incident and scattered He^+ ions (E_f/E_i) of 0.94, is resolved. By comparison with the theoretical ratio for platinum, 0.936 (see Figure 2.4), this peak can clearly be attributed to ions scattered from platinum surface atoms. Deposition of Pd onto Pt(111) leads to a gradual decrease of the Pt peak and a concomitant increase of a second peak with a ratio of $E_f/E_i = 0.89$. Again, the observed ratio fits well with the theoretical value of 0.886 for palladium, indicating that the latter peak corresponds to He^+ ions scattered from palladium surface atoms. The elemental sensitivity factors for palladium and platinum have been evaluated in separate experiments which are not shown. It has been found that the elemental sensitivity factors are about the same, and consequently, the Pd/Pt ratio can simply be calculated by fitting the area of both peaks using Gaussian lines. From the Pd/Pt ratio, in turn, the Pd coverage is determined.

Representative examples for Pd surface coverages in the range of $40\% < \Theta_{Pd} < 80\%$ are shown in Figure 3.5b. The calculated palladium coverage is indicated at each spectrum. In the last spectrum only a single peak of $E/E_0 = 0.89$ with the maximum intensity is resolved. This proofs that the Pt surface is completely covered by Pd atoms, as already suggested in previous AES/LEED studies by Attard and co-workers [42, 44]. The palladium coverage of this spectrum is denoted as ~1ML, however regarding the results of LEIS it can just be stated that the surface is completely covered by palladium. That the coverage is indeed only one 1ML will be shown in the following, where the cyclic voltammograms of the UVH prepared electrodes are discussed.

After the determination of the LEIS spectra, the respective Pt(111)-xPd sample was immediately transferred to the electrochemical cell, in order to establish the relationship between the palladium surface coverage and the corresponding voltammetric profile. Considering that the voltammetric response of the Pt(111) electrode modified with a Pd film is well established in sulfuric acid solution [43, 46, 66], in this work the UHV-prepared Pt(111)-Pd systems were electrochemically characterized in 0.05 M H_2SO_4 at room temperature, as displayed in Figure 3.6. For comparison the CV of pure Pt(111) is included as well.

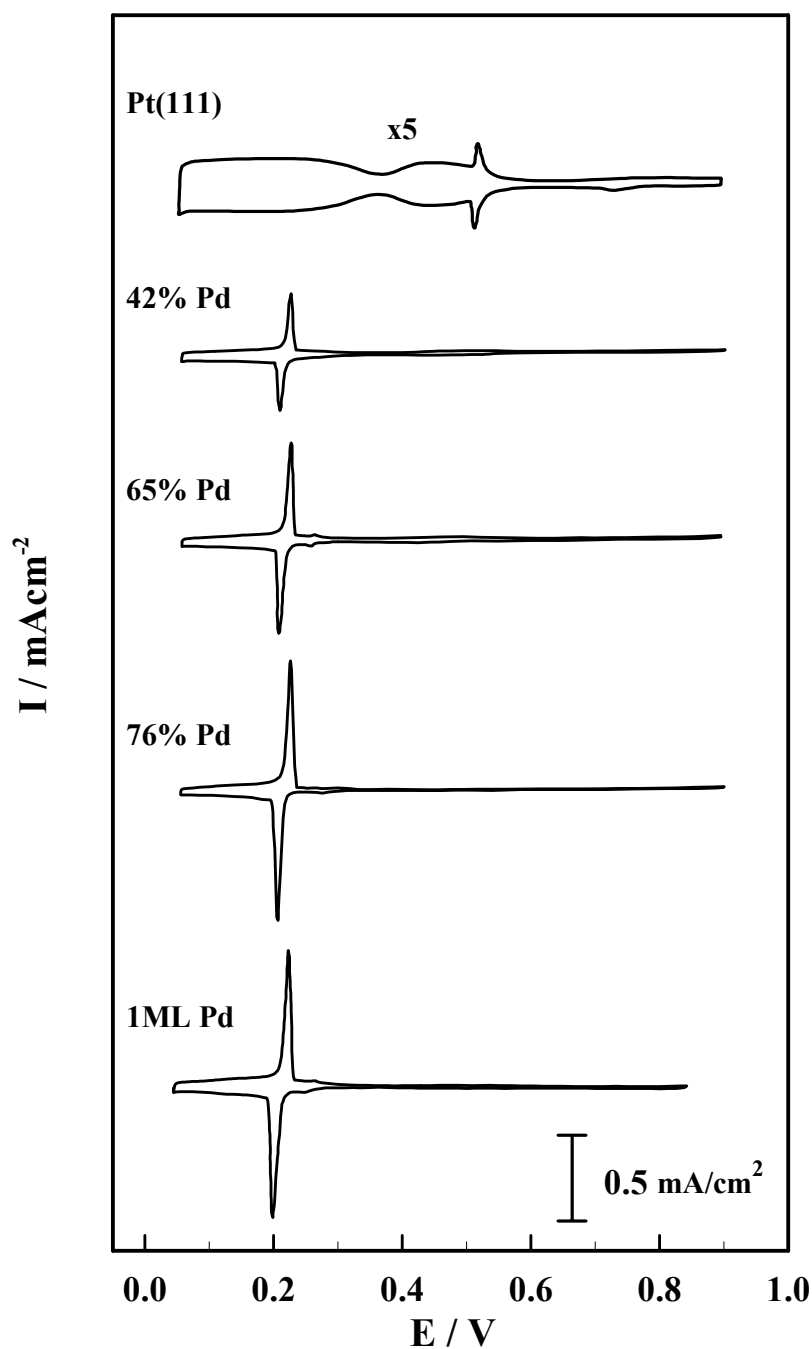*Figure 3.6: Series of cyclic voltammograms of Pt(111)-xPd electrodes in contact with 50 mM H₂SO₄; scan rate 50 mV/s at room temperature*

The cyclic voltammograms of the UHV-prepared Pt(111)-xPd surfaces are more or less identical with the voltammograms observed for the electrochemically deposited palladium films. As discussed in the previous section, the coupled processes of hydrogen

adsorption/desorption and (bi)sulfate desorption/adsorption (0.05 V < E < 0.375 V) give rise to a single very sharp peak centered at ca. 0.23 V. Comparing the voltammograms obtained for the surfaces with different palladium coverage, a correlation of the maximum current density at 0.23 V with the palladium coverage is apparent. Clearly, an increase in the surface coverage by Pd leads to a concomitant increase in the height of the main peak at 0.23 V. This is essentially the same observation as in the electrochemical deposition procedure, where an increase in the deposition time leads to an increase of the maximum current density at 0.23 V. Notice that, for the UHV-prepared surface indicated as a ~1 ML Pd film, the peak associated with the formation of the second Pd layer (at ca. 0.28 V) is not observed in the cyclic voltammogram, suggesting that indeed just 1 ML is evaporated on the Pt(111) surface.

Summarizing, it can be clearly stated that the voltammetric response of the UHV prepared samples is the same as for the electrochemically deposited palladium films.

3.3 Calibration curve for Pt(111)-xPd surfaces

Given the fact that the voltammograms of the UHV prepared films are identical with the voltammograms of the electrochemically deposited Pt(111)-xPd electrodes a calibration curve similar to the one of Alvarez et al. (see section 3.4) can be developed.

In the following the cyclic voltammograms shown in Figure 3.6 are analyzed. Integration of the current densities reveals that the hydrogen adsorption pseudocapacitance increases from 160 $\mu C/cm^2$ on unmodified Pt(111) to 320 $\mu C/cm^2$ on Pt(111) covered with 1 ML of Pd as reported for electrochemically deposited films [46]. The difference between the total charge in the H_{upd} potential region (Q_{Hupd}) and the charge deduced from sulfate adsorption (80 $\mu C/cm^2$) [46] equals 240 $\mu C/cm^2$, implying that the Pt(111)-1ML Pd surface is covered by 1 ML of H_{upd} (for any adsorbate, 1ML is defined as one molecule/adatom adsorbed per Pt surface atom, or 1.5×10^{15} molecules/cm^2, which is equivalent to 240 $\mu C/cm^2$ if the molecule is fully discharged). The evaluation of the charge densities Q_{Hupd} in the potential range (0.05 and 0.375 V) of underpotentially deposited hydrogen was performed by integrating the current densities both in the forward and back scan. Both values were corrected by the double layer charge evaluated from Pt(111) in pure sulfuric acid solution. Note, that subtracting always the *same* double layer for all voltammograms reduces the uncertainty in the charge integration. The mean value of both results was defined as Q_{Hupd}. The relationship between Θ_{Pd}, evaluated from the LEIS measurements, and Q_{Hupd}, inferred from the corresponding cyclic voltammograms, is shown in Figure 3.7. Clearly, the integrated

charge increases linearly from a value of ca. $165 \, \mu C/cm^2$ ($\Theta_{Pd} = 0$ ML) to a charge of ca. $320 \, \mu C/cm^2$ ($\Theta_{Pd} = 1$ ML).
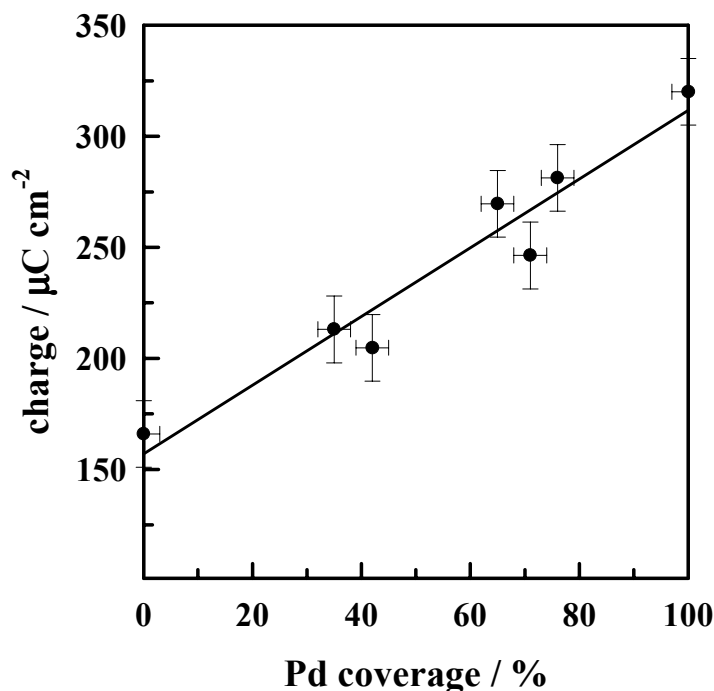
Figure 3.7: Calibration curve for θ_{Pd} of electrochemically deposited palladium films on Pt(111)

This calibration curve can now be used to evaluate *quantitatively* the surface coverage of palladium which is deposited *electrochemically* on Pt(111). The surface coverage of palladium is determined from Figure 3.7, simply by integrating the charge in the H_{upd} region ($0.05 \, V < E < 0.375 \, V$) on the Pt(111)-xPd electrodes and extrapolating the Θ_{Pd} value from the calibration curve. Following this procedure, the fast and easy in-situ preparation of palladium films on Pt(111) is combined with a straightforward characterization of the palladium surface coverage of the investigated surfaces.

3.4 Discussion

Unlike in UHV, the evaluation of the palladium coverage Θ_{Pd} of Pt(111)-xPd surfaces prepared in an electrochemical cell is not straightforward. The only attempt of an in-situ determination of Θ_{Pd} of electrochemically deposited palladium films on Pt(111) has been reported by Alvarez et al. which is in the following compared to the procedure applied in this

work. In contrast to the method for evaluating Θ_{Pd} presented here, the determination of Alvarez and coworkers is solely based on the integration of the current densities in the observed cyclic voltammograms upon palladium deposition in sulfuric acid. The authors assumed that the charge under the peak at 0.23 V is completely due to charge transfer to the palladium sites of the surface [48], whereas the remaining charge, integrated between 0.06 and 0.7 V and corrected by a horizontal baseline to subtract the double layer contribution, was assigned to the substrate sites which are not covered by palladium adatoms. Given these assumptions the authors plotted both integrated current densities against each other. The palladium coverage was then obtained by the ratio of both charge densities, the peak at 0.23 V and the remaining charge, respectively. There are some drawbacks in this procedure. First of all, the assignment of the current densities to the different processes is not unambiguous. Furthermore, this procedure requires very defined voltammograms and several uncertainties are introduced into the determination of Θ_{Pd} by the integration of the different current densities. Especially the correction of the electrochemical double layer is not straightforward and somehow depends on the applied procedure. However, for pure in-situ studies there is up to date no other procedure available in determining the palladium coverage.

As mentioned before, in this work a different approach for the determination of the palladium coverage is introduced. By employing UHV analytical tools Θ_{Pd} of UHV prepared films can be *unambiguously* determined. The observed voltammogram of the UHV prepared electrode in sulfuric acid solution (after the transfer to an electrochemical cell) can be compared to the well known voltammogram of electrochemically deposited palladium films. In fact identical voltammograms are obtained for the electrochemical- and UHV-prepared palladium films. Therefore a calibration curve for *electrochemically* prepared Pd films can be developed by comparing the ex-situ determined palladium coverage with the integrated current densities in the cyclic voltammogram of the UHV-prepared films. In contrast to Alvarez et al. here the complete charge of the anodic and cathodic scan in voltammogram is integrated and divided by two. As a baseline correction the *same* value for the double layer capacity is taken for all voltammograms. Therefore, this double layer correction is only for comparing the current densities with data in the literature, but introduces no additional uncertainty in the determination of Θ_{Pd}.

The clear advantage of this procedure is that no assumptions on underlying processes of the voltammetric features have to be made. The variable Θ_{Pd} is unambiguously determined by the LEIS spectra and can directly be compared to the integrated current densities of the observed voltammograms. In principle no double layer correction in the voltammogram is necessary.

3.5 Summary

The electrochemical behavior of thin palladium films on Pt(111), prepared in UHV as well as in an electrochemical cell, in sulfuric acid solution is compared. The electrochemical deposition in sulfuric acid solution containing small amounts of palladium is an easy to apply, slow process and therefore favorable for palladium deposition, especially in the submonolayer regime. The determination of the palladium surface coverage by electrochemical methods, however, is not straightforward. By contrast, in UHV θ_{Pd} can be easily obtained by applying LEIS. It is demonstrated that the respective Pt(111)-xPd surfaces, prepared in UHV and electrochemically, show the same voltammetric behavior in sulfuric acid solution and therefore have the same film morphology.

Therefore it was possible to establish a calibration curve for the Pd coverage of electrochemically deposited Pt(111)-xPd films (with $0 \leq x \leq 1$) by comparing the integrated charge density in the H_{upd} region of several UHV-prepared Pt(111)-xPd surfaces with the Pd surfaces coverage established by LEIS. This calibration curve is used in the following chapters to evaluate *quantitatively* the surface coverage of palladium which is deposited *electrochemically* on Pt(111). Following this procedure both the fast and easy in-situ preparation is combined with a straightforward characterization of the investigated surfaces.

Chapter 4

CO electrooxidation

During the last decades the adsorption behavior and the oxidation of carbon monoxide has been investigated extensively in UHV [67] as well as in an electrochemical environment. The wealth of investigations is triggered by the fundamental role of CO_{ad} in both, catalysis as well as a test molecule in fundamental studies concerning the adsorbate-substrate interactions of adsorbed molecules.

In electrocatalysis CO has an eminent importance for the development of low-temperature fuel cells, because CO_{ad} blocks the active sites of the anode catalyst, primarily platinum alloys, for the reaction of the fuel [3]. In a PEMFC[10] the most important problem of the anode catalysts is their high sensitivity towards CO contaminations in the hydrogen feed gas [4], whereas in the DMFC CO_{ad} is formed as a poisoning intermediate during the oxidation of methanol [68, 69]. Consequently, in electrochemistry by far the most studies concerning CO were performed on platinum and platinum binary alloys, where the addition of a more oxophilic metal is used to provide the surface at lower potentials with OH_{ad}, a species needed for the oxidation of CO [70].

The chapter is organized as follows. After shortly introducing the most important results of previous work on CO_{ad} on Pt(111) and Pd(111) single crystals, in the next sections the adsorption behavior and the electrooxidation of carbon monoxide on the well characterized Pt(111)-xPd ($0 \leq x \leq 1$ Pd monolayer (ML)) surfaces will be described. Since in alkaline solution only OH^- adsorption has to be considered for the electrooxidation of CO, at first the results from measurements in 0.1 M KOH are presented.

Subsequently, the measurements performed in perchloric acid solution are introduced. When analyzing the electrooxidation of CO_{ad} in acid solution also specific adsorption of anions from the supporting electrolyte has to be taken into account. Thus, the CO oxidation reaction is affected by further parameters, compared to a simpler mechanism in alkaline solution.

---

[10] **P**olymer **E**lectrolyte **M**embrane **F**uel **C**ell

4.1 Literature: CO adsorption and electrooxidation

In recent studies various methods were employed to elucidate the structure of CO adlayers on Pt(hkl). The first ex-situ determination of the electrochemically formed CO_{ad} structure on Pt(111) was reported by Wieckowski and co-workers [71, 72]. In these studies the LEED patterns of a Pt(111) electrode which was emersed from CO containing electrolyte and subsequently transferred to UHV have been interpreted in terms of compressed domains of a c(4×2) structure. The importance of the observations in this study lies in the fact that the saturation coverage of CO_{ad} at an emersed electrode is higher than that observed in the gas-phase at room temperature. That this conclusion is indeed true in-situ, i.e. in an electrochemical environment, was proven by in-situ STM. In contrast to the reported c(4×2) structure, these investigations, however, established (in a CO saturated solution) a hexagonal close packed (2×2)-3CO adlayer structure at low potentials, whereas at higher potentials a ($\sqrt{19} \times \sqrt{19}$)R23.4°-13CO unit cell is formed [73, 74]. Investigations by in-situ X-Ray diffraction revealed an average domain size of the (2×2)-3CO structure of 80 - 120Å whereas the CO structure formed at more positive potentials shows no long-range order [75]. Infrared spectra have provided additional insight in the adsorption sites of the CO molecules in the two adlayer structures. Whereas the cathodic adlayer structure consists of CO molecules adsorbed on three-fold hollow and on-top sites, CO bands of on-top and bridge bonded CO are found at higher potentials [73, 74]. Therefore in IRAS the transition between the two adlayer structures can be easily detected by the appearance of the bridge bonded CO species. Recently it was demonstrated by utilizing SHG[11] that the transition in the CO adlayer is associated with a redistribution of the electronic charge at the metal surface. This is attributed due to a variation in the charge transfer between the CO adsorbed on the different coordination sites and the metal [76].

The formation and stability of the (2×2)-3CO structure depends on several factors, including the CO concentration in the solution [77]. In contact with CO-free solution only CO adsorbed at on-top and on bridge sides is detected [76]. In CO saturated solution the transition from the (2×2)-3CO to the ($\sqrt{19} \times \sqrt{19}$)R23.4° structure is linked to the oxidative removal of CO_{ad} and is therefore sensitive on the defect/step density on Pt(111), where OH_{ad} is formed at first [78, 79]. Furthermore, it has been demonstrated recently, that on Pt(111) specific anion adsorption is stabilizing the (2×2)-3CO structure. Adsorbed Br shifts the transition between the two structures to more positive potentials and is concomitantly increasing the average domain size to about 350Å [80].
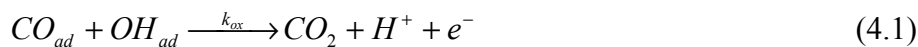
---

[11] **S**econd **H**armonic **G**eneration

Due to the difficult handling of Pd single crystals in electrochemistry for Pd(111) only few studies on the adsorption behavior of CO exist. It is reported by Weaver and co-workers that at CO saturation coverages on Pd(111), two different absorption bands can be observed by IRAS, which were assigned to bridge bonded CO and CO adsorbed on three-fold hollow sites, respectively [81]. However, no ordered CO adlayer structure on Pd(111) in an electrochemical environment is reported so far. Recent CO adsorption studies on a pseudomorphic Pd monolayer on Pt(111) [48, 66] revealed only one CO adsorption band at saturation coverage, assigned to bridge-bonded CO. The fact that two absorption bands were observed on the Pd(111), could be assigned to CO adsorbed at bridge-sites and steps/defect sites [66], respectively. The steps/defects are massively introduced by the electropolishing procedure of the Pd(hkl) electrodes.
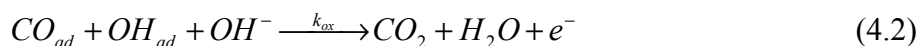
The CO oxidation reaction at the solid-liquid interface is influenced by several factors, including the coadsorption of solution species, potential-driven charge transfer, and the presence of a strong electric field at the solid-liquid interface. Although different models exist in the literature for the CO oxidation reaction, it is unambiguous that the two adlayer structures have a different reactivity towards oxidation. Rather than discussing every aspect of CO oxidation here in detail, the interested reader is referred to the original references [76, 77, 82-85]. Here only some widely accepted aspects of CO oxidation are introduced on which the discussion in the subsequent sections is based.

Systematic studies revealed that CO oxidation is a structure sensitive process on Pt(hkl) electrodes, having a different onset potential as well as different reaction rates at the respective low index (hkl) surfaces [79, 85]. A clear correlation is found between the onset of CO oxidation and the electrode potential where OH^- adsorption begins. It has been concluded, that both species have to be adsorbed on the surface in order to react with each other. Consequently, the CO oxidation reaction is of first order concerning the OH_{ad} as well as the CO_{ad} concentration. In alkaline solution the oxidation is reported to proceed already at very low potentials, even in the H_{upd} potential region [85]. Thus, also OH_{ad} formation takes place at very low potentials in alkaline solution (high OH^- concentration). On the other hand, in acid solution specifically adsorbed anions influence the reactivity of the CO adlayer. At low potentials the OH^- adsorption is blocked by more strongly adsorbed anions. Moreover, a correlation is found between the adsorption strength of anion adsorption from the supporting electrolyte and the onset potential of the CO oxidation reaction. The onset potential is clearly increasing with increasing adsorption strength of the anions.

Consequently, on platinum the oxidation of CO_{ad} is assumed to proceed between CO and adsorbed OH_{ad} through a Langmuir-Hinshelwood mechanism, i.e.

$$CO_{ad} + OH_{ad} \xrightarrow{\quad k_{ox} \quad} CO_2 + H^+ + e^- \tag{4.1}$$

in acid solution and

$$CO_{ad} + OH_{ad} + OH^- \xrightarrow{\quad k_{ox} \quad} CO_2 + H_2O + e^- \tag{4.2}$$

in alkaline solution, respectively [86].

4.2 Investigations in alkaline solution

4.2.1 Cyclic voltammetry

Since the CO oxidation proceeds between CO_{ad} and OH_{ad} through a Langmuir-Hinshelwood mechanism, special attention has to be paid to the formation of OH_{ad}. Therefore it is instructive at first to monitor the onset of OH^- adsorption on the bare surfaces by cyclic voltammetry.

In Figure 4.1 the cyclic voltammogram of a Pt(111)-1ML Pd electrode at 298 K in 0.1 M KOH solution (solid curve) is compared with the CV of bare Pt(111), obtained under the same experimental conditions (dashed curve). It can be seen that the voltammogram of bare Pt(111) in KOH, as in sulfuric acid solution, exhibits three separate potential regions: the hydrogen underpotential deposition region (H_{upd}, $0 < E < 0.4$ V) is directly followed by the double layer potential region (ca. 0.4 V $< E < 0.6$ V) and subsequently by the so-called 'butterfly region' ($0.6 < E < 0.9$ V), which in alkaline solution is commonly assumed to represent the discharge of OH^- to form a hydroxyl adlayer [87], hereafter denoted as OH_{ad}. At more positive potentials the "irreversible" oxide formation is observed at $E > 0.8$ V. Notice that, recently it was demonstrated that on Pt(111) in alkaline electrolyte some amount of OH_{ad} can even be present in the H_{upd} region [88]. Based on thermodynamic considerations, it was estimated that the Pt-OH_{ad} bond energy in the H_{upd} potential region is in the range of ca. 206-216 kJ/mol [88]. This is considerably higher than the estimated Pt-OH bond energy in the "butterfly region", which is ca 136 kJ/mol [88].
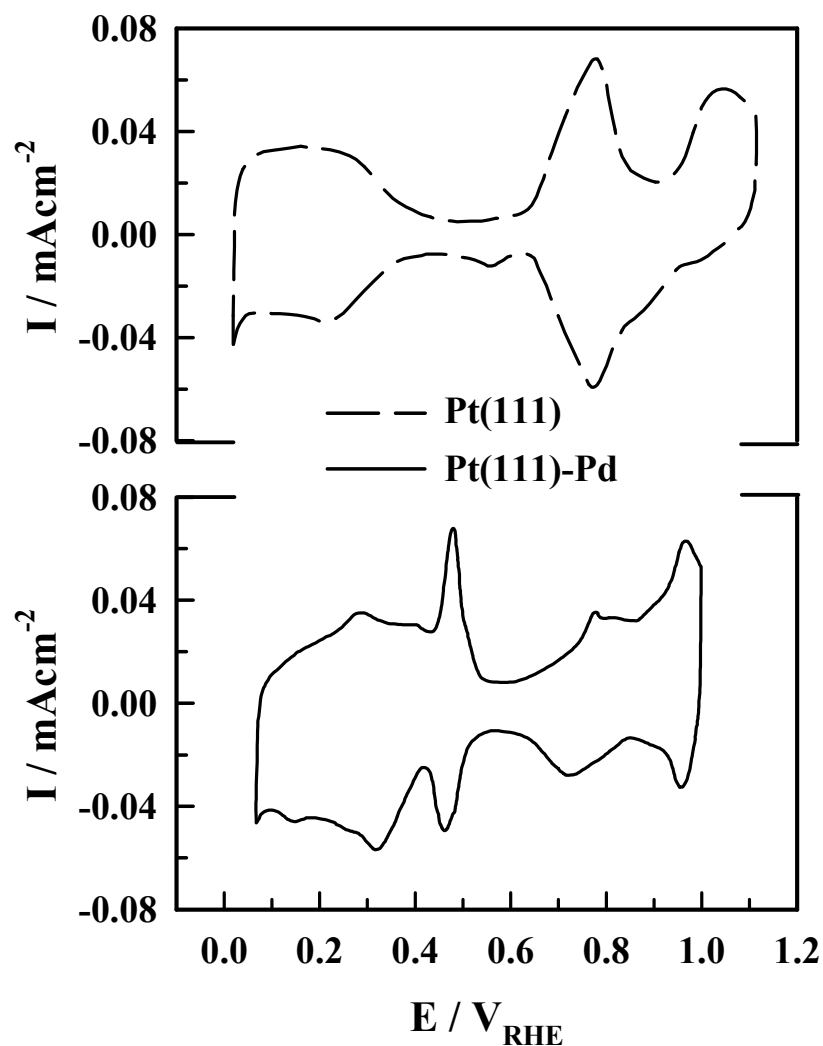
Figure 4.1: Cyclic voltammetry of Pt(111)-1ML Pd (full line) and Pt(111) (dashed line) recorded in 0.1 M KOH (sweep rate 50 mV/s) at room temperature

When a monolayer of Pd is deposited on Pt(111), the voltammogram changes dramatically. In particular, the feature of the formation of H_{upd} ($0.05 < E < 0.34$ V) is not unambiguously separated in the CV from the OH^- adsorption process. A broad peak, assigned to H_{upd} ($0.05 < E < 0.34$ V), is *immediately* followed first by a relatively sharp reversible peak at 0.475 V, and then by two broad peaks which are not completely reversible. The assignment of the H_{upd} charge is based on the fact that integrating the charge in the voltammogram between $0.05 < E < 0.34$ V leads to a value corresponding to 1 ML H_{upd}. Based on the assumption that only 1 ML of hydrogen can be adsorbed on the surface the peak at 0.475 V can be assigned to reversible adsorption of OH_{ad}. The "true oxide formation" begins at higher potentials, most likely at about 0.95 V.

Using these assignments the charges associated with the H_{upd} and OH$^-$ adsorption process are depicted in Figure 4.2. Note, that the current densities were integrated after subtraction of the double layer regime in the voltammogram of bare Pt(111) for *both*, the Pt(111) and the Pt(111)-1ML Pd surface. This was necessary since, as already mentioned, for the CV of the Pt(111)-1ML Pd surface no double layer region exists, which unambiguously divides the H_{upd} and the OH$^-$ adsorption process.

That indeed a full monolayer of H_{upd} is completed on Pt(111)-1ML Pd has been suggested earlier for sulfuric acid solution [46]. Based on the cyclic voltammograms presented here it seems to be reasonable also for alkaline solution. In this section the discussion will be focused more on the OH$^-$ adsorption regime rather than the H_{upd} potential region, which is introduced more detailed in section 4.3.
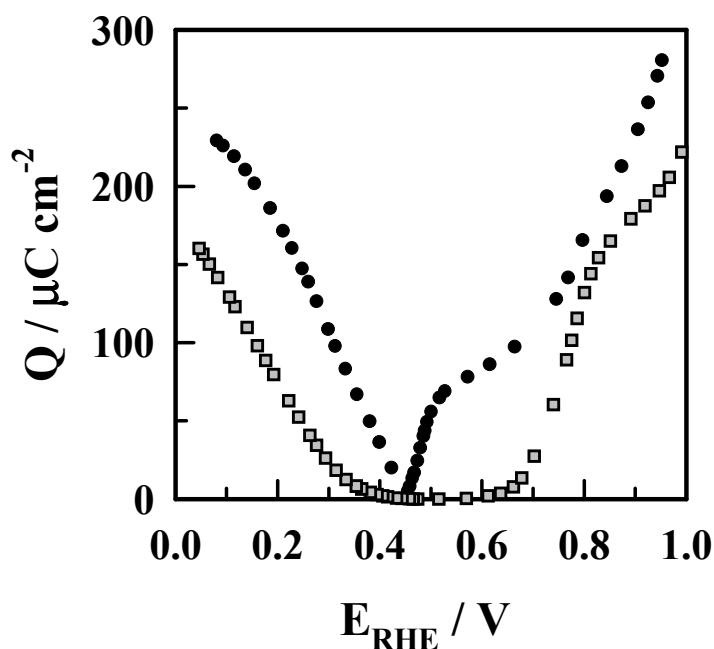
Figure 4.2:Integrated charges of H_{upd} and OH$^-$ adsorption process from Figure 4.1; Pt(111)-1ML Pd (circles); Pt(111) squares

It can be seen in Figure 4.2 that using the above assignments the OH$^-$ adsorption is sharply increasing on the Pt(111)-1ML Pd surface. By contrast no OH$^-$ adsorption takes place on bare Pt(111) until 0.65 V. The sharp increase of the OH$^-$ adsorption on Pt(111)-Pd indicates that the strict separation of the potential regions of the H_{upd} process and the OH$^-$ adsorption may be oversimplified. Therefore it is proposed that the potential regions of both processes overlap on the Pt(111)-1ML Pd surface. Consequently, the OH$^-$ adsorption on the Pt(111)-1ML Pd surface starts in the H_{upd} potential region and H_{upd} is completely desorbed

only after the peak at 0.475 V. The onset of OH⁻ adsorption in the H_{upd} potential region was also suggested, as pointed out before, for the bare Pt(111) surface. On the Pt surface, however, the rate of OH⁻ adsorption is rather small at low potentials, taking place only at defect sites and becoming apparent only when probing the surface with CO_{ad} [85, 88]. Regardless of the true potential for the incipient OH⁻ adsorption on the Pd surface, Figure 4.2 clearly shows that in comparison to the Pt(111)-OH_{ad} interaction, the reversible adsorption of OH⁻ on the Pd covered surface is shifted towards more negative potentials. This confirms previous findings that the Pd-OH_{ad} bond is stronger than the Pt-OH_{ad} bond, e.g. Pd is a more oxophilic metal than Pt [40]. As we demonstrate below, the differences in the bond energy between Pt-OH_{ad} and Pd-OH_{ad} will have a significant effect on the electrocatalysis of CO on the Pt(111)-xPd surfaces.

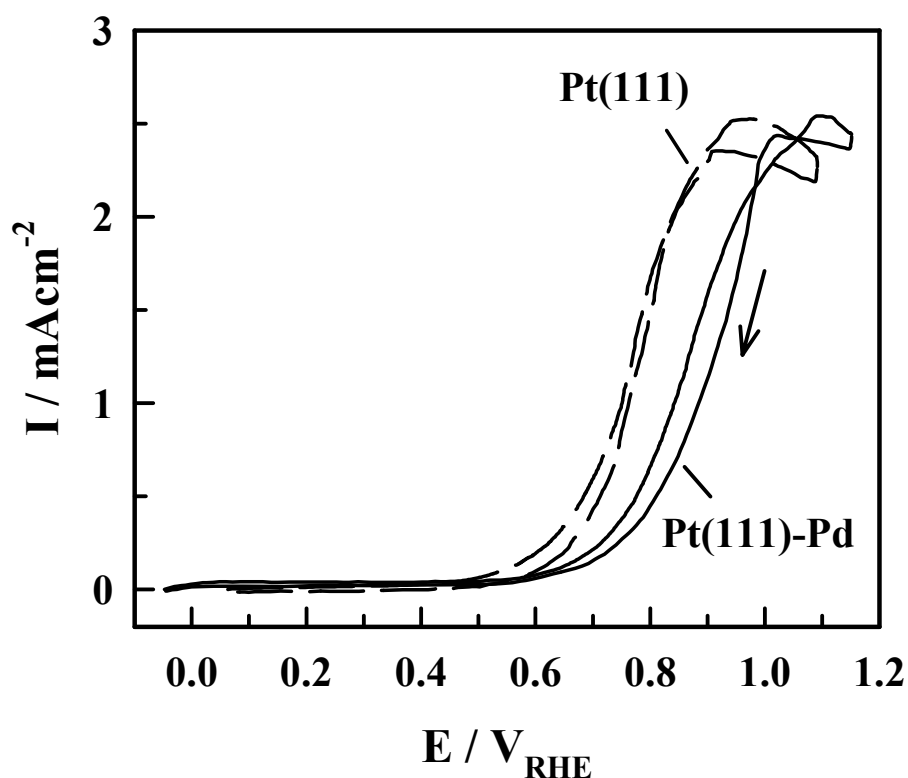## 4.2.2 RDE measurements

Figure 4.3: RDE CO_b electrooxidation on Pt(111)-1ML Pd and Pt(111) (dashed line) in 0.1 M KOH at room temperature; the adsorption and start potential is –0.05V; 50 mV/s, rotation rate 2500 rpm

The reactivity of a surface towards CO oxidation can be easily detected by CO stripping voltammetry or by oxidation of CO dissolved in the bulk of the electrolyte, hereafter denoted as CO_b. For the latter method it is advantageous to apply the RDE technique in order to provide the surface with a continuous flux of CO.

In Figure 4.3 the oxidation of CO_b on Pt(111) and Pt(111)-1ML Pd electrodes is compared at ambient temperature. It is obvious that the overall reaction rate of CO_b oxidation is much faster on Pt(111) than on the palladium modified electrode. Note that the difference in the onset potential compared to the potentiostatic FTIR measurements, which will be introduced in the next section, can be explained by the relatively high scanning rate of 50 mV/s. The nucleation of OH_{ad} proceeds too slow in order to see any significant (macroscopic) current before the potential for massive oxidation is reached.

The low reaction rate of CO_b on the Pd covered electrode is a surprising result and at first sight contradicts the just proposed shift of the OH^- adsorption regime to more negative potentials compared to the bare Pt(111) surface. Up to this point, two possible explanations can be given for the low reactivity of the Pt(111)-1ML Pd surface towards CO_b oxidation: first a slow surface diffusion of the reactants and secondly a higher binding energy of the reactants which could increase the activation energy for the reaction.

The influence of the binding energy (or adsorption enthalpy) of the reactants on the reaction rate leads often to so-called "volcano plots", where a maximum in the reaction rate is observed at a medium binding energies of the reactants. Consequently, this would mean for this special case here, that the binding energy of OH_{ad} on Pt(111)-Pd has already exceeded the ideal value for the reaction to proceed. In the next section further investigations on the CO oxidation reaction are performed by FTIR spectroscopy in order to clarify this point.

4.2.3 FTIR measurements

The characteristic C-O stretching bands for bare Pt(111) in CO saturated 0.1 M KOH solution as a function of the electrode potential are shown in Figure 4.4. The background spectra are collected at 0.9 V, where CO_{ad} is completely oxidized. As previously described by different authors [64, 89], at potentials below 0.3 V characteristic C-O stretching bands near 2070 cm^{-1} and 1740 cm^{-1} predominate in the spectra. These bands can be assigned to CO bound on a-top and three-fold hollow sites, respectively. Going to more anodic potentials, the band of the hollow species is replaced by a new C-O stretching band at about 1800 cm^{-1}, which can be related to the presence of bridge-bonded CO.
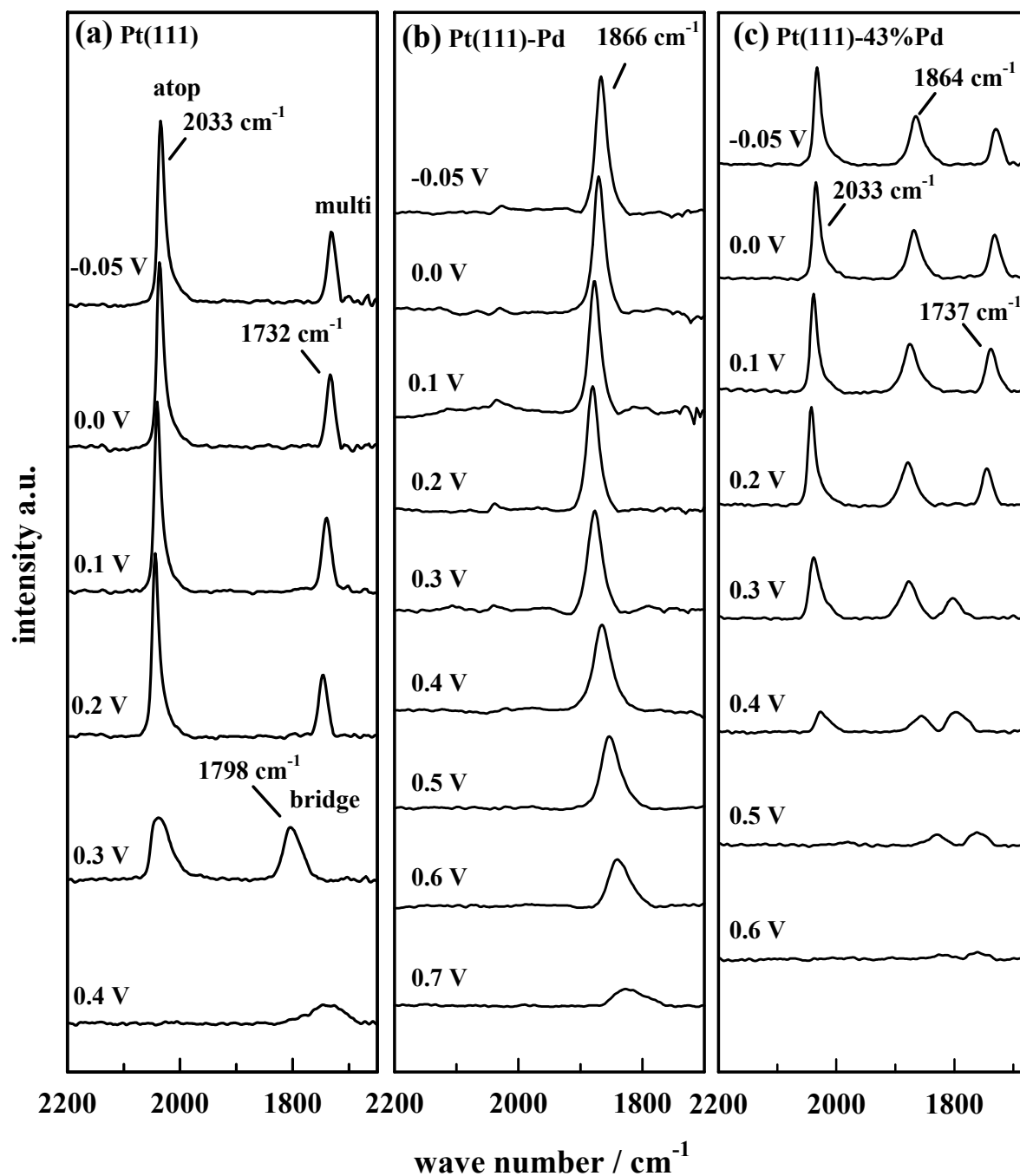
Figure 4.4: Series of infrared spectra of CO_{ad} on (a) Pt(111), (b) Pt(111)-1ML Pd and (c) Pt(111)-43% Pd obtained by stepping the applied potential in a positive direction in CO sat. 0.1 M KOH solution, each spectrum was accumulated from 50 interferometer scans at the potential indicated, the background potential was taken at 0.9 V vs. RHE;

As discussed in the literature overview (section 4.1), the comparison of the potential dependent intensity changes for the three-fold and bridge CO bands with surface X-ray scattering (SXS) data suggests that the combination of the on-top band and the three-fold

hollow band is related to the p(2 x 2)-3CO structure whereas the loss of this ordered structure is reflected by the transition of the three-fold hollow band into the bridge-bonded CO band [75]. This change in the adsorption geometry is accompanied by the onset of CO oxidation (CO_3^{2-} production in Figure 4.5c), which begins at a potential as low as 0.2 V. As discussed in reference [85, 88], CO_{ad} is oxidatively removed in the H_{upd} potential region by OH_{ad} which is adsorbed at the defect/step sites of the Pt(111) surface. More details about the structure stability of a CO_{ad} layer and the kinetics of CO oxidation the interested reader may find in reference [85, 88].

For Pt(111) covered with a full monolayer of Pd FTIR spectra in CO saturated 0.1 M KOH (Figure 4.4b) reveal only one single absorption band near 1870 cm^{-1}. Previous FTIR investigations of CO adsorption on Pd in acid solutions also showed only one absorption band at about 1900 cm^{-1}, which was assigned to bridge bonded CO_{ad} [64, 66, 81]. In line with these studies, the band for CO on 1 ML of Pd in alkaline solution is also assigned as CO_{ad} at bridge sites. Note that the observation of the C-O stretching bands being at lower wave numbers than in acid solutions (ca 30 cm^{-1}) may be related to the lower electric field effective at the surface in alkaline solution, as previously discussed for the Pt(111)-CO_{ad} system in alkaline solution [90]. A closer inspection of Figure 4.4b reveals that besides the major Pd-CO band also a tiny band at about 2020 cm^{-1} is present in the spectra. From Figure 4.4a it is clear that this band corresponds to adsorption of CO on very *small* Pd-free platinum islands. Therefore, it is concluded that if only a single band near 1870 cm^{-1} is observed in the spectra, the Pt(111) electrode is covered with a pseudomorphic palladium monolayer.

Figure 4.5b shows that for sweeping the potential from –0.05 V to more positive values the integrated intensities for CO_{ad} on Pt(111)-1ML Pd remain constant, suggesting that the initial slow oxidation of CO (production of CO_3^{2-} in Figure 4.5c) is accompanied by a concomitant re-adsorption of CO from the CO saturated thin layer solution. Note that with increasing the potential the absorption band is becoming broader, indicated by the change of the full width of half maximum (FWHM) from 20 cm^{-1} at 0 V to 31.5 cm^{-1} at 0.4 V. Above 0.4 V, however, the decrease in the integrated intensity of CO (Figure 4.5b) parallels a fast oxidation of CO at these high anodic potentials. Note also, that due to an interplay of the electrochemical Stark effect [16] and dipole-dipole coupling the absorption frequency of CO is dependent on the electrode potential [76]. This effect will be discussed in more detail on the basis of the FTIR measurements performed in perchloric acid solution (see section 4.3.2).

For the characterization of the adsorption behavior of CO on Pt(111)-xML Pd electrodes further FTIR spectroscopic measurements were performed. Even though FTIR spectra were recorded on different samples, only one surface with $\Theta_{Pd} = 0.43$ ML, shown in Figure 4.4c, will here be introduced as an example to demonstrate all important features of

CO surface electrochemistry on a Pd modified Pt(111) surface in the Θ_{Pd} submonolayer range in alkaline solution. Figure 4.4c shows a set of absorption spectra for adsorbed CO on Pt(111)-0.43ML Pd in CO saturated 0.1 M KOH. At low potentials, three different C-O stretching bands near 1730 cm^{-1}, 1870 cm^{-1} and 2035 cm^{-1} can be distinguished in the spectra. By comparison with Figure 4.4a and b, these bands can clearly be assigned to multi-coordinated CO adsorbed on Pt, CO bridge bonded on Pd and on-top CO adsorbed on Pt, respectively. Figure 4.5c shows that the oxidation of CO, as on the previous two surfaces, begins at around 0.2 V, concurrent with the loss of Pt-CO$_{ad}$ at three fold hollow sites and the emergence of Pt-CO$_{ad}$ on bridge sites. At more positive potentials, further CO$_3^{2-}$ production (Figure 4.5c) is accompanied by the loss of Pt-CO$_{ad}$ and Pd-CO$_{ad}$ at the bridge sites and Pt-CO$_{ad}$ at on-top sites. A detailed analysis of the band positions and the integrated intensities as a function of the applied potentials will be postponed until the IR spectra obtained in perchloric acid solution have been presented in section 4.3.2.
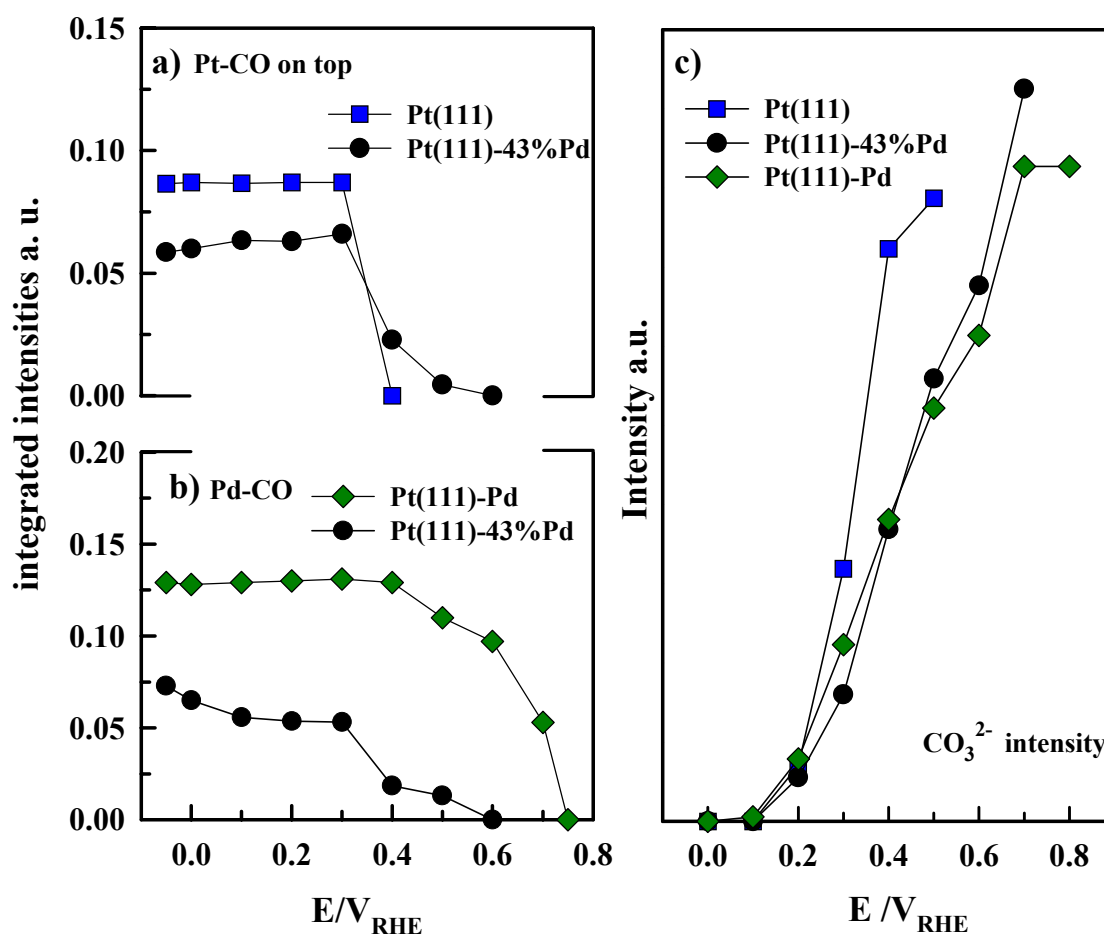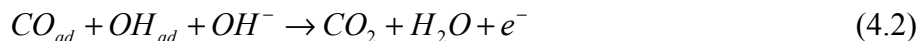

Figure 4.5: Integrated band intensities of on-top Pt-CO bands (a) and Pd-CO bands (b) as a function of the electrode potential c) CO$_3^{2-}$ production for all three surfaces as a function of the electrode potential, data extracted by using –0.05 V as background potential

An important point that can be clarified from the in-situ FTIR measurements is, that although the onset of CO_3^{2-} production associated with the CO oxidation on Pt(111) and Pt(111)-1ML Pd surfaces is very similar (close to 0.2 V), the rate of CO_3^{2-} produced on Pt is higher than on Pt(111)-1ML Pd. A comparison (Figure 4.5c) clearly shows that despite the same onset potential of CO oxidation the absorption bands of CO on Pt(111)-1ML Pd can still be observed at potentials as high as 0.7 V. This suggests that the rate of CO oxidation, in accordance with the RDE measurements, is much faster on Pt(111) than on a Pt(111)-1ML Pd electrode. The kinetics of CO oxidation on Pt(111)-0.43ML Pd, established from the onset/slope of CO_3^{2-} production in Figure 4.5c, lies between the one observed with pure Pt(111) and Pt(111) modified by 1ML of Pd. In fact, as will be demonstrated more clearly in perchloric acid solution, a monotonic increase in the palladium surface coverage leads to a gradual decrease in the catalytic activity of the Pt(111)-xPd surfaces. This implies that the catalysis of CO on these surfaces takes place *independently* on Pt and Pd sites, i.e. in contrast to Pt-Pd(hkl) single crystal alloy surfaces [91] the Pt(111)-xPd systems do not behave as a pseudo metal.

4.2.4 Discussion: CO oxidation in alkaline solution

The most important finding of the previous section is the low kinetic rate of the CO oxidation on the Pt(111)-Pd surface in alkaline solution. This might be a surprising result considering that the adsorption of OH_{ad} is enhanced on Pt(111)-1ML Pd (see Figure 4.1). In order to resolve this paradoxon one should recall the overall reaction mechanism, which can be represented by three steps:

$$OH^- \rightarrow OH_{ad} + e^- \tag{4.3}$$

$$CO_b \rightarrow CO_{ad} \tag{4.4}$$

$$CO_{ad} + OH_{ad} + OH^- \rightarrow CO_2 + H_2O + e^- \tag{4.2}$$

Based on this reaction scheme, the CO oxidation rates are determined by both the surface coverages of CO_{ad} and OH_{ad} and the probability of interaction of these two adsorbed species. For the latter aspect surface diffusion of the reactants and the energy barrier for the reaction are the determining factors. Since in alkaline solution no anion adsorption from the electrolyte, except OH^- adsorption, takes place, in the discussion no blocking of active sites due to anion adsorption has to be taken into account. Recent studies have convincingly shown that surface diffusion of CO_{ad} on Pt is rather high and that the adsorption of OH_{ad} at defect

sites is the determining factor [77, 80, 85, 92-95]. For bare Pt(111) it has been shown by RDE measurements, that in alkaline solution OH^- adsorption takes place even in the H_{upd} potential region and is hidden in the CV by the broad double layer. The here presented FTIR measurements confirm this finding. On the Pt(111)-1ML Pd surface the same onset of CO oxidation is found as on bare Pt(111). However the reaction *rate* is decreased on the palladium film. One suggestion to interpret this finding could be that the coverage of OH_{ad} is decreased on the palladium film (compared to the bare Pt(111) surface). However, based on the cyclic voltammograms of both surfaces a higher concentration of OH_{ad} is suggested on the palladium film compared to the bare Pt(111) surface (see Figure 4.2). Furthermore, the number of defect sites is increasing upon Pd deposition and thus the formation of OH_{ad} on the palladium film should be increased.

Therefore a different explanation of the reduced activity of the Pt(111)-Pd surface towards CO oxidation has to be found. It is important to stress once more at this point, that the kinetics of reaction (4.2) does not only depend on the surface coverage of OH_{ad}, but is also strongly affected by the delicate balance between the *coverage and the nature* of the electroactive species. That is, as in the electrochemical kinetics of inorganic/organic compounds, the CO oxidation is governed by the same electrocatalytic law: while the reaction rate passes through a maximum for metals adsorbing CO and OH^- moderately strong, the kinetic rates are very slow on those metals which adsorb CO and OH^- either strongly or weakly. This behavior is well known and is often expressed in "volcano plots", where the electrocatalytic activity of a material is plotted against the adsorption enthalpies of the reactants (for example ref. [96] for the hydrogen evolution reaction). Previous studies have shown that while the adsorption energy of CO is not significantly different on Pt(111)-1ML Pd from the one found for Pt(111), the adsorption of anions on Pd is much stronger than on Pt. Consequently, the Pd-OH_{ad} bond is much stronger than the Pt-OH_{ad} bond. Therefore it is reasonable that the catalytic activity of OH_{ad} towards the oxidation of CO_{ad} is significantly reduced on Pt(111)-1ML Pd in comparison with OH_{ad} which is adsorbed on Pt(111). This is especially important at more anodic potentials in the RDE measurements where, in contrast to the FTIR measurements, the flux of CO_b to the surface is not hindered and high reaction rates are reached. Therefore when comparing the reaction on both surfaces the concentration of OH_{ad} on the Pt(111)-Pd, is at least as high as on the bare Pt(111) surface and the kinetic rates are decreased on the Pd surface due to an increased activation barrier for reaction (4.2). However for a detailed description of the reaction of the CO oxidation reaction on the Pt(111)-1ML Pd surface further studies are required.

4.2.5 Conclusion: CO oxidation in alkaline solution

The CO adsorption behavior and the kinetics of CO oxidation on bare Pt(111) and Pt(111)-xPd electrodes in 0.1 M KOH has been studied by means of cyclic voltammetry, RDE measurements and Fourier transform infrared (FTIR) spectroscopy. The spectra for CO adsorbed on a pseudomorphic monolayer of Pd and a Pd submonolayer, with a Pd coverage of about 40 % Pd, are compared to those of the unmodified Pt(111) surface, all surfaces having identical 2D lattice structures. The infrared absorption bands of CO bound on bare Pt(111) and Pt(111)-1ML Pd can clearly be distinguished. At surfaces with palladium films of submonolayer coverage the CO adsorption and electrooxidation process on the palladium islands as well as on the free Pt(111) sites can be investigated at the same time.

The kinetics of CO oxidation on these surfaces was determined by monitoring the CO_3^{2-} production during oxidative removal of CO_{ad} from Pd-free and Pd-modified Pt(111). The oxidation of CO_{ad} on Pt(111) and on Pt(111)-xPd surfaces starts at the same potential, ca. at 0.2 V. The oxidation rate, however, is considerably lower on Pd-modified Pt(111) than on bare Pt(111). It is proposed that the kinetics of CO oxidation is determined by the nature of the adsorbed hydroxyl anions (OH_{ad}), which are much stronger adsorbed (less active) on the highly oxophilic Pd layers.

4.3 Investigations in perchloric acid solution

In contrast to alkaline solution in acid solution the reactivity of electrocatalysts is often controlled by specific anion adsorption from the electrolytes. These spectator species, not involved in the reaction, are blocking the adsorption sites for the reactants. The different acid solutions are commonly characterized as electrolytes with strongly adsorbing anions (Cl^-, hydrochloric acid), weakly adsorbing anions (SO_4^{2-}, sulfuric acid) and non adsorbing anions (ClO_4^-, perchloric acid). In this section, investigations were performed in perchloric acid solution, i.e. an electrolyte with non-absorbing anions. The results of the adsorption behavior and the electrooxidation of CO_{ad} are compared to the results obtained in alkaline solution. In perchloric acid solution the peak of reversible OH^- adsorption in the cyclic voltammogram of bare Pt(111) is located at the same potential as in alkaline solution. However, the CO adlayer is known to be considerably more stable towards oxidation at higher potentials. As mentioned, for platinum this behavior has been ascribed to a site blocking effect.

The investigations in perchloric acid solution are performed by utilizing cyclic voltammetry and FTIR spectroscopy. One aim of the following experiments is to investigate

if a corresponding mechanism (as on Pt(111)) is also active for the reactivity of Pt(111)-Pd surfaces towards the CO oxidation reaction in acid solution. Therefore, the focus of the investigations is on the role of possible spectator species blocking the adsorption sites.

4.3.1 Cyclic voltammetry

4.3.1.1 Perchloric acid solution
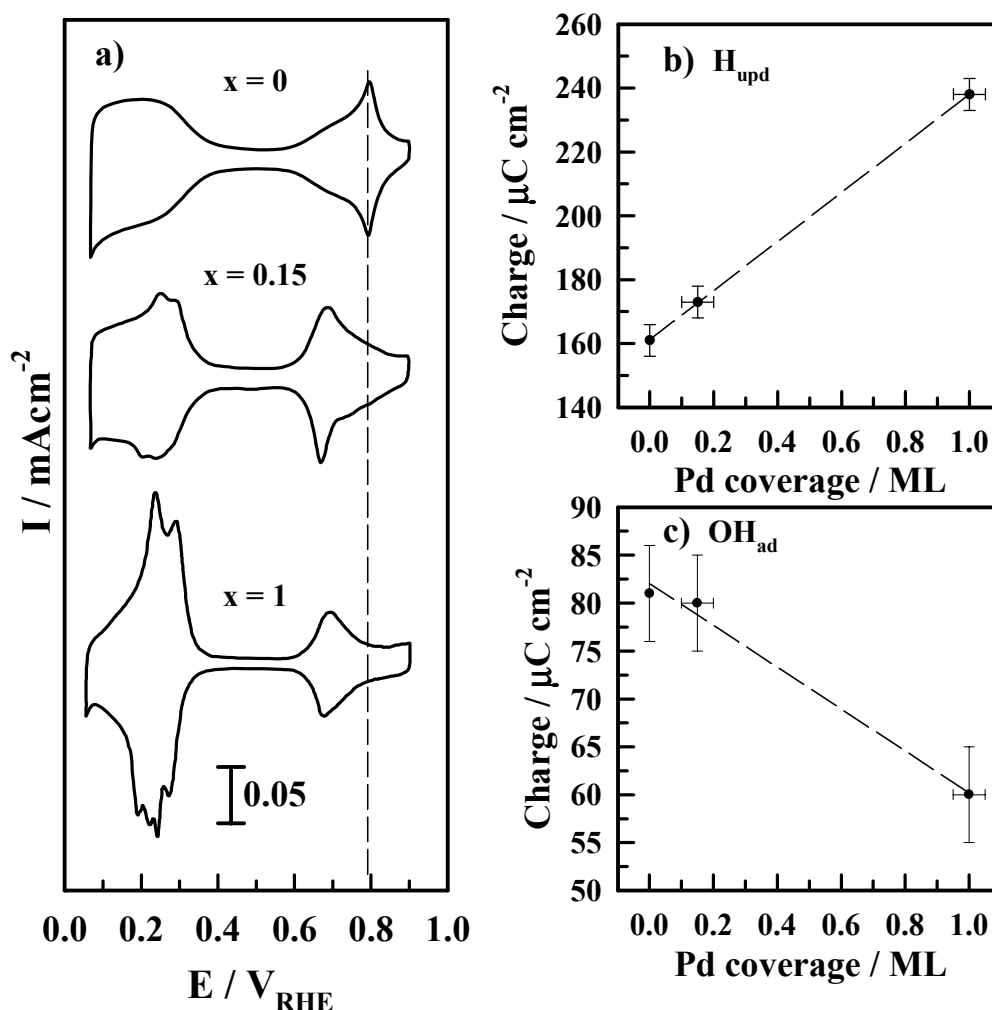
Figure 4.6: a) Cyclic voltammograms of Pt(111)-xPd electrodes in 0.1 M HClO₄; scan rate 50 mV/s at room temperature; the palladium coverage x is increasing from x = 0 to x = 0.15 and x = 1 (counted from top); b) CV H_{upd} peak area vs. palladium coverage; c) CV peak area of OH⁻ adsorption peak vs. palladium coverage

In Figure 4.6a the cyclic voltammogram of bare Pt(111) in perchloric acid solution is compared to the voltammograms of two Pt(111)-xPd electrodes (with x = 0.15 and x = 1,

respectively) in order to establish how the systematic increase of the Pd surface coverage is modifying the voltammetric profiles of Pt(111). As the CV's recorded in sulfuric acid and potassium hydroxide, the CV of bare Pt(111) in perchloric solution exhibits three characteristic potential regions: the hydrogen underpotential deposition region (H_{upd}, $0 < E < 0.375$ V) is followed first by the so-called "double-layer" potential region ($0.375 < E < 0.6$ V) and then by the so-called "butterfly" feature ($0.6 < E < 0.85$ V). In perchloric acid the interpretation of the processes which control the shape of the butterfly feature are still controversial, e.g., it has been suggested that at least a part of the feature (the sharp spike) is associated with either co-adsorbed chloride (being present as an impurity in $HClO_4$ at a concentration of at least 10^{-7} M in even the most meticulously prepared electrolyte [97]) or to perchlorate anions [98] co-adsorbed with oxygenated species (hereafter denoted as hydroxyl, OH_{ad}). These conclusions are supported by the fact that in the absence of specific anion adsorption (for example in KOH electrolyte) the butterfly feature contains substantially more charge but no spike [87, 88]. The difference in the pseudocapacitance between $HClO_4$ and KOH solution was interpreted in terms of competitive adsorption of specifically adsorbing anions (Cl_{ad}, ClO_4^-) and OH_{ad} in perchloric acid solution. Note also, that the peak potential for OH^- adsorption in perchloric acid solution is the same as in alkaline solution.

Figure 4.6 shows that the deposition of Pd on Pt(111) produces significant changes in the cyclic voltammogram. A close inspection of Figure 4.6 reveals that there are three characteristics in the voltammetric profiles that demonstrate the effect of Pd. The first characteristic is a linearly increase of the charge in the H_{upd} region with an increase of the Pd surface coverage, presumably due to a stronger Pt(111)-Pd-H_{upd} interaction compared to the Pt(111)-H_{upd} interaction. As shown in Figure 4.6b, the H_{upd} charge increases linearly from about (161 ± 5) $\mu C/cm^2$ for bare Pt(111) to a value of (240 ± 5) $\mu C/cm^2$ for a full monolayer of Pd on Pt(111). These charges correspond to hydrogen coverages of (0.67 ± 0.02) ML and (1.00 ± 0.02) ML, respectively. This observation is not new, and has been reported previously for H_{upd} in sulfuric acid [46] and alkaline [99] solutions.

The second characteristic, which has not been noted before, is that the peak position for the butterfly feature is shifting negatively by an increase of Θ_{Pd}, by ca. 0.1 V for Pt(111) modified with a pseudomorphic Pd layer compared to bare Pt(111). This finding is consistent with the stronger affinity of Pd towards oxygen [100, 101], as discussed in the previous section for the oxide formation on Pt(111)-Pd in alkaline solution [99]. The third characteristic is that the charge associated with the "butterfly" formation decreases by an increase of Θ_{Pd} (see Figure 4.6c). This is a surprising result, and clearly contradicts the just proposed high oxophilicity of Pd. In Figure 4.6c it is shown that under the experimental conditions applied here (50 mV/s, 293 K) the charge under the "butterfly" feature decreases from ca. 80 $\mu C/cm^2$ on Pt(111) to ca. 60 $\mu C/cm^2$ on Pt(111)-1ML Pd in perchloric acid

solution. At slow sweep rates (10 mV/s) on the Pt(111)-1ML Pd surface the charge under the "butterfly" feature decreases down to ca. 50 $\mu C/cm^2$, while the charge for Pt(111) remains the same.

One possible explanation of this apparently conflicting behavior of palladium atoms in $HClO_4$ is the supposition that the adsorption of OH^- on the Pd sites in $HClO_4$ is inhibited by the competitive adsorption of anions. This hypothesis can be supported by the previous findings. First, as mentioned before, chloride anions, being present as an impurity in "ultrapure" $HClO_4$, are known to be strongly adsorbing anions. Secondly, anion adsorption on palladium is considerably stronger than on bare Pt. This can be seen, for example, in the shift of the adsorption potential of sulfate on Pt(111)-Pd compared to bare Pt (see Figure 3.2). Sulfate is so strongly bound to Pt(111)-Pd that, as soon as H_{upd} is desorbed, sulfate adsorption begins. This behavior results in a coupled hydrogen desorption/sulfate adsorption peak on the Pt(111)-Pd surface.

Since in perchloric acid solution the main trace impurity is chloride, here special attention has been paid on the influence of chloride co-adsorption on Pt(111)-Pd electrodes.

4.3.1.2 Effect of chloride

In order to elucidate the role of Cl^- impurities, present in "pure" $HClO_4$, on the adsorption of H_{upd} and OH_{ad} on a Pt(111)-Pd electrode, in the present work the Cl^- concentration was intentionally increased in the vicinity of the electrode surface. In electrochemical experiments, the rate of mass transport of reactants to the electrode surface can usually be increased by the application of several methods: including the rotation of the electrode (or the stirring of the solution), a decrease of the sweep rate, an increase of the temperature, and an increase of the reactant concentration in the electrolyte. An enhanced mass-transport of the small amount of Cl^- (ca. 10^{-7} M) from the bulk of "pure" $HClO_4$ solution to the electrode surface by forced convection should have a similar effect as the addition of chloride to the electrolyte. Therefore in Figure 4.7 the voltammetric profiles of the Pt(111)-Pd electrode in 0.1 M $HClO_4$ and in 0.1 M $HClO_4$ containing 10^{-6} M Cl^- are presented with and without rotating the electrode, respectively. As can be seen in Figure 4.7c and d, the rotation of the electrode (1600 rpm) has a significant effect on both the shape of the H_{upd} peaks and on the adsorption of OH^-. In particular, the observed H_{upd} peaks in the voltammogram of the rotated electrode exhibit an asymmetry, in contrast to the relatively symmetrical H_{upd} peaks observed on a stationary electrode. This asymmetry displays the fact, that upon rotating the electrode the current density in the H_{upd} peak is increased in the cathodic sweep of the CV, whereas in the anodic sweep the observed current densities in the H_{upd} potential region are the same in the stationary experiments and under enhanced mass-transfer conditions. On the other

hand in the OH⁻ adsorption potential region no peak can be observed anymore when rotating the electrode, indicating the complete blocking of the OH_ad adsorption by another species.
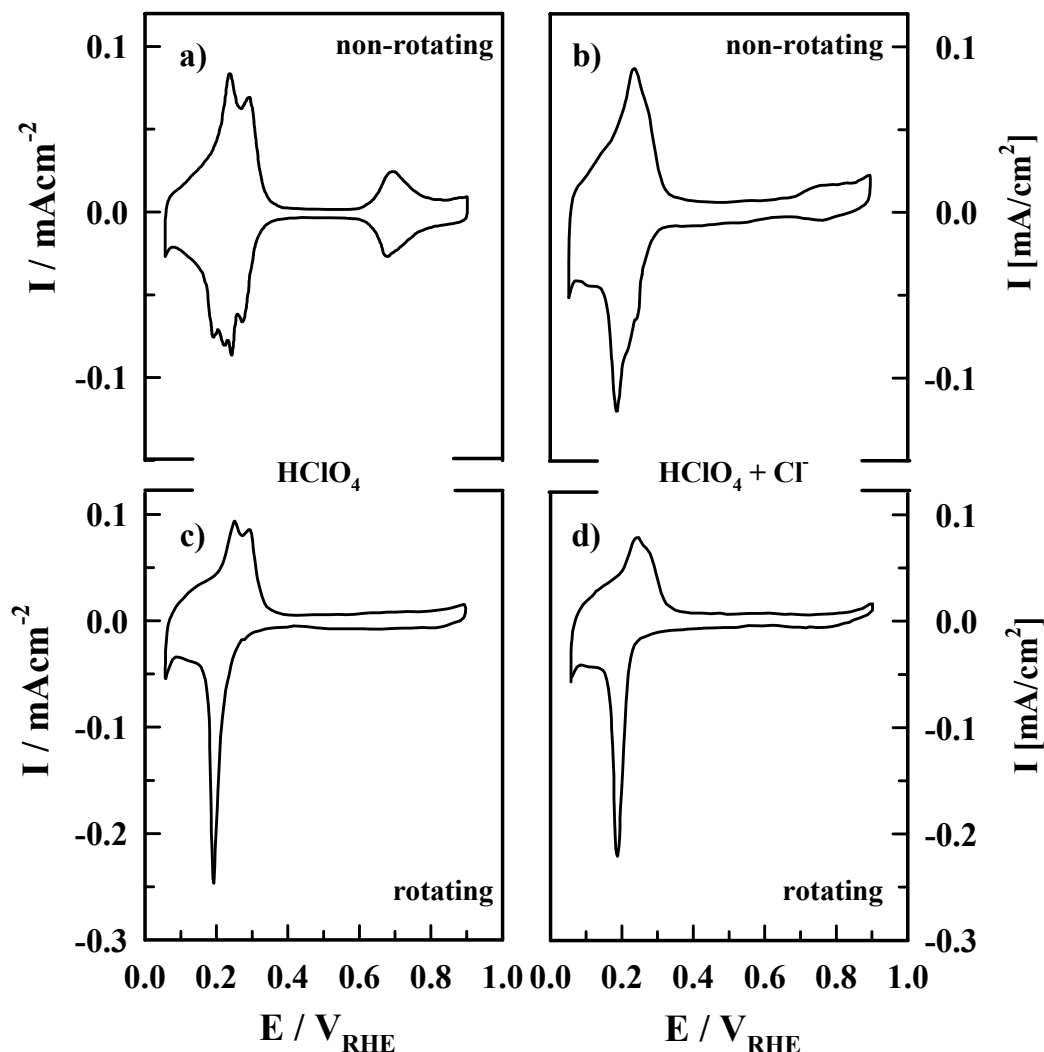
Figure 4.7: Cyclic voltammograms of Pt(111)-1ML Pd; scan rate 50 mV/s at room temperature; a) in 50 mM HClO₄; b) in 0.1 M HClO₄ containing 10⁻⁶ M HCl c) same conditions as in (a) but rotation of electrode with 1600 rpm; d) same conditions as in (b) but rotation of electrode with 1600 rpm

In the experiments presented in Figure 4.7b Cl⁻ is *intentionally* added to the solution. Interestingly, the observed voltammetric features in the presence of small amounts of chloride (10^{-6} M HCl) added to the solution are qualitatively similar to the effect induced by a rotation of the electrode in "pure" HClO₄. Whereas the H_{upd} region in the anodic scan remains unaffected by the addition of small amounts of chloride, in the cathodic scan the various H_{upd} peaks are merging into a single peak located at 0.2 V. Furthermore the OH⁻ adsorption is largely suppressed. These results support the supposition that trace amounts of Cl⁻ and *not* the

high concentration of perchlorate anions control the adsorption properties of the Pt(111)-Pd interface.

Before introducing the effect of chloride on the CO electrooxidation on Pt(111)-Pd surfaces in perchloric acid, FTIR measurements in the "ultrapure" electrolyte, 0.1M HClO$_4$ will be discussed. However, special emphasize will be placed on the question how the possible chloride adsorption from the electrolyte is affecting the electrocatalytic properties of the Pt(111)-Pd surface.

4.3.2 FTIR measurements

In the previous chapter (4.2) the electrooxidation of carbon monoxide on Pt(111)-xPd in alkaline solution has been studied by FTIR spectroscopy [99]. The results clearly demonstrated that the kinetic rate of CO oxidation is inhibited on Pt(111) modified by Pd, although the adsorption of OH$^-$ sets in at lower potentials on the Pd film. As an explanation for these results it was suggested that the kinetic rate of CO oxidation is strongly affected by the delicate balance between the coverage and the nature of the electroactive species, the Pd-OH$_{ad}$ interaction being too strong to effectively oxidize adsorbed CO. In order to demonstrate that in acid solution competitive anion adsorption also plays a significant role in the kinetics of CO oxidation at the Pt(111)-xPd interfaces, the representative FTIR results for molecular level characterization of the surface chemistry of CO$_{ad}$ on the Pd modified Pt(111) surface in HClO$_4$ with and without Cl$^-$ are summarized in the next two sections. When appropriate, these results will be compared with the corresponding results obtained in alkaline solutions.

4.3.2.1 Perchloric acid solution

As in alkaline solution in-situ FTIR measurements were performed in perchloric acid solution on several thin palladium films with different Pd coverages supported on Pt(111). Figure 4.8 depicts potential dependent series of infrared spectra of CO adsorbed on three different Pt(111)-xPd surfaces in CO saturated perchloric acid solution. The background spectra were recorded at 1.0 V. Since the CO adsorption behavior in perchloric acid solution is similar to the adsorption behavior in alkaline solution, and hence similar IR spectra are obtained, the main features of the spectra are only described shortly. Note, however, the higher stability of the CO adlayer towards oxidation and the aforementioned shift of the IR absorption bands of CO$_{ad}$ of ca. 20 cm^{-1} to higher frequencies in perchloric acid solution in comparison to alkaline solution.
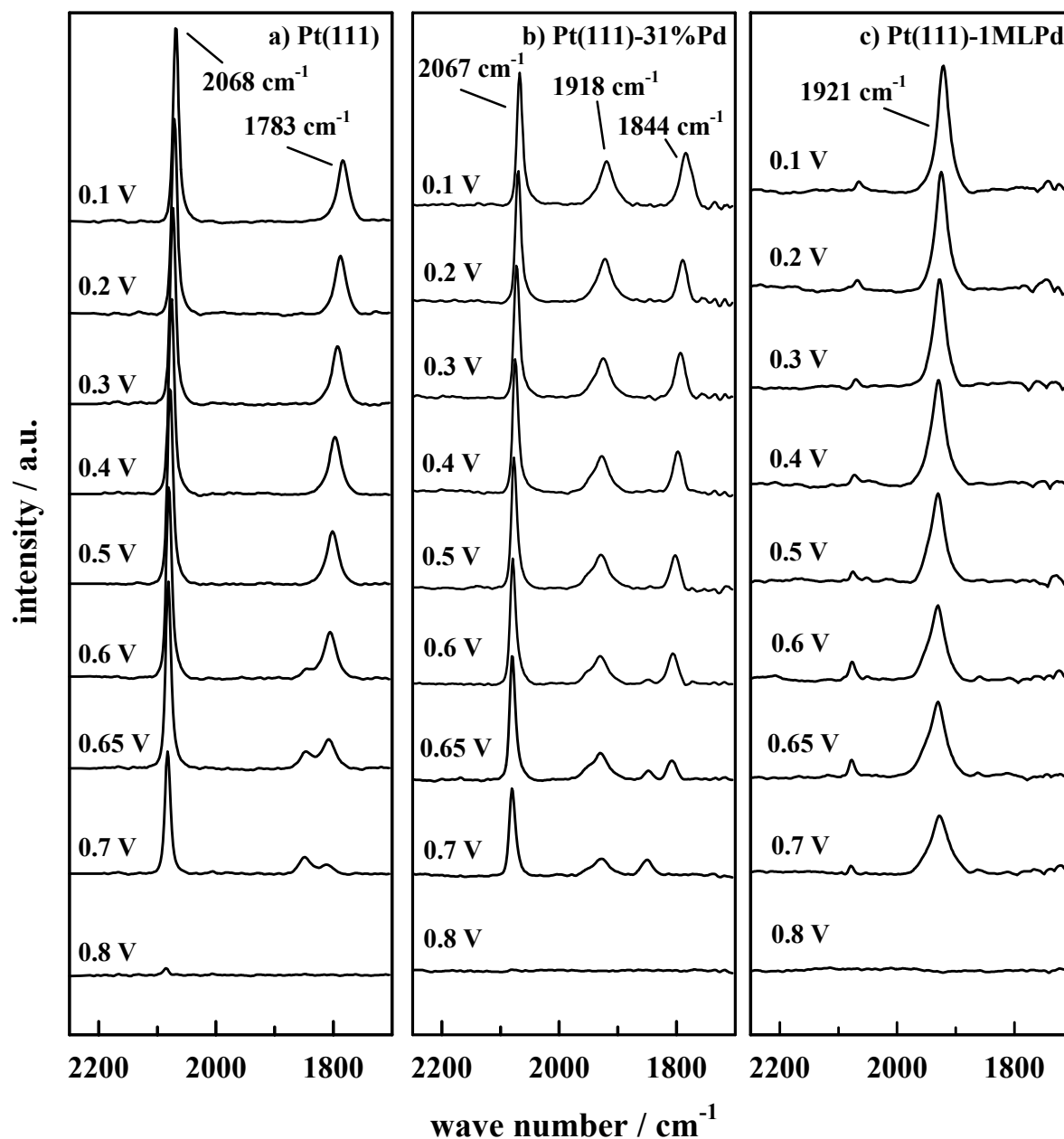
Figure 4.8: Series of infrared spectra of CO_{ad} on (a) Pt(111), (b) Pt(111)-31% Pd and (c) Pt(111)-1ML Pd obtained by stepping the applied potential in a positive direction in CO sat. 0.1 M $HClO_4$ solution, each spectrum was accumulated from 100 interferometer scans; the applied potential is indicated, the background potential was taken at 1.0 V vs. RHE;

For CO_{ad} on Pt(111) (x = 0, Figure 4.8a) at cathodic potentials below 0.6 V the characteristic C-O stretching bands near 2070 and near 1790 cm^{-1}, corresponding to CO adsorbed on on-top and three-fold hollow sites, respectively, can be distinguished. Going to more anodic potentials, the band of the hollow species is replaced by a new C-O stretching band at about 1840 cm^{-1}, which can be related to the presence of bridge bonded CO. The

three-fold hollow band in combination with the on-top band is related to a p(2 x 2)-3CO structure, whereas the loss of this ordered structure is reflected by the appearance of the bridge-bonded CO band, located near 1840 cm^{-1} [75], corresponding to a ($\sqrt{19} \times \sqrt{19}$)R23.4°-13CO unit cell. The change in the CO adsorption geometry is accompanied by the onset of CO_{ad} oxidation, which begins at a potential of about 0.55 V. It is apparent that the transition of the CO adlayer is considerably slower than in alkaline solution. As discussed before [75, 76, 94], upon the change in the adlayer about 15% of CO_{ad} are oxidatively removed by the reaction with OH_{ad} to form CO_2 through a Langmuir-Hinshelwood mechanism.

For Pt(111) covered with a full monolayer of Pd FTIR spectra in CO saturated 0.1 M HClO$_4$ (Figure 4.8c) reveal only one single absorption band near 1920 cm^{-1}. This finding is consistent with FTIR investigations of Inukai et al. [47] and Gil et al. [66], where the absorption peak has been assigned to bridge-bonded CO_{ad}. In line with these studies, the band for CO_{ad} on 1 ML of Pd observed here will be assigned to CO adsorbed at Pd bridge sites. In Figure 4.8b a series of FTIR measurements of CO_{ad} on a Pt(111)-xML Pd electrode with x = 0.31 can be seen. Even though FTIR spectra were recorded at surfaces modified by electrochemical Pd deposition in submonolayer-to-monolayer quantities, only this representative series of spectra will here be introduced in order to demonstrate all important features of CO surface electrochemistry on a Pd modified Pt(111) surface in perchloric acid solution. At low potentials, three different C-O stretching bands near 1800 cm^{-1}, 1920 cm^{-1} and 2070 cm^{-1} can be distinguished in the spectra. By comparison with Figure 4.8 a and c, these bands can clearly be assigned to CO adsorbed on three-fold hollow sites on Pt, CO bridge bonded on Pd and CO adsorbed on-top of Pt, respectively. No coupling takes place between CO adsorbed on Pt and CO adsorbed on Pd sites. Moreover the spectra of the submonolayer of Pd are a superposition of the spectra obtained on bare Pt(111) and those from the full monolayer of Pd, respectively.

Figure 4.9: Band position of the on-top Pt-CO band (a) and the Pd-CO band (b) (taken from Figure 4.8) as a function of the electrode potential in CO sat. 0.1 M HClO₄ solution

In Figure 4.9 the band positions of the CO absorption bands on the different surfaces are compared. Data from another Pt(111)-xPd surface with x = 0.54 are included as well. Note, that due to an interplay of the electrochemical Stark effect [16] and dipole-dipole coupling the absorption frequency of CO is dependent on the electrode potential [76]. At a constant CO coverage (cathodic potentials) the absorption frequencies show due to the Stark effect a linear dependence on the applied potential. Upon the beginning of the electrooxidation of CO_{ad} (about 0.55 V) the CO coverage decreases and, hence, the effect of the reduced dipole-dipole coupling is overcompensating the electrochemical Stark effect. This leads to a decreasing of the absorption frequency with increasing applied potential. Note, that at very small CO coverages the determination of the band position becomes difficult due to the small intensity. Furthermore Figure 4.9 shows that the absorption frequencies for CO

adsorbed on on-top platinum sites as well for CO adsorbed on palladium are lying closely together on the different surfaces. However, although the adsorption frequencies on the different surfaces are almost identical, as a trend it can be noticed that with increasing the palladium coverage the absorption frequency of CO_{ad} on Pd is increasing as well. The same is true for CO bound to Pt in the reverse order. With increasing palladium coverage the absorption frequency of Pt-CO is slightly decreasing. In other words, the larger the mean size of the areas of CO bound to one metal, the larger is the absorption frequency of the specific CO_{ad} band. Therefore, the dipole-dipole coupling seems to be sensitive also to the size of the area of the CO islands bound to one specific metal. At least for CO bound to platinum this can be ascribed to the tendency of a more ordered p(2 x 2)-3CO structure when increasing the size of the CO island.

Summarizing, it can be stated that the adsorption behavior of CO on the patches of the two metals is the same as on the respective bare surface. The structure of the CO adlayer on Pd islands and free Pt patches is more or less independent of the Pd coverage except on very high or very low coverages. Therefore, it is interesting to examine more closely the integrated intensities of the CO bands as a function of the electrode potential. These are given for the Pt-CO on-top bands and the Pd-CO bands in Figure 4.10. Calculating the ratio for on-top CO bound on platinum of the Pt(111)-xPd surfaces with x = 0, x = 0.31 and x = 0.54, respectively, we found a ratio of 1/0.65/0.38 which reflects pretty well the calculated palladium coverage (and hence the free Pt-sites) for the first two surfaces. The ratio of the latter surface, however, is slightly different from θ_{Pd}. On the other hand CO bound to palladium gives rise to only one absorption band. This may simplify the evaluation of the palladium coverage by the ratio of the integrated band. Figure 4.10b depicts the integrated band intensities for CO bound on palladium found for the three surfaces. From these data the ratio of the band intensities for CO bound on the different Pt(111)-xPd surfaces can be calculated to 1/0.57/0.37 for x = 1, x = 0.54 and x = 0.31. It can be seen that indeed the integrated band intensities reflect (within the uncertainty) the calculated palladium coverages using the calibration curve introduced in the third chapter. When examining the integrated band intensities the above mentioned increased stability of the CO adlayer in acid solution compared to alkaline solution can be clearly seen. Here, the effect of *palladium* on the CO oxidation reaction in acid solution will be discussed more detailed. From Figure 4.10b it is apparent, that the integrated intensities of CO adsorbed on Pd are slightly decreasing with stepping the potential to higher values.
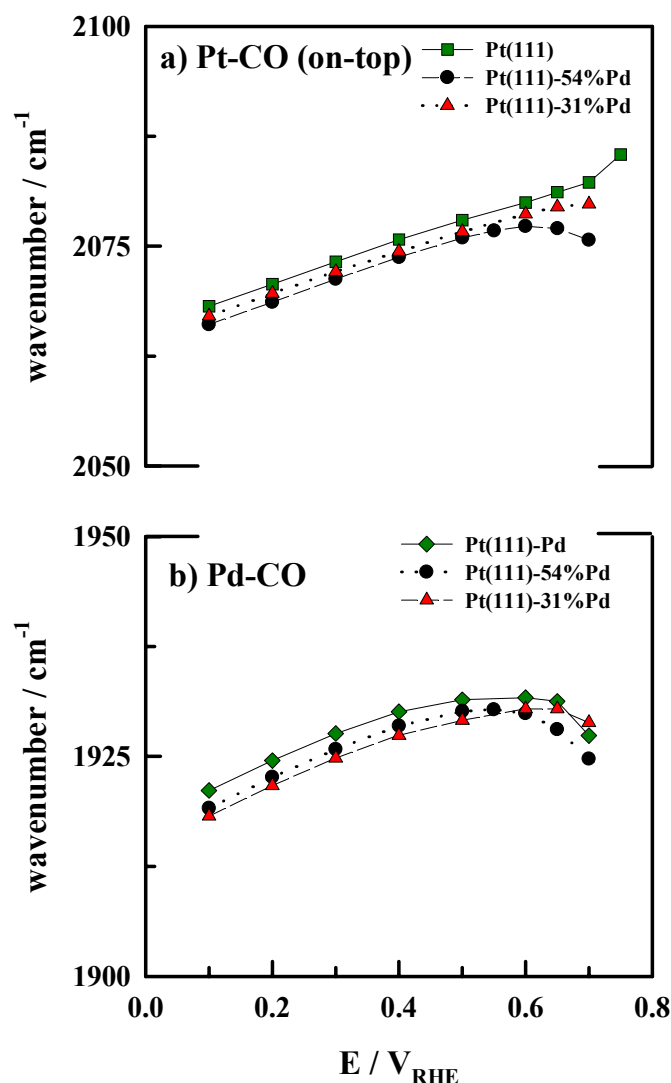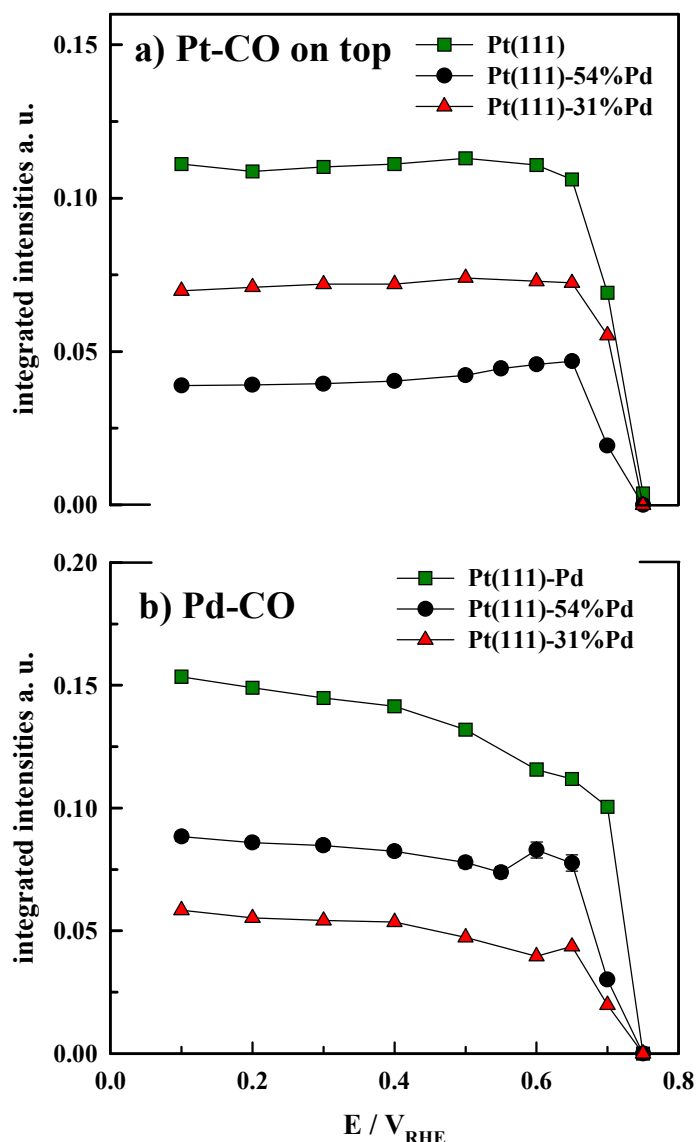
Figure 4.10: Integrated band intensities of on-top Pt-CO bands (a) and Pd-CO bands (b) (taken from Figure 4.8) as a function of the electrode potential in CO sat. 0.1 M HClO₄ solution

That this effect is *not* due to a partial oxidation of CO_{ad} on Pd is by no means clear and becomes apparent only when looking at the CO_2 production. The influence of Pd on the CO oxidation in argon saturated perchloric acid solution is demonstrated in Figure 4.11. The evolution of the absorption band of dissolved CO_2 (formed under oxidation of CO_{ad}) on three Pt(111)-xPd surfaces is plotted against the applied potential. These measurements were recorded in CO free perchloric acid solution in order to suppress an eventual readsorption of CO from the electrolyte and to separate the amount of CO_2 formed on the different surfaces more clearly. It can be clearly seen that on bare Pt(111) the onset potential of CO oxidation

(ca. 0.55 V) is lower than on the palladium monolayer (ca. 0.65 V). The onset potential for CO oxidation on the half covered surface lies in between the latter two values.
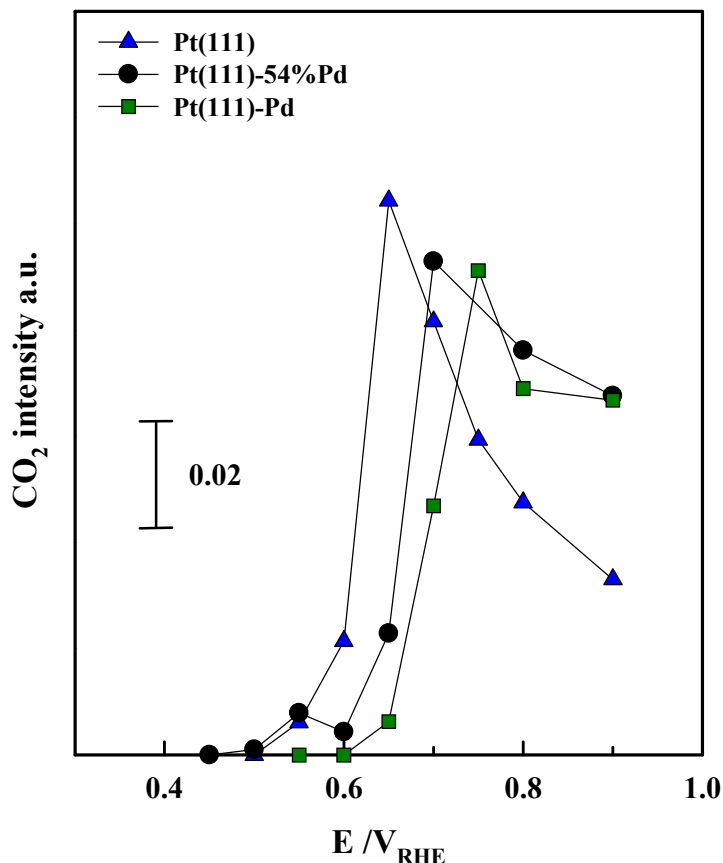
Figure 4.11: CO_2 production for three Pt(111)-xPd surfaces in argon saturated perchloric acid solution as a function of the electrode potential; data extracted by using –0.05 V as background potential

When comparing these values it is crucial that the experimental procedure for all measurements is the same, since factors such as defect density of the surface and the recording time of the spectra can influence the results. Additionally, it is important to note that very small amounts of CO_2 in the path of the IR beam in the spectrometer can lead to small CO_2 bands in the spectra which are not due to the oxidation of CO_{ad}. This leads to a higher uncertainty at low CO_2 concentrations and consequently to small variations in the onset potential where CO_2 is detected at first (see Pt(111)-54% Pd surface). A misinterpretation of the data, however, can be excluded since a *massive* absorption band from CO_2 in the gas phase can be separated from CO_2 in solution, due to the splitting of the absorption band in the gas phase, indicating the rotation of the molecule.

Considering all these arguments it can be stated that, despite of the lower adsorption potential for OH⁻ species, Pd shifts the CO-oxidation to more positive potentials. Bearing in mind that the adsorption of OH⁻ on the Pd sites is strongly inhibited by the presence of Cl⁻ in $HClO_4$ it is reasonable to suggest that Cl⁻ can effectively suppress the adsorption of OH⁻, and thus the rate of CO oxidation (CO_2 production in Figure 4.11). FTIR investigations for the elucidation of the possible role of chloride trace impurities in the electrolyte are presented in the next section.

4.3.2.2 Effect of chloride
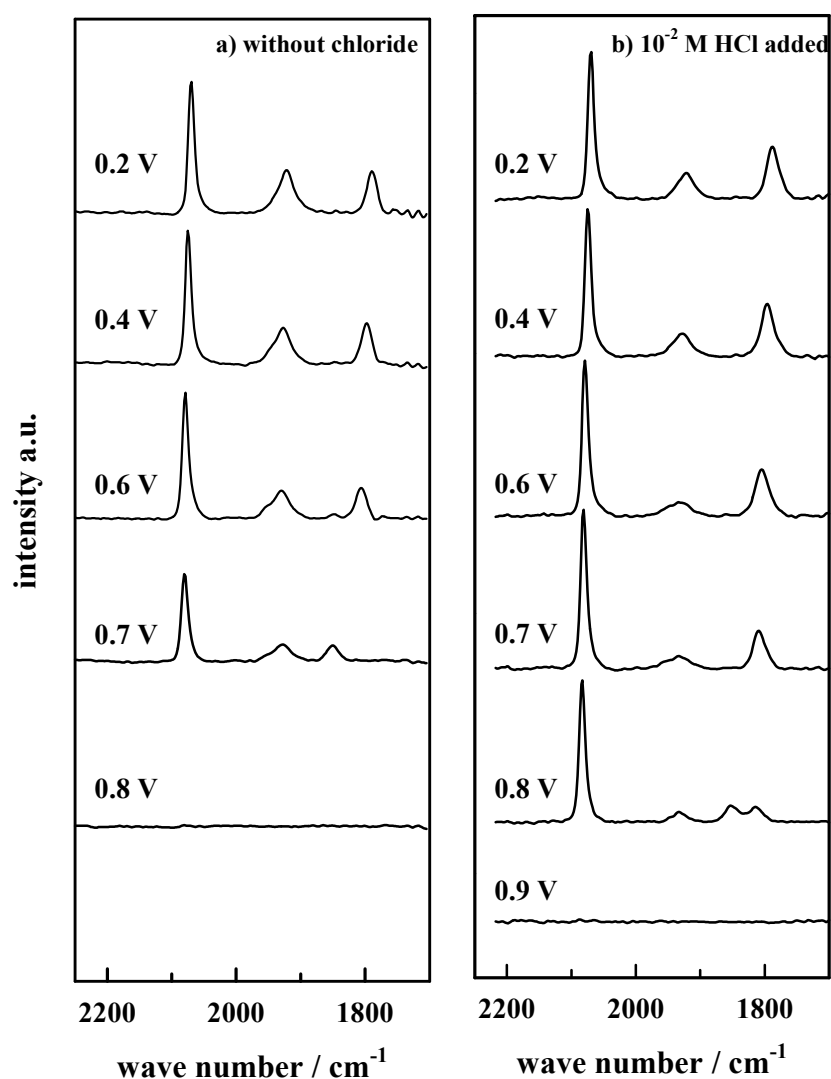
Figure 4.12: Series of infrared spectra of CO_{ad} on Pt(111)-31% Pd in CO sat. 0.1 M $HClO_4$ solution; in (b) 10^{-2} M HCl are added; each spectrum was accumulated from 100 interferometer scans at each potential indicated, the background potential was taken at 1.0 V vs. RHE;

In order to support the hypothesis of competitive anion adsorption, the effect of Cl^- on the rate of CO oxidation (CO_2 production) is investigated in $HClO_4$. The CO_2 production is compared in pure $HClO_4$, and in $HClO_4$ containing different amounts of Cl^- at the same pH of the solution (constant OH^- concentration). The corresponding FTIR results are shown in Figure 4.12 for CO adsorption on a Pt(111)-xML Pd electrode with $x = 0.31$. The measurements of Figure 4.12a are performed in perchloric acid whereas the spectra in Figure 4.12b are recorded in the same solution containing 10^{-2} M HCl, both solutions being CO saturated (the evaluated palladium coverage in Figure 4.12b is slightly different, $x = 0.29$).
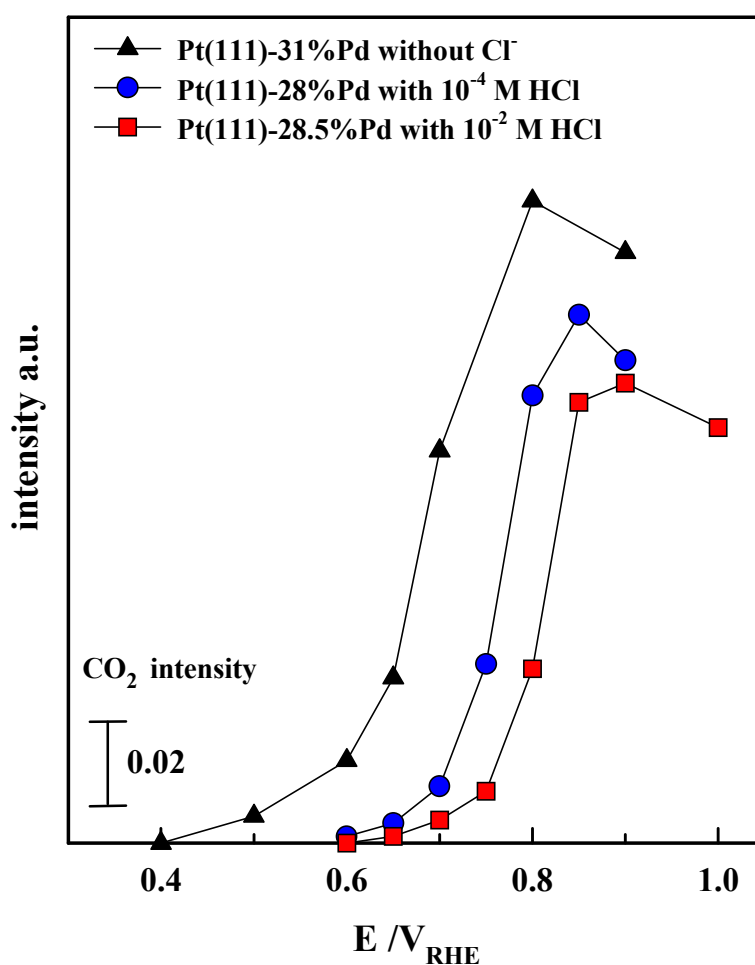
Figure 4.13: Comparison of the CO_2 production evaluated from the spectra shown in Figure 4.12 by using 0.05 V as background potential

Comparing the two series it is obvious that chloride is increasing the stability of the CO_{ad} layer towards oxidation. Whereas in the chloride free electrolyte the CO adlayer is completely oxidized at 0.8 V, in the chloride containing electrolyte at 0.8 V both CO adsorbed on palladium and on platinum still can be detected. This clearly demonstrates the stabilizing

effect of specific anion adsorption from the electrolyte on the CO adlayer. However, that indeed the *onset* potential of CO-oxidation is shifted to more anodic potentials by Cl⁻ is shown by monitoring the CO_2 production in dependence of the chloride concentration in the electrolyte, depicted in Figure 4.13. It can be seen that the CO oxidation in the pure perchloric acid solution sets in at between 0.5 V and 0.6 V whereas the addition of 10^{-2} M HCl shifts the onset of CO_{ad} oxidation to a potential higher than 0.7 V. Therefore specific anion adsorption influences the onset of CO oxidation in electrolytes containing strongly absorbing anions. This is a strong indication that indeed Cl⁻ from pure perchloric acid solution can suppress the adsorption of OH⁻.

4.3.3 Discussion: CO oxidation in perchloric acid solution

Starting the discussion with the relationship of the palladium coverage and the integrated band intensities of the CO bands. It has been suggested in the text that the integrated band intensities can be directly linked to the Pd surface *coverage*. The argument was, that the adsorption behavior of CO on the patches of the two metals is the same as on the respective bare surface and the structure of the CO adlayer on Pd islands and free Pt patches is more or less independent of Pd coverage except on very high or very low coverages. Therefore, the integrated intensities of the CO bands should be directly related to the palladium coverage of the respective surfaces. It was shown that a better agreement exists between the Pd coverage estimated from the integrated band intensities with that given by the calibration curve introduced in chapter 3, when using the Pd-CO band rather than the Pt-CO band. Regarding this difference in the accuracy of the estimated Pd coverage from the integrated intensities of the CO bands on Pt and Pd, respectively, one has to take into account that on platinum there are two different adsorption sites for CO (in the potential region below 0.6 V), whereas for CO bound to palladium only one adsorption site is found. That this ordered CO structure on Pt(111) complicates the estimation of the Pd coverage from the integrated band intensities of CO_{ad} on Pt becomes clear when comparing the CO band intensities of bare Pt(111) with the CO adlayer structure established from STM. Considering the real space model of the cathodic p(2x2)-3CO structure the occupancy of CO bound to on-top sites is 1/3 whereas 2/3 of the CO_{ad} molecules occupy three-fold hollow sites. However, this ratio is obviously not represented by the integrated band intensities. This becomes apparent when examining the FTIR spectra shown in Figure 4.8a. It is obvious that an intensity transfer of the three-fold hollow band to the on-top band takes place.

Furthermore, besides this well known intensity transfer, the integrated band intensities of adsorbed molecules must be interpreted with caution, since the matrix element, which determines the absorption intensity, is dependent on the coverage of the IR active molecule [10]. This becomes clear when considering the decrease in the integrated band intensities of the Pd-CO band. It has already been mentioned that the integrated band intensities are

decreasing with stepping the potential to higher values. Since no CO_2 bands are seen in the spectra below 0.65 V (see Figure 4.11) this decrease can not be due to oxidation of CO bound to Pd. The main reasons for this at first sight puzzling finding may be that when stepping the electrode potential to more positive values the CO adlayer on Pd becomes less ordered. This effect, apparent from the increase in the FWHM of the absorption bands with increasing potential, may lead to a change in the matrix element due to a change in the average CO_{ad}-CO_{ad} distance on Pd. However, since no data exist about the structure of CO_{ad} on Pt(111)-1ML Pd this suggestion is somehow speculative and further investigations are needed to clarify this point. However, from the above discussion it becomes clear that when using CO as a probe for the coverage of a metal deposit on an electrode attention has to be paid to other factors influencing the absorption band. Furthermore, it must be stressed, that this method is applicable at all, only if metal *islands* are formed upon deposition and the adlayer structure of the molecule is the *same* on the metal islands as on the respective bare metal surface.

The fact that Pd grows in islands on Pt(111) provides one with the opportunity to investigate the electrochemical properties of Pt(111) and Pt(111)-Pd surfaces simultaneously. By varying θ_{Pd} the properties of both metals easily can be distinguished. In the following the focus will be on the comparison of the CO electrooxidation properties of the Pt(111)-xPd surfaces with those of the two pure metals Pt and Pd, respectively.

Comparing the FTIR spectra obtained in perchloric acid and alkaline solution it is obvious that although the adlayer structure of CO adsorbed on the Pt(111)-xPd surfaces is the same in the two electrolytes, the CO oxidation in perchloric acid is considerably hindered at lower potentials. This finding is typically observed in the case when specific anion adsorption from the electrolyte are blocking the defect sites of the surface, where OH^- adsorption takes place first. However, perchlorate anions are often considered as non-absorbing anions, but in a certain amount trace impurities of other anions are always present in perchloric acid solution. Therefore in this chapter special attention was paid to specific anion adsorption on Pd, when only very small concentrations of anions other than perchlorate are being present in the electrolyte.

One important observation, showing the stronger interaction of Pd with anions compared with that of Pt, is the decrease in the current density of the "butterfly" upon Pd deposition (see Figure 4.6). Compared to bare Pt(111) the amount of OH_{ad} on the palladium islands is decreased, although the adsorption starts earlier in the CV (at more negative potentials). This decreased OH^- adsorption leads to a increase of the onset potential of CO oxidation as demonstrated in Figure 4.11 in argon saturated perchloric acid solution.

These are surprising results, and clearly contradict the here proposed high oxophilicity of Pd. As a possible explanation it was put forward that the adsorption of OH^- on the Pd sites

in $HClO_4$ might be controlled (inhibited) by the competitive adsorption of impurity chloride anions, and *not* by the high concentration of perchlorate anions. This hypothesis has been supported by the FTIR measurements by adding chloride to the perchloric acid solution, where it was found that the CO adlayer is considerably stabilized by chloride and the onset of CO oxidation is shifted to more anodic potentials (see Figure 4.13).

Based on the strong Pd-Cl interaction also the H_{upd} potential region of the cyclic voltammograms of Pt(111)-xPd can be explained. Upon rotating the electrode, the voltammogram exhibits an asymmetry in the H_{upd} region, in contrast to the relatively symmetrical H_{upd} peaks observed on a stationary electrode. Interestingly, a very similar behavior has been reported for the adsorption of hydrogen on Pt(100) in $HClO_4$ containing 5×10^{-6} M Cl^- [26], leading to a slightly higher Cl^- concentration than here. In order to explain the asymmetry of the H_{upd} peaks on Pt(100) in the presence of traces of Cl^-, the authors suggested that the diffusion controlled adsorption of Cl^- is responsible for the observed asymmetry. For further details of the experiments see reference [26]. Here the same argumentation is adopted and described in the following.

It is suggested here, that the asymmetry of the H_{upd} peaks induced by the rotation of the Pt(111)-Pd electrode is due to an increased mass-transport of Cl^- from the bulk of the $HClO_4$ solution to the electrode surface and due to the enhanced adsorption of Cl^- anions on the Pd sites. Consequently, the surface coverage of Cl_{ad} should be increased on the RDE, resulting in an almost complete blocking of the OH^- adsorption. This leads to a shift of the H_{upd} peak, which follows the desorption of Cl_{ad}, to lower potentials when sweeping the potential from the positive limit to negative potentials, thereby producing a sharp peak located at ca. 0.2 V. After desorption, Cl^- diffuses away from the surface, and then re-adsorbs slowly in the positive sweep reaching the maximum surface coverage at the positive potential limit. The asymmetry observed in the H_{upd} potential region is, therefore, completely controlled by the different Cl_{ad} surface coverage in the positive and negative sweep direction. Diffusion and H_{upd} desorption controls simultaneously the Cl^- adsorption during the anodic sweep. Clearly, under enhanced mass-transfer conditions even traces of Cl^- present in 'pure'' $HClO_4$ are controlling completely the oxide formation on the Pt(111)-Pd surface. A further confirmation of this hypothesis is obtained from the experiments in which Cl^- is intentionally added to the solution, see Figure 4.7b. The observed effect of small amounts of chloride (10^{-6} M HCl) added to the solution is qualitatively similar to the effect of rotation.

Very recently, it was shown that with an increased amount of chloride added to the perchloric acid (10^{-3} M HCl) , the cyclic voltammogram of Pt(111)-1ML Pd is becoming symmetrical again and simultaneous desorption/adsorption peaks can be seen in the anodic cycle of the H_{upd} potential region and vice versa in the cathodic cycle [91].

It must be noted here, that the described effects are not due to contaminations caused by the experimental cleanliness. All measurements performed in the course of this work were identical to the literature data which existed already from previous studies. For bare Pt(111) test measurements showed no significant influence on the cyclic voltammograms of neither rotating the electrode nor the addition of 10^{-6} M HCl to the perchloric acid solution (see also ref. [102]). Only at Cl⁻ concentrations as high as 10^{-5} M the CV of bare Pt(111) was affected.

4.3.4 Conclusion: CO oxidation in perchloric acid solution

A combination of cyclic voltammetry and in-situ FTIR investigations has been used in order to describe the electrochemical behavior of thin palladium films supported on Pt(111) in perchloric acid solution. Utilizing FTIR it has been shown that upon electrodeposition of palladium on Pt(111), pseudomorphic Pd islands are formed on the surface. The palladium affects the cyclic voltammetry in perchloric acid in three characteristic ways. First of all, the hydrogen coverage in the H_{upd} potential region is calculated to be 1ML, independent of the pH of the solution. This high coverage is attributed to the strong interaction of Pd with hydrogen and/or the absence of lateral repulsion within the H_{upd}. At positive potentials the adsorption potential of OH⁻ is shifted in the negative direction, whereas the charge density of the "butterfly" peak is considerable lower on Pt(111)-1ML Pd than on bare Pt(111). These findings are related to a competition of the available adsorption sites between impurity chloride anions and OH⁻ species. This hypothesis is supported by additional cyclic voltammograms recorded at varying chloride concentration and scan rate.

In this light the electrooxidation of CO_{ad} on Pt(111)-xPd films in perchloric acid solution is discussed. It is demonstrated that on the palladium films the kinetic rate constants as well as the onset potential of oxidation are different than on bare Pt(111). Despite of the shift of OH⁻ adsorption towards more negative potentials on the palladium films, the CO oxidation is shifted towards more positive potentials. This, at first sight contradictory behavior, is ascribed to the competition of specific (impurity) chloride adsorption and the formation of OH_{ad} on the Pd sites. At lower potentials in perchloric acid solution trace amounts of chloride are stabilizing the CO adlayer towards electrooxidation on the thin palladium films. At higher potentials, however, as demonstrated in alkaline solution the kinetic rate constant for CO oxidation on palladium is reduced due to the stronger Pd-OH bond.

4.4 Summary: CO oxidation

The CO adsorption behavior and the electrooxidation of CO adsorbed on Pt(111)-xPd electrodes has been studied in alkaline as well as in perchloric acid solution.

The CO adsorption behavior is used as a probe for the film morphology. It is shown that upon Pd deposition onto Pt(111) no Pd-Pt surface alloying takes place rather than two dimensional Pd islands are formed. From the absence of a second Pd-CO band in the FTIR spectra it is established, that using the here applied deposition procedure a complete Pd monolayer is formed before three dimensional growth sets in.

Cyclic voltammetry reveals that on Pt(111)-1ML Pd the surface is completely covered by H_{upd}, independently of the pH of the electrolyte. Pd deposited on Pt(111) leads to a lower OH^- adsorption potential than on bare Pt(111) in alkaline as well as in perchloric acid solution. In perchloric acid solution, however, Cl^- trace impurities are limiting the amount of OH_{ad}.

Chloride adsorption is also responsible for the differences in the electrooxidation of CO_{ad} on the Pd surfaces between alkaline and acid solution. In alkaline solution the oxidation of CO_{ad} on Pt(111) and on platinum surfaces modified with Pd starts at the same potential, ca. at 0.2 V. However the CO oxidation *rate* is considerably lower on Pd-modified Pt(111) than on bare Pt(111). The kinetics of CO oxidation is determined by the stronger Pd-OH bond in comparison to the Pt-OH bond. In contrast, in perchloric acid solution also the onset of CO electrooxidation is affected by palladium. The beginning of CO oxidation on the palladium films is shifted towards more positive potentials with increasing Pd coverages. At lower potentials in perchloric acid solution trace amounts of chloride are stabilizing the CO adlayer towards electrooxidation on the thin palladium films. At higher potentials, however, as in alkaline solution, the kinetic rate constant for CO oxidation on palladium is reduced due to the stronger Pd-OH bond.

Chapter 5

The oxygen reduction reaction

The oxygen reduction reaction (ORR) is considered to be one of the most important electrocatalytic reactions because of its role in electrochemical energy conversion, several industrial processes, and corrosion [103]. Consequently, for many years it has been in the focus of electrochemical interest. However, oxygen reduction still continues to be a challenge for electrochemists because of its complex kinetics and the need for better cathode electrocatalysts for fuel cells [103]. Especially recent efforts to develop improved fuel cell cathodes have revived interest in improving electrocatalysts for O_2 reduction [104].

The substantial difficulties in the search for better electrocatalysts for fuel cells become clear when considering that there is up to date no electrode material for which there is even a *measurable* current from oxygen reduction at the equilibrium potential, 1.23 V *vs.* the normal hydrogen electrode (NHE) [82]. Even for the most catalytically active electrode materials, i.e., expensive platinum group metals, measurable currents are obtained only below 1 V, i.e. at an overpotential higher than 0.2 V. It is customary, therefore, in kinetic studies of the ORR to use the current density at a fixed potential, e.g., at 0.9 V, as a measure of the reaction rate instead of the exchange current density. On the other hand the extremely high overpotential for oxygen reduction shows that there is still a great potential in enhancing the effectiveness of energy conversion on the basis of fuel cells.

In order to optimize the *cost* of fuel cell catalysts different strategies can be applied. One possibility is to replace Pt, still the catalyst of choice at least for acid-based fuel cells [104], partially or entirely by a less noble and cheaper material and/or to maximize the surface area of the catalyst with the most active microstructures. On the other hand, several attempts have been made to modify the intrinsic activity of platinum itself by making bimetallic surfaces [105]. In this work, the ORR is investigated on model electrodes of platinum group metals and no attempts are made to replace Pt by non-noble materials. Moreover, the focus is on the fundamental understanding of the reaction at the metal (platinum)-electrolyte interface and the optimization of the catalytic properties of the platinum surface.

The chapter is structured as follows. In the first section details on the oxygen reduction reaction are given. The most important results of previous work concerning the ORR on platinum group single crystal electrodes as well as the reaction pathway and the mechanisms of the oxygen reduction reaction are discussed. Before coming to the experimental results of this work, the application of the RRDE technique in investigating electrocatalytic reactions is introduced and the kinetic equations used are briefly derived.

In the next section measurements of the ORR on Pt(111)-xPd surfaces in alkaline solution are introduced. Triggered by the exceptionally high activity of the Pd film, both the influence of the palladium coverage in alkaline solution and the influence of anions in acid solution on the ORR are studied. Finally, a summary of the experimental findings is given.

5.1 Details: Oxygen reduction reaction

5.1.1 Literature: ORR at platinum group metals

The experimental relation between the current density, I, and the electronic properties of metals which are known to influence the heat of adsorption of oxygen, manifests itself in "volcano-type" curves, with the platinum group metals at or near the top of the "volcano plot" [106]. The "volcano" relationship for the ORR appears to be valid for alloys as well as for pure metals, showing variations in reaction rates by $5-6$ orders of magnitude [107, 108]. In such plots, however, the scale for the reaction rate is usually a logarithmic scale, where rates differ by orders of magnitude. On a finer scale, additional factors must be accounted for in order to explain the full range of catalytic response on different surfaces. The optimization of an electrocatalyst for the ORR must, therefore, accommodate many contributing factors, including the rate dependence on the geometry of the surface atomic structure.

Early kinetic and mechanistic studies were carried out on polycrystalline electrodes. It was proposed that on platinum group metals the reaction pathway of the ORR is very similar, and that at low overpotentials the order of activity increased in the sequence Rh < Pd < Pt [100]. Furthermore it was concluded that the kinetic reaction rates were strongly dependent on the nature of the anion of the supporting electrolyte. Recent studies on the structure sensitivity of the ORR on Pt single crystals in the rotating ring disk configuration have shown that the reaction rates of the ORR vary with the crystal face in a different manner depending on the electrolyte used [109, 110]. It has been proposed that the structure sensitivity arises not only from the sensitivity of the adsorption energy of the reactive intermediates to the adsorption site geometry but more importantly from the structure sensitivity of anion adsorption from the supporting electrolyte. These adsorbed anions, e.g., sulfate [111], hydroxyl [24], and halides

[112] are not intermediates in the ORR but are thought to act as spectator species which impede the kinetics of the reaction. In contrast to Pt(hkl), there are no kinetic studies of the ORR on Pd(hkl) and Rh(hkl) surfaces. As already mentioned electrochemical studies with Pd(hkl) electrodes are relatively scarce because of the immense difficulties in the surface preparation and stability caused by the absorption of hydrogen into the bulk lattice which is disordering the surface when cycling the electrode. To circumvent these problems epitaxial palladium films on Pt(111), which are also studied in this work, have recently been used to investigate the ORR in perchloric acid as well as in sulfuric acid [46]. It was found that in sulfuric acid the ORR is strongly inhibited at the Pt(111)-Pd surface whereas in perchloric acid the activity of the Pt(111)-Pd surface is only slightly lower than the activity of the bare Pt(111) electrode. However, no studies of the ORR on Pt(111)-Pd electrodes in *alkaline* solution have been reported so far.

5.1.2 Reaction pathway

The oxygen reduction reaction follows a complex reaction mechanism which includes the transfer of two or four electrons, depending on the reaction pathway. The reaction may include a number of elementary steps involving different reaction intermediates. However, of the various reaction schemes proposed for the ORR (for an overview see references [101, 103, 113]), only a *simplified* version based on the schemes given by Bagotsky et al. [114] and Wroblowa et al. [115], is introduced here. Without considering every detail of the complicated pathway by which O_2 is reduced at metal surfaces, this scheme appears to be rather effective in describing the *most important* factors affecting the activity of a given electrocatalysts towards the ORR [105, 116]:
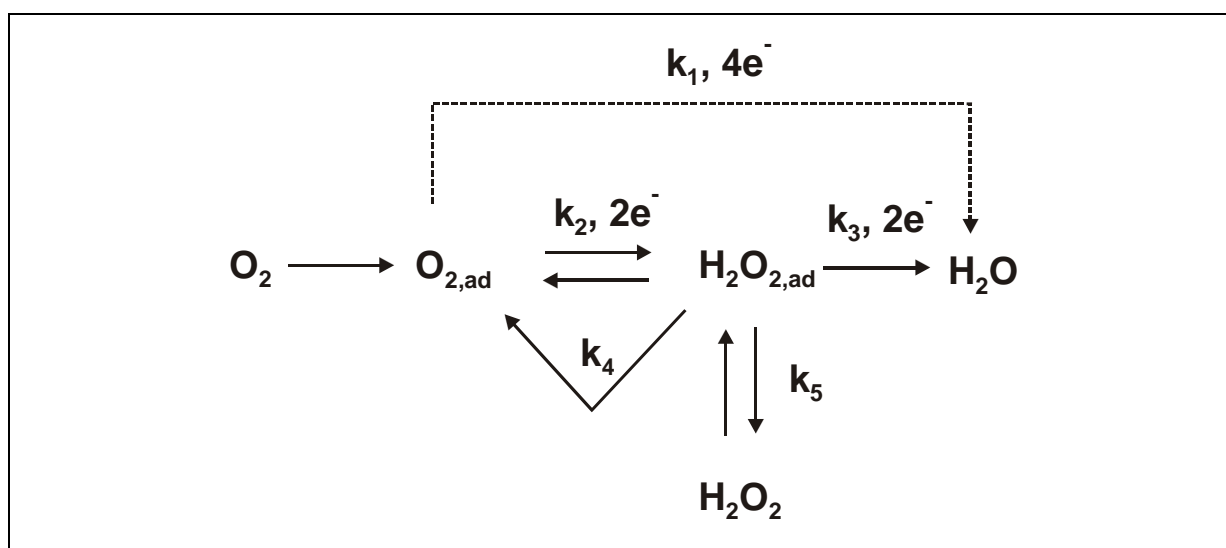

Figure 5.1: Reaction scheme for the oxygen reduction reaction mechanism (in acid solution)

Based on the reaction scheme given in Figure 5.1, O_2 can be electrochemically reduced either directly to water with the rate constant k_1 without intermediate formation of $H_2O_{2,ad}$ (so-called "direct" $4e^-$ reduction) or to $H_2O_{2,ad}$ with the rate constant k_2 ("series" $2e^-$ reduction). The adsorbed peroxide can be electrochemically reduced to water with the rate constant k_3 ("series" $4e^-$ pathway), catalytically (chemically) decomposed on the electrode surface (k_4) or desorbed into the bulk of the solution (k_5). Although a number of important problems pertaining to the interpretation of the reaction pathway for the ORR on Pt(hkl) have yet to be resolved, recent studies [112, 117, 118] suggest that mainly a series pathway via an $(H_2O_2)_{ad}$ intermediate is operative on all Pt and Pt bimetallic catalysts and the direct four-electron reduction occurs only with negligible rates. This can be considered as a special case of the general mechanism where k_1 is essentially zero, i.e., there is no splitting of the O-O bond before a peroxide species is formed. Peroxide, on the other hand may (k_5=0) or may not ($k_5 \neq 0$) be further reduced to water. In either case, the rate determining step appears to be the addition of the first electron to $O_{2,ad}$ to form a superoxide radical. The rate expression is then [101, 112, 119] ,

$$I = nFkc_{O_2}(1-\Theta_{ad})^x \exp(-\beta FE/RT)\exp(\gamma r \Theta_{ad})/RT) \qquad (5.1)$$

where n is the number of electrons, k is the rate constant, c_{O_2} is the concentration of O_2 in the solution, Θ_{ad} is the total surface coverage by anions (Θ_{anions}) and OH_{ad} (Θ_{OHad}), x is either 1 or 2 depending on sites requirements of the adsorbates, I is the observed current, E is the applied potential, β and γ are the symmetry factors (assumed to be ½, i.e. the same behavior is found for both directions of the reaction), and r is a parameter characterizing the rate of change of the apparent standard free energy of adsorption with the surface coverage by adsorbing species, e.g., the adsorption energy decrease with increasing Θ_{ad}. In deriving equation 5.1, it is assumed that the reactive intermediates, $(O_2^-)_{ad}$ and $(HO_2^-)_{ad}$, are adsorbed at low coverage, i.e., they are not a significant part of Θ_{ad}. Therefore, the kinetics of O_2 reduction is determined either by the free platinum sites available for the adsorption of O_2 (1-Θ_{ad} term in equation 5.1) and/or by the change of the Gibbs energy of adsorption of the reaction intermediates with Θ_{OHad} or spectator species Θ_{anions} ($r_{ad}\Theta_{ad}$ term in equation 5.1). In other words, the case of r = 0 is synonymous with Langmuir adsorption conditions, i.e. no interaction takes place between the adsorbed molecules, whereas for r $\neq$ 0 Frumkin adsorption conditions are obtained, i.e. the Gibbs energy of adsorption of the reaction intermediates is dependent on the surface coverage by anions. In the following sections, this reaction pathway and rate expression will be used in order to analyse the effects of the factors on the kinetics of the ORR on the Pt(111)-xPd surfaces.

5.1.3 The application of the RRDE for investigating the electro-catalytic reactions

When investigating an irreversible electrode reaction at high overpotentials, such as the oxygen reduction reaction, the contribution of the back reaction can be ignored and the polarization curves (I vs. E) at an RRDE have typically the form shown in Figure 5.2. Note that in this case negative (reduction) currents are shown, the following description however is also appropriate for describing oxidation reactions like the hydrogen oxidation reaction.

Three distinctive potential regions can be observed in the polarization curves. First, the limiting current plateau region (0.2 V < E < 0.75 V), where the current density only depends on the rotation rate of the RRDE (see basic description of the RRDE in Chapter 2.1.4), then the mixed kinetic-diffusion control potential region (0.75 V < E < 0.925 V) and at last the potential region of very low current density, where the current density is totally determined by the kinetics of the electron transfer and the mass transport does not affect the current density (E > 0.925 V).
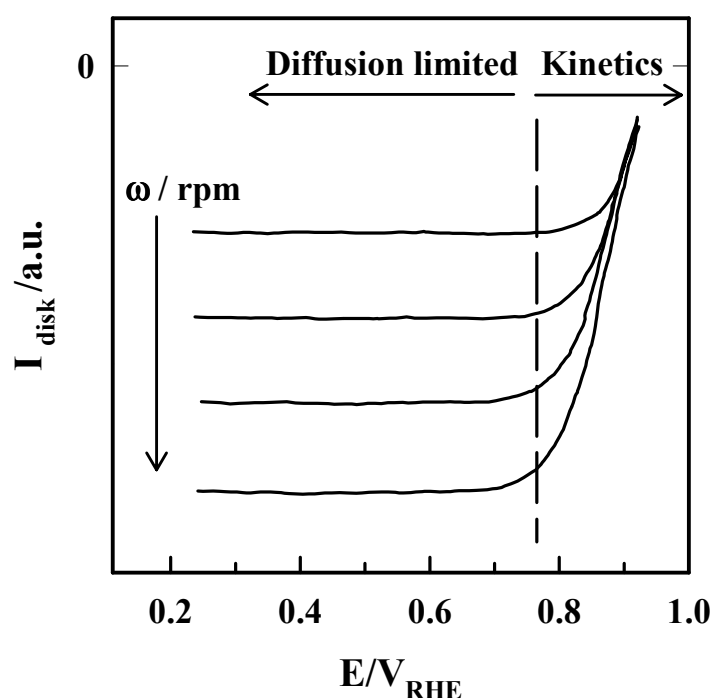

Figure 5.2: Typical family of polarization curves for the disk current at different rotation rates when investigating the ORR with the RRDE technique

For kinetic studies the potential regions of interest are those where (at least some) kinetic control of the measured current densities is present. Consequently, for the ORR only

the mixed kinetic-diffusion control region is examined where the current density is controlled in parts by mass transfer and by the kinetic reaction rate. In this potential region the reaction rate is sufficient enough to be relevant for applied processes and still the kinetic (or activation controlled) current, i.e. the part of the observed current which is controlled by the kinetic rate constant, can be extracted from the measurements. In order to illustrate the way of extracting the "true kinetics" from the measurements, it is instructive to compare the equation of the current measured at the disk electrode expressed in terms of the kinetic rate constant $\vec{k}$ [6, 7] :

$$I = nF\vec{k}c_\sigma \qquad (5.2)$$

and the expression of the current based on the Nernst diffusion layer model (see Chapter 2.1.4):

$$I = nF\frac{D}{\delta}(c_0 - c_\sigma) \qquad (2.6)$$

When eliminating I, one obtains the following expression for the surface concentration of the reactants:

$$c_\sigma = \frac{D}{\delta}\frac{c_0}{\vec{k} + \frac{D}{\delta}} \qquad (5.3)$$

Substituting equation (5.3) into (2.6) and inverting it finally leads to:

$$\frac{1}{I} = \frac{1}{I_k} + \frac{1}{I_{d,RDE}} = \frac{1}{nF\vec{k}c_0} + \frac{1}{nF\frac{D}{\delta}c_o} = \frac{1}{nF\vec{k}c_{O_2}} + \frac{1}{B\omega^{0.5}} \qquad (5.4)$$

Where I_k is the kinetically controlled current, hereafter called the kinetic current, and $I_{d,RDE}$ the diffusion limited current in the RDE configuration. Note, that in the latter expression of eq. 5.4 for the sake of simplicity in the further discussion the diffusion layer thickness δ is expressed in terms of the Levich constant B and the rotation rate ω. Furthermore, for the bulk concentration of the reactant, the concentration of O_2 is inserted.

For an analysis of the kinetic controlled current, the inverse current density I^{-1} at a fixed potential is plotted against the inverse square root of the rotation rate $\omega^{-0.5}$ resulting in a so-called Levich-Koutecky plot. From equation 5.4 it is obvious that these Levich-Koutecky plots for various potentials yield straight lines with the intercept (with the y-axis) corresponding to the inverse of the *kinetic currents* and the slope corresponding to the *B*

value. The former also becomes clear when considering that the intercept is equivalent with an infinite rotation rate and, hence, due to an infinite mass transfer to the electrode at the intercept the current is completely controlled by the activation energy of the reaction.

An alternative expression of the kinetic current, derived from eq. 5.4 is the following equation:

$$I_k = \frac{I \times I_D}{I_D - I}$$

$$(5.5)$$

This equation can be used to correct the observed disk current at the RDE for mass transport and thus obtain I_k as a *function* of potential from the polarization curves in the mixed kinetic-diffusion controlled region (provided the limiting current is known with sufficient accuracy). It should be noted here that equation (5.5) can be used to correct for mass transport only when constant current densities are obtained, as in the application of the R(R)DE. The fact that it is not applicable for stationary electrodes in the absence of defined mass-transport is underlining the importance of the R(R)DE technique when studying electrode kinetics.

5.2 ORR in alkaline solution

Based on the conclusion that in acid solution the electrocatalytic activity of a surface towards the ORR is mainly determined by the structure sensitive adsorption of anions from the supporting electrolyte, measurements in alkaline solution are the most direct probe of the inherent activity of an investigated catalyst. In alkaline solution only the effects of OH_{ad} at lower potentials and the oxide formation at higher potentials have to be taken into account.

5.2.1 RRDE measurements

Figure 5.3 summarizes a family of polarization curves for the ORR on a Pt(111)-Pd electrode in O_2-saturated 0.1 M KOH solution at room temperature. The ring electrode is potentiostated at 1.3 V in order to oxidize HO_2^- (in alkaline solution) which is produced on the disk electrode under diffusion control. Consequently, HO_2^- can be quantitatively collected on the ring electrode. As demonstrated below, in alkaline solution at higher potentials oxide formation is inhibiting the kinetics of the ORR. Therefore, for the sake of comparability of the data collected in alkaline solution, a strict procedure was applied for recording the polarization curves. Before beginning the measurement the electrode was held for 30 s at the start potential, then the potential is swept with a scan rate of 50 mV/s to the negative potential limit and directly back to the positive potential limit. For the further examination of the data, e.g. the Levich-Koutecky plot or the Tafel plot, always the polarization curves of the *anodic*

potential sweep are used. This procedure has the advantage that the polarization curves are obtained from the ORR on the 'bare' metal surface, i.e. the reaction is not perturbed by oxide formation on the electrode.
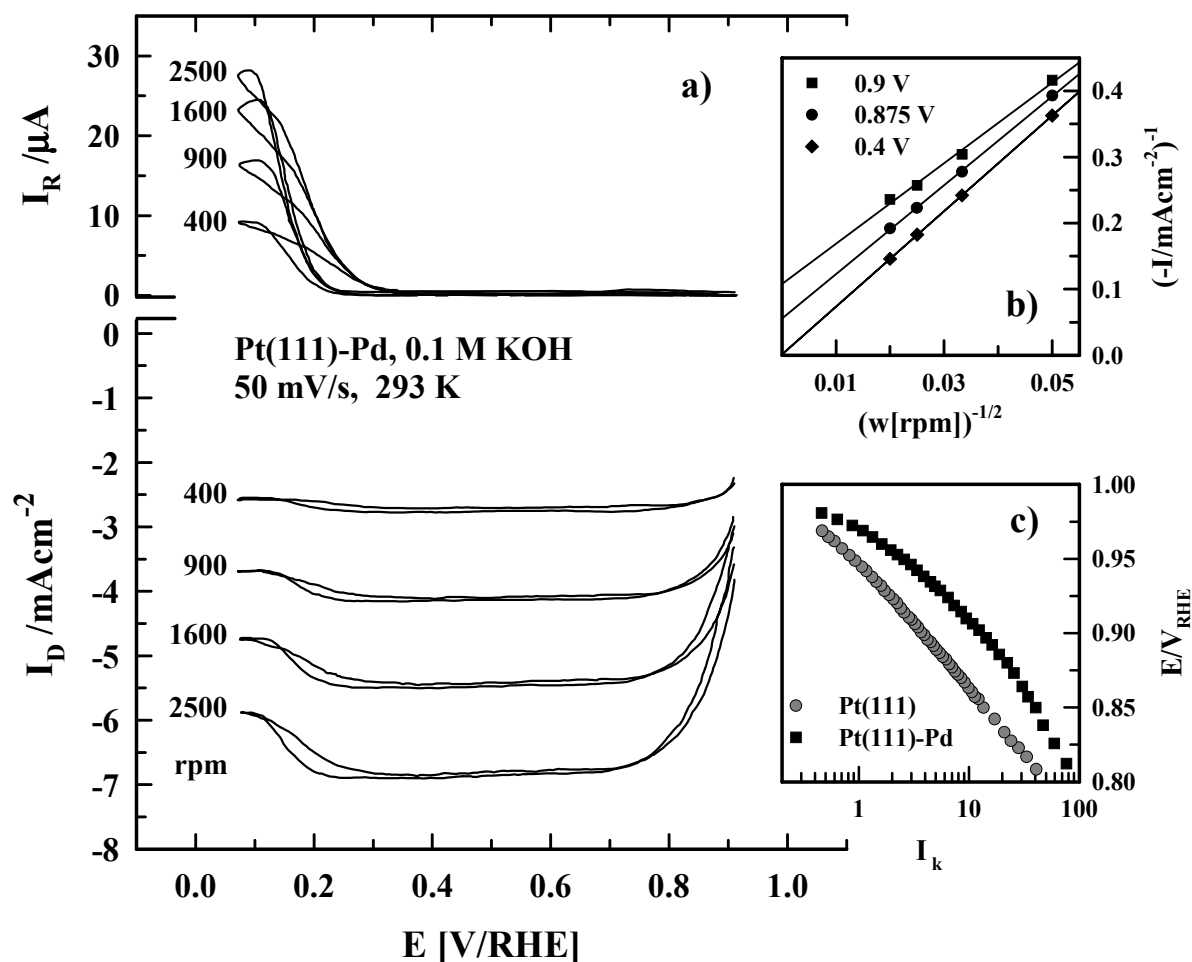
Figure 5.3: a) Polarization curves for the ORR on a Pt(111)-1ML Pd disk electrode and corresponding peroxide oxidation current on the ring electrode in 0.1 M KOH at different rotation rates; 50 mV/s; 293 K; b) corresponding Levich-Koutecky plot at 0.9 V, 0.875 V and 0.4V ; c) Tafel plot of the true kinetic current at 1600 rpm, for comparison data for Pt(111) under the same conditions are included as well

For the discussion of the data, however, it is convenient to start at the mixed kinetic-diffusion control potential region (0.8 V < E < 1 V). Beginning at the positive potential limit almost no reduction current can be observed on the disk electrode due to the slow kinetics of the ORR. Sweeping the potential negatively, the current increases due to the lowering of the activation energy when shifting the Fermi level of the electrode, before reaching the diffusion

limited current I_D, which is controlled by the mass transfer of the reacting species, i.e. O_2, to the surface. Below ca. 0.3 V, however, the disk current is decreasing again. This decrease in the disk current is concomitant with the detection of peroxide on the ring electrode (see Figure 5.3). Whereas in the potential region positive of 0.3 V essentially no ring currents are detected, below 0.3 V increasing ring currents are measured, i.e. below 0.3 V considerable amounts of peroxide are formed on the disk electrode. This enhanced peroxide formation can be explained by adsorption of H_{upd} and its role as a site blocking species [120].

In Figure 5.3b a Levich-Koutecky plot, derived from the data in Figure 5.3a, is shown. As discussed in the previous chapter, in the potential region of diffusion limited currents, e.g. at 0.4 V, the intercept of the straight line is essentially zero, i.e. the *measured* current density is completely determined by the rate of mass transfer and no (zero) kinetic controlled currents are measured. From the intercepts of the data in the mixed diffusion-kinetic region the kinetic rate constant can be calculated. Here, however, the focus is more on *comparing* the activities of different electrocatalysts towards the ORR rather than deriving absolute kinetic values. Therefore it is more appropriate to calculate the kinetic current densities as a function of the electrode potential using equation (5.5).

In Figure 5.3c the kinetic currents of the ORR at a fixed rotation rate of 1600 rpm on the Pt(111)-Pd electrode are compared in a Tafel plot with the kinetic currents on a bare Pt(111) electrode obtained under the same conditions. Quite obviously, the Pd modified Pt(111) is much more active for the ORR as compared to the unmodified Pt(111) surface (note the logarithmic scale). By comparing the kinetic current densities at 0.9 V, an activity improvement of a factor of ca. 4 can be observed. Keeping in mind that the Pt(111) electrode in alkaline solution was the most active catalyst for the ORR, the catalytic improvement is an *important* new observation, which in the following is investigated in more detail. Note also, that in contrast to bare Pt(111) on Pt(111)-Pd no linear dependency exists between *log I_k* and the applied potential *E*. For Pt(111) in the potential region of mixed kinetic-diffusion control a constant (negative) Tafel slope of ca. 85 mV per decade (mVdec^{-1}) is observed. For Pt(111)-Pd, however, no straight line can be fitted to the kinetic current densities in dependence of the applied potential. In principle the tangent at each point has a different slope. Yet, for a rough estimation of the *range* of the Tafel slopes observed, in the potential region of 0.925 V < E < 0.975 V a negative Tafel slope with ca. 50 mVdec^{-1} is calculated, whereas in the potential region of 0.80 V < E < 0.90 V a negative Tafel slope of ca. 100 mVdec^{-1} is obtained.
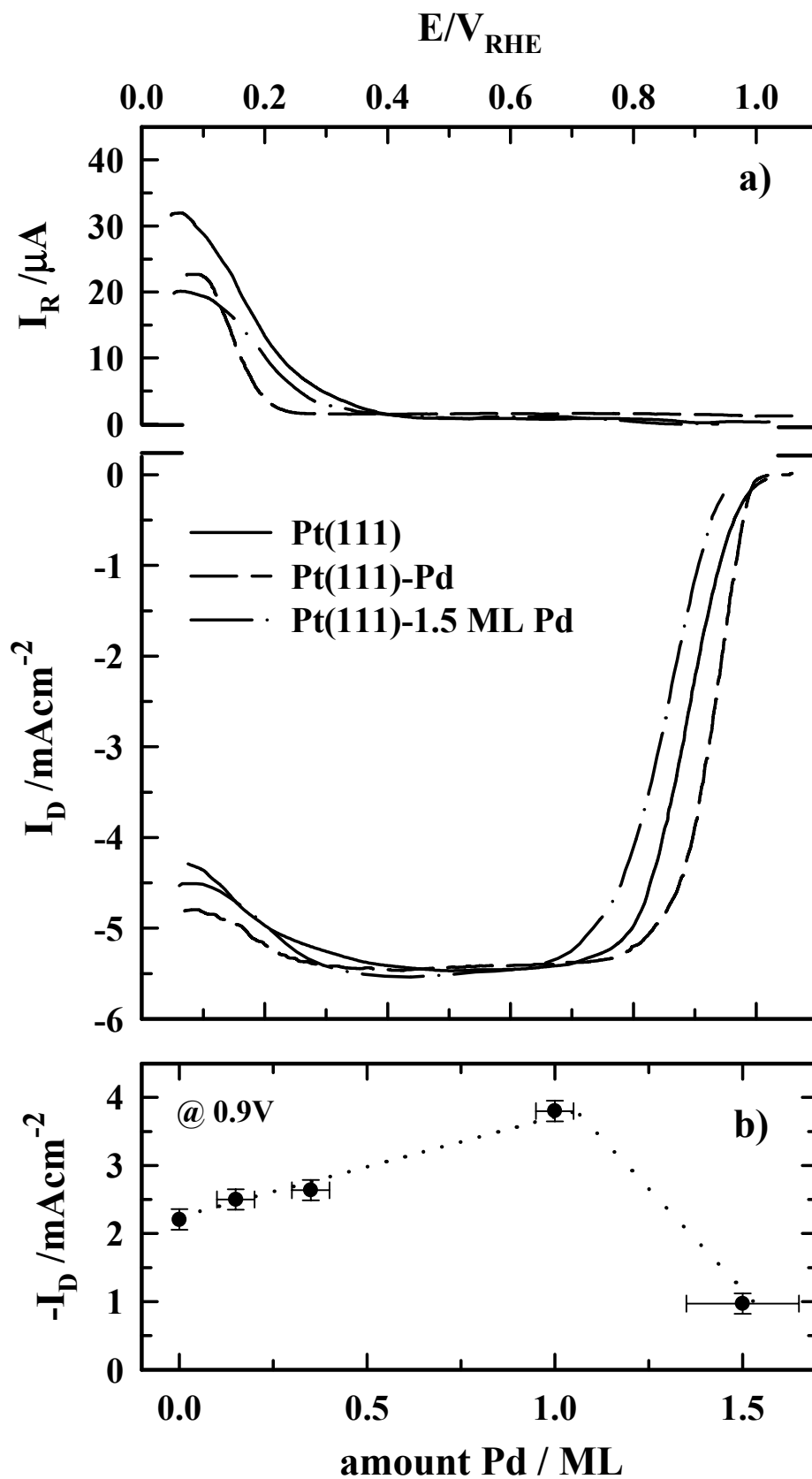
Figure 5.4: a) Polarization curves for the ORR on Pt(111)-xPd disk electrodes (with 0 ≤ x ≤ 1.5) in 0.1 M KOH; 50 mV/s; 293 K; b) corresponding currents at a fixed potential of 0.9 V

In Figure 5.4a the polarization curves of the ORR on Pt(111)-xPd electrodes, with x = 1 and x ≈ 1.5 are compared to the unmodified Pt(111) at a fixed rotation rate. Interestingly, while Pt(111)-1ML Pd is more active than bare Pt(111), the current densities in the mixed kinetic-diffusion potential region, and hence the kinetic rates, are decreasing again if more than one monolayer of palladium is deposited on a Pt(111) electrode. For a palladium film of roughly 1.5 ML coverage the current density of the ORR is drastically lowered and this surface is much less active than the unmodified Pt(111) surface.

Another important observation is the reduced peroxide formation on palladium in the H_{upd} region compared to platinum. In Figure 5.4a it can be seen that on both Pt(111)-xPd surfaces, less peroxide is produced than on bare Pt(111). This observation will be treated later more closely when discussing the reaction pathway of the oxygen reduction. Before that, however, the influence of Pd on the electrocatalytic activity is analyzed.

Of specific interest is the question if the enhanced electrocatalytic activity is a property of the palladium *film* supported on Pt(111) or if Pd is enhancing the reaction rate in some other way, for example by influencing the electronic properties of platinum, in which case only small amounts of palladium would be needed to increase the activity of Pt(111). In order to elucidate the influence of palladium coverage on the improved catalytic activity of Pt(111) further polarization curves of the ORR on Pt(111)-xPd electrodes with, x <1, are recorded. For a convenient test of the activity of different electrocatalysts for the ORR usually the current densities at a fixed potential in the mixed kinetic-diffusion region are compared. Such a plot is shown in Figure 5.4b where the current densities at 0.9 V are plotted against the palladium coverage of the film. Although the data are only limited, clearly the increase of the electrocatalytic activity with the palladium coverage of the film can be seen with the maximum in activity towards the ORR when a full monolayer of palladium is completed on the Pt(111) electrode, but no three-dimensional Pd islands are formed. Since palladium is growing in islands on the Pt(111) surface, it is obvious that the high electrocatalytic activity towards the oxygen reduction is a property of the pseudomorphic monolayer of Pd deposited on Pt(111). For a further elucidation of the properties of the Pt(111)-Pd surface also time dependent measurements have been conducted.

In contrast to acid solution, in alkaline solution the oxidation reduction currents are not stable over a longer period of time, rather than a decrease in the current density can be observed when halting the potential in the mixed kinetic-diffusion control region. This behavior is shown in Figure 5.5 for the Pt(111)-Pd surface. The initial polarization curve is compared to the current densities at fixed potentials when the potential is halted for ten minutes. After ten minutes the further decrease of the current densities is only small, and

therefore these points represent the quasi steady state activity of the Pt(111)-Pd electrode towards the ORR in alkaline solution.
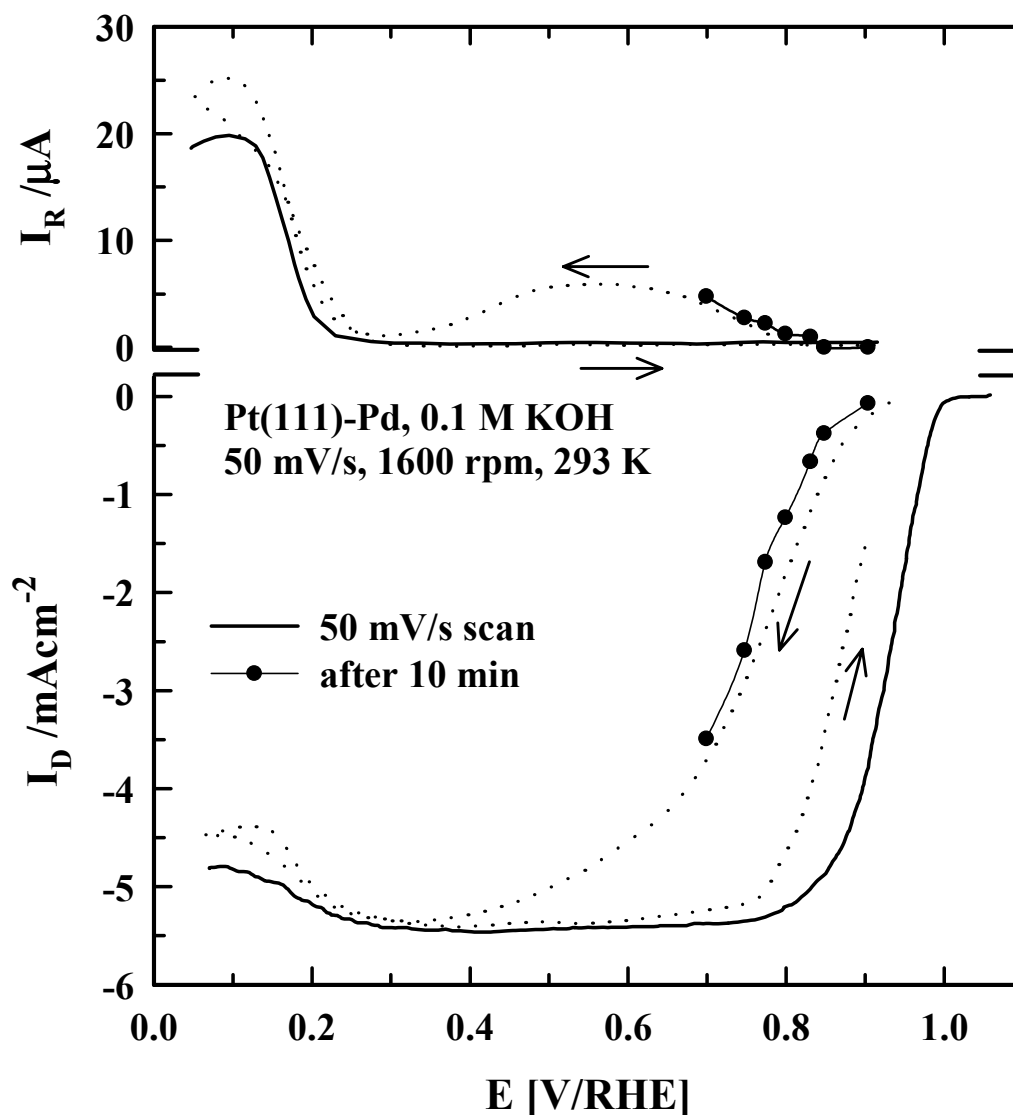
Figure 5.5: a) Polarization curve for the ORR on a Pt(111)-1ML Pd disk electrode in 0.1 M KOH; 50 mV/s; 293 K; the thick dots indicate the remaining current density 10 min after halting at a fixed potential when coming from the lower potential limit; the dotted line represents the polarization curve of the remaining activity at the end of the measurements

For recording the "fixed points" always the same procedure has been applied. Beginning at 0.95 V the potential is scanned to 0.05 V, where the potential is halted for 30 s in order to reduce all surface oxides. Then the potential is scanned to the respective point and is stopped for ten minutes and the disk and ring currents are recorded. Subsequently, the potential is swept to the start potential and the measurement is repeated with a new fixed

value. During the whole measurement the electrode rotates with 1600 rpm and the scan rate is 50 mV/s. The "fixed potentials" begin with the lowest value of 0.7 V and are successively increased by 50 mV. The dotted line is the polarization curve measured at the end of the whole experiment and indicates the remaining activity of the surface towards the ORR.

From Figure 5.5 it is obvious that the polarization curves, recorded with 50 mV/s, represent only transient behavior, the oxygen reduction rate being drastically decreased after ten minutes. The deactivation of the surface can, at least in parts, be reversed when reducing the metal surface at lower potentials. From the dotted line, however, it is obvious that after *several* halts at the chosen potentials, the initial activity of the surface can not be *completely* restored. As observed for the deviation of the current densities from the diffusion limited value in the H_{upd} region, the deactivation with time at a fixed potential is concomitant with the detection of peroxide oxidation on the ring electrode. In fact when halting the potential a clear correlation of the *increase* of the peroxide formation with time and the *decrease* of the O_2 reduction current is observed. However, after reducing the metal surface at negative potentials again no peroxide formation can be detected on the ring electrode (see dotted line of ring current in Figure 5.5). Note, that the shown behavior is not unique to Pt(111)-Pd electrodes, because it is observed on bare Pt(111) as well. Further measurements have revealed (not shown) that the rate of deactivation at 293 K is almost the same on Pt(111)-Pd and Pt(111), whereas at elevated temperatures (333 K), in the temperature range of fuel cell operation, a considerable increase in the stability of Pt(111)-Pd towards oxidation compared to Pt(111) is observed. Consequently, the observed quasi steady state current densities for the ORR at 333 K are about two times higher on Pt(111)-Pd than on Pt(111).

5.2.2 Discussion: ORR in alkaline solution

The experimental results in the previous section clearly demonstrate the enhancement of the electrocatalytic activity of Pt(111) towards the ORR in alkaline solution if the electrode is modified by a pseudomorphic palladium monolayer. This is an *important* result since up to now Pt(111) *was* the most active catalyst in alkaline solution.

Analyzing the findings, at first, we will concentrate on the discussion of general aspects observed on all surfaces in the potential region of mixed kinetic-diffusion controlled current densities. At potentials positive of the H_{upd} region, based on previous work [120], it has been suggested that the structure sensitive kinetics of the ORR on Pt(hkl) in KOH solution mainly arises from the structure sensitive adsorption of OH_{ad} on the different surface orientations and that oxide formation is strongly inhibiting the reaction. The latter conclusion is clearly supported by the experimental findings when halting the electrode potential at a fixed value and investigating the deactivation of the electrode (see Figure 5.5). Based on

equation 5.1, the kinetic current of the ORR is determined mainly by the availability of free adsorption sites, that is the $(1-\theta_{ad})^x$ term, and/or by the change of Gibbs energy of adsorption of reaction intermediates with Θ_{OHad} ($r_{OHad}\Theta_{OHad}$ term in equation 5.1). In chapter 4 it is shown that OH$^-$ adsorption takes place even in the H$_{upd}$ potential region. Under the experimental conditions applied for the oxygen reduction (scan rate of 50 mV/s) at higher potentials the Pt(111)-Pd surface is almost completely covered by OH$_{ad}$ (see Figure 4.2). The observed decrease in activity, however, is a rather slow process (compared to the adsorption process of OH$^-$ anions) and therefore the deactivation can be unambiguously assigned to the slow oxidation process of the surface. Unfortunately, very little is known about the formation of surface oxides. Even the difference between reversible OH$_{ad}$ and irreversible formation of oxygenated species is far from clear. Discussing these terms one has to keep in mind that under electrochemical conditions the surface is under constant interaction with molecules from the electrolyte, and hence, the analytical tools are only limited. The following discussion is therefore mainly based on suppositions that are, however, always consistent with the experimental observations.

At first the simplified case is considered, in which oxygen adsorption takes place only at "bare" metal sites. Consequently, the irreversible form of adsorbed oxygenated species (or surface 'oxides') effectively blocks the available adsorption sites for molecular oxygen. In contrast, the reversible form of OH$_{ad}$ has no site blocking effect. In fact, these two properties can be used to define the term irreversible and reversible form of oxygenated species. That is, only a surface covered with the reversible form of OH$_{ad}$ can be active for the oxygen reduction. Once the irreversible 'oxide' is formed at more positive potentials, the surface looses its activity towards the ORR, i.e., the kinetics of oxygen reduction of the electrocatalysts (by definition) closely follows the tendency of the surfaces to become strongly (irreversibly) oxidized in alkaline solution.

Based on the kinetic model given in chapter 5.1.2 these suggestions can be discussed using equation 5.1. As mentioned, the rate determining step of the ORR seems to be the addition of the first electron to O$_{2,ad}$ to form a superoxide radical (O$_{2,ad}$)$^-$. Among the factors affecting the rate with which this reaction step occurs is, most importantly, the availability of free Pd (Pt) sites. The adsorption behavior of OH$^-$ (as well as other anions from the supporting electrolyte such as sulfate or chloride) is considerably different on Pt(111)-Pd and bare Pt(111), respectively. It is therefore proposed that, although the formation of the reversible form of OH$_{ad}$ on Pt(111)-Pd is increased, the formation of irreversible surface oxides, blocking the reaction sites, is lower on Pt(111)-Pd than on bare Pt(111). Consequently, the number of free adsorption sites ($(1-\Theta_{ad})^x$ term) is strongly affected when modifying Pt(111) with a palladium monolayer resulting in considerably distinct activities. One argument pointing in this direction is the fact, that the order in activity of the different low index Pt(hkl)

electrodes is found to be directly correlated with the adsorption properties of OH⁻ and the tendency of the surface to become strongly oxidized [120]. On the other hand, the structure sensitivity of the adsorption energy of the reactive intermediates ($r_{ad}\Theta_{ad}$ term) seems to play only a minor role.

When reducing the surface oxides by sweeping to cathodic potentials the activity of the surface can, at least partially, be restored. The fact that the electrocatalytic activity cannot be completely restored after the series of measurements by reduction of the oxides can be assigned to some degree of surface roughening on the palladium film. The experimental findings suggest that this deactivation mechanism is valid for Pt(111) as well as for Pt(111)-Pd. However, the remaining activity shows, that the palladium film is *much* more stable towards irreversible oxidation and the concomitant surface roughening than bare Pt(111), especially at elevated temperatures. For Pt it is well known that when applying oxidation-reduction cycles the cyclic voltammetry of Pt(hkl) electrodes is irreversibly altered (see review of Pt(hkl) preparation by Clavilier in reference [121]). This observation is generally attributed to a place exchange between platinum surface atoms and oxygenated species during the oxidation process. When the oxides are reduced, pits remain in the surface, which are not refilled by platinum atoms due to their low mobility. Based on the results presented here such a site exchange process seems not to be active on the (ideal) palladium film and, hence, the oxide formation causes (almost) no roughening of the surface. Indeed, the same conclusion of an enhanced stability has been reported on the basis of SXS measurements in acid solution [49]. And very recent (still unpublished) results indicate also for alkaline solution an enhanced stability towards roughening of the palladium film [122]. Consequently, based on the discussion above, the tendency of a surface to become strongly oxidized may be directly correlated with the surface roughening during oxidation.

The steady state measurements show that both platinum and palladium are not noble in alkaline solution. Keeping in mind that very little is known about oxide formation (under electrochemical conditions) on either surface Pt(111)-Pd and bare Pt(111) another hypothesis concerning the high catalytic activity of Pt(111)-Pd may be given. On Pt(111)-Pd the oxide may cluster thereby forming islands of oxide and islands of "bare" metal sites. Due to the weaker Pt-OH interaction and presumably higher repulsive interaction between OH$_{ad}$ on Pt(111) the irreversible oxide layer (OH$_{irr}$) may be in a form which for the same amount of OH$_{irr}$ covers more reactive sites on Pt(111) than on Pt(111)-Pd.

Another important aspect in kinetic studies is the reaction mechanism. Elucidating the *pathway* of the oxygen reduction reaction at first the Levich-Koutecky plot in Figure 5.3 is analyzed. The slope of the straight line is in the order of 7.2 and 6.1 $(mAcm^{-2})^{-1}/rpm^{1/2}$ at

0.4 and 0.9 V, respectively. Considering the area of the electrode of 0.283 cm^2, a *B* factor of $3.93 \cdot 10^{-2}\, mA\,/\,rpm^{-1/2}$ and $4.6 \cdot 10^{-2}\, mA\,/\,rpm^{-1/2}$, respectively, is obtained. This value fits well, especially in the potential region of diffusion limited currents, with the theoretical value of $3.99 \cdot 10^{-2}\, mA\,/\,rpm^{-1/2}$ for a four-electron reduction using literature data for O$_2$ solubility, $c_0 = 1.21 \cdot 10^{-3}$ *mol/L*, viscosity $v = 1.0008 \cdot 10^{-2}$ *cm^2/s* and oxygen diffusivity, $D = 1.86 \cdot 10^{-5}$ *cm^2/s* [123, 124]. A similar value, $4.0 \cdot 10^{-2}\, mA\,/\,rpm^{-1/2}$, is found for bare Pt(111) under the same conditions [111]. This is a further indication that the oxygen reduction pathway is the same on Pt(111) and Pt(111)-Pd. However, it cannot be distinguished between a direct four-electron reduction and a serial four-electron pathway (see Figure 5.1)

For a further discussion, it is instructive to examine the ring currents during the deactivation process. In the polarization curves (see Figure 5.3) no peroxide oxidation currents can be detected on the ring electrode in the potential region of mixed kinetic-diffusion control as well as in the diffusion limited current region. In Figure 5.5, however, it can be seen that when halting the potential in the mixed kinetic-diffusion region, concomitantly with the decrease in the disk current, the peroxide detected on the ring electrode is increasing. Based on the scheme in Figure 5.1, the consequence of the oxide formation on the surface in a serial pathway is simply a decrease in the available pairs of adsorption sites (note, that an adsorption site is not necessarily identical to only one atom) needed for the breaking of the O-O bond in the peroxide species. Consequently, the amount of peroxide which is further reduced to water is decreasing and the amount of peroxide which is desorbed from the surface is increasing. In other words the term $(1-\theta_{ad})^x$ in equation 5.1 determines the ratio of the rate constants of the "four electron serial pathway" (reduction to water, k_3) and the "two electron pathway" (desorption of peroxide, k_5).

In the H$_{upd}$ region on the palladium films is always *less* peroxide detected than on bare Pt(111). This observation is not unique to platinum, but is also observed when increasing the electrocatalytic activity of gold single crystals towards the ORR by modifying the surface with palladium [116]. Furthermore, temperature dependent measurements have shown that the activity of Au(hkl) [116] and Pt(hkl) [111] towards oxygen reduction closely follows the ability of reducing peroxide which is intentionally added to the solution. All these findings directly point to the importance of the reduction of peroxide intermediates (k_3 in the reaction scheme) in the overall oxygen reduction process. It appears, that the ORR mainly proceeds through the serial pathway ($k_2 + k_3$) (see scheme in Figure 5.1) with the intermediate formation of peroxide species.

Therefore, a second factor (besides the availability of free adsorption sites) affecting the electrocatalytic activity towards oxygen reduction may be the ability of a catalyst to further reduce peroxide to water. The electrochemical decomposition of HO$_2^-$ (k_3) involving

the cleavage of the oxygen-oxygen bond appears to be a highly activated process. On the basis of measurements on gold and platinum single crystal electrodes it has been proposed that the electrochemical reduction of peroxide is significantly catalyzed by the Pt-OH and Au-OH layer, respectively [116]. This conclusion fits with the observations presented in this work and may also account for the exceptionally high activity of the Pt(111)-Pd surface. As discussed in chapter 4, Pd has a higher oxophilicity than platinum. It has been shown that the amount of OH_{ad} is increasing with the Pd coverage, however, from the observed deactivation process of the Pt(111)-Pd surface it is evident that the irreversible oxide formation on Pt(111)-Pd is slower than on bare Pt(111). That means on the pseudomorphic palladium film over a wide potential range a high coverage of reversible adsorbed OH_{ad} is obtained. Therefore in line with the results obtained on gold single crystals by Schmidt et al. [116], it may be that the higher oxophilicity of Pd is increasing the activity of the Pt(111) surface towards the ORR. However, criterions what kind of physical properties adsorbed OH_{ad} must exhibit in order to become catalytically active for peroxide reduction are by far not clear and certainly further work is needed to answer this important question unambiguously, but most likely the OH_{ad} coverage, adsorption energy, and the electronic configuration of the modified metal surface play a central role.

Therefore, an important question is whether the high activity of the pseudomorphic palladium film towards the oxygen reduction is an intrinsic property of bulk palladium, or whether the underlying substrate is substantially influencing the electronic properties of the thin Pd film in such a way that the ORR is increased. Unfortunately due to the difficulties in preparing Pd single crystal electrodes, there are no experimental data to answer this question unambiguously. Electro-polishing of Pd(hkl) electrodes leads to rough surfaces and consequently different electrocatalytic properties. On the other hand electrochemical deposition of more than one monolayer of palladium on Pt(111) yields a three-dimensional growth and therefore also rough surfaces. Consequently, the observed decrease in the catalytic activity when more than one monolayer of palladium is deposited does not implicitly contribute to answer the above question. The decrease with the palladium coverage if more than one monolayer is deposited appears to be too high as to be ascribed to electronic effects. Therefore, it is suggested that the three-dimensional growth mode, which sets in at $\theta_{Pd} > 1$, is responsible for the deactivation of the surface. Most reasonably the steps, which are introduced by the deposition, are favoring the formation of surface oxides and, hence, are inhibiting the oxygen reduction. Therefore the deactivation is following the same mechanism which is accountable for the order of activity of Pt(hkl) electrodes towards the ORR in alkaline solution, decreasing from $(111) > (100) > (110)$ [116, 120]. This explains also that the initial activity of the surface cannot be completely restored, when reducing the surface oxides at cathodic potentials, due to the introduction of defects to the surface.

Previous work on pseudomorphic palladium films on different substrates conducted in UHV by Goodman et al. shows that the electrocatalytic activity of a thin metal film supported on another metal substrate can be considerably higher than both the unmodified substrate as well as the respective bulk single crystal of the film material [125]. However, in the case of Pt(111)-Pd there is a lack of UHV studies concerning the electronic properties of the thin metal film. The more or less linear increase of the current density at 0.9 V with the palladium coverage, however, gives a hint that indeed the properties of the *system* Pt(111)-Pd are important, i.e. the underlying substrate does influence the electronic and, hence, the electrocatalytic activity of the pseudomorphic palladium film.

At last, the deviation of the diffusion limited current in the H_{upd} region will be shortly discussed. As already mentioned in the polarization curves recorded with a scan rate of 50 mV/s, in the mixed kinetic-diffusion control region and in parts of the diffusion limited current region, no peroxide oxidation currents can be detected on the ring electrode. However, scanning the potential in the H_{upd} potential region the disk currents deviate from the diffusion limited value. This decrease in the disk current is concomitant with the observation of peroxide oxidation currents on the ring electrode. Therefore at low potentials the deviation of the disk current can be quantitatively related to the formation of HO_2^- (in alkaline solution), and consequently, following the previous conclusions, to a change of the reaction pathway from a serial four-electron pathway to a two-electron pathway (see Figure 5.1). This behavior can be observed for the unmodified Pt(111) electrode as well as for the various Pt(111)-xPd electrodes. However, comparing the amount of peroxide formation in the H_{upd} region on the Pt(111) and Pt(111)-Pd surface it can be seen, that on the palladium covered surface less peroxide is produced. This smaller peroxide production is concomitant with a smaller deviation of the disk current in the H_{upd} region from the diffusion limited value compared to the bare Pt(111) electrode. Considering the previous result that at low potentials Pt(111)-Pd is covered by a complete monolayer of H_{upd} in contrast to about 0.66 ML H_{upd} formed on bare Pt(111), this is a surprising result. Since only limited data are available and the nature of adsorbed hydrogen on Pt(hkl) and especially on Pt(111)-Pd is not known, one can only speculate about the ultimate cause of this finding. One possible explanation may be a higher adsorption energy of HO_2^- (at low potentials) on the Pt(111)-Pd surface than on the bare Pt(111) surface acting as a catalytic driving force for the breaking of the O-O bond. Furthermore, a higher defect density on the Pd film may lead to an increase in the number of active sites required for the dissociative adsorption of HO_2^-.

From the discussion above it is clear, that there are many open questions which have to be solved in order to explain the exceptionally high catalytic activity of the Pt(111)-Pd

surface towards the ORR in alkaline solution. Since previous measurements described in the literature concerning the ORR on a Pt(111)-Pd electrode in *acid solution* reported a *decreased* catalytic activity in comparison to the bare Pt(111) electrode, in this work further measurements were conducted in perchloric acid solution in order to elucidate the reason for the inhibiting effect of acid solutions on the Pt(111)-Pd surface.

5.3 ORR: Anion effect

In this section the focus is on the inhibiting effect of specifically adsorbed anions on the kinetics of the ORR. Measurements are performed in perchloric acid solution containing various amounts of chloride anions, which are *intentionally* added to the solution. Considering that high-surface area catalysts are often synthesized from halide containing educts and that trace levels of chloride may also be present in the water contained in the fuel cell feed-stream [126-128], the effect of Cl$^-$ on the catalytic activity is not only important from a theoretical point of view, but also of great practical importance [105].

5.3.1 Measurements

In Figure 5.6 polarization curves of the Pt(111)-Pd and the unmodified Pt(111) surface are compared in different O$_2$ saturated solutions. The measurements in sulfuric acid solution and perchloric acid solution are taken from reference [46]. From Figure 5.6 a clear correlation between the adsorption strength of the anions in the supporting electrolyte and the activity towards the ORR can be observed on *both* surfaces. In sulfuric acid solution the inhibition of the oxygen reduction is the highest of the three solutions, whereas at both surfaces in alkaline solution the highest activity can be observed. This observation is not new and has been noted previously. What is important to note, however, is that the adsorption strength of the anions in the supporting electrolyte *also* affects the *rank order* in the activity of the two surfaces. That is, in sulfuric acid solution a large difference in activity of unmodified Pt(111) and Pt(111)-Pd can be observed. The currents in the potential region of mixed kinetic-diffusion control are considerably inhibited on Pt(111)-Pd compared to Pt(111) under the same experimental conditions. On Pt(111)-Pd no diffusion limited current can be observed even at low potentials. In perchloric acid solution the difference in activity of the two surfaces is considerably smaller, but still Pt(111) is more active than Pt(111)-Pd. Eventually, in alkaline solution the activity of the Pt(111) surface is increased by the pseudomorphic palladium monolayer (see Figure 5.6). This interesting observation is further investigated in the following.

Figure 5.6:Polarization curves for the ORR on Pt(111)-1ML Pd disk electrode and corresponding peroxide oxidation current on the ring electrode in a) 0.05 M H₂SO₄, b) 0.1 M HClO₄ and c) 0.1 M KOH. The dotted line represents unmodified Pt(111) under the same conditions; 50 mV/s; 293 K

At first, a closer look is taken at the ORR on Pt(111)-Pd as well as on unmodified Pt(111) in pure perchloric acid. Figure 5.7 shows the polarization curves in O_2 saturated perchloric acid solution when the same experimental procedure is applied as in the measurements in alkaline solution. That is, before beginning the potential sweep the surface is held for 30 s at the start potential, here 0.9 V, before scanning the potential to the negative limit and then directly back to the anodic limit. The ring is potentiostated at 1 V.
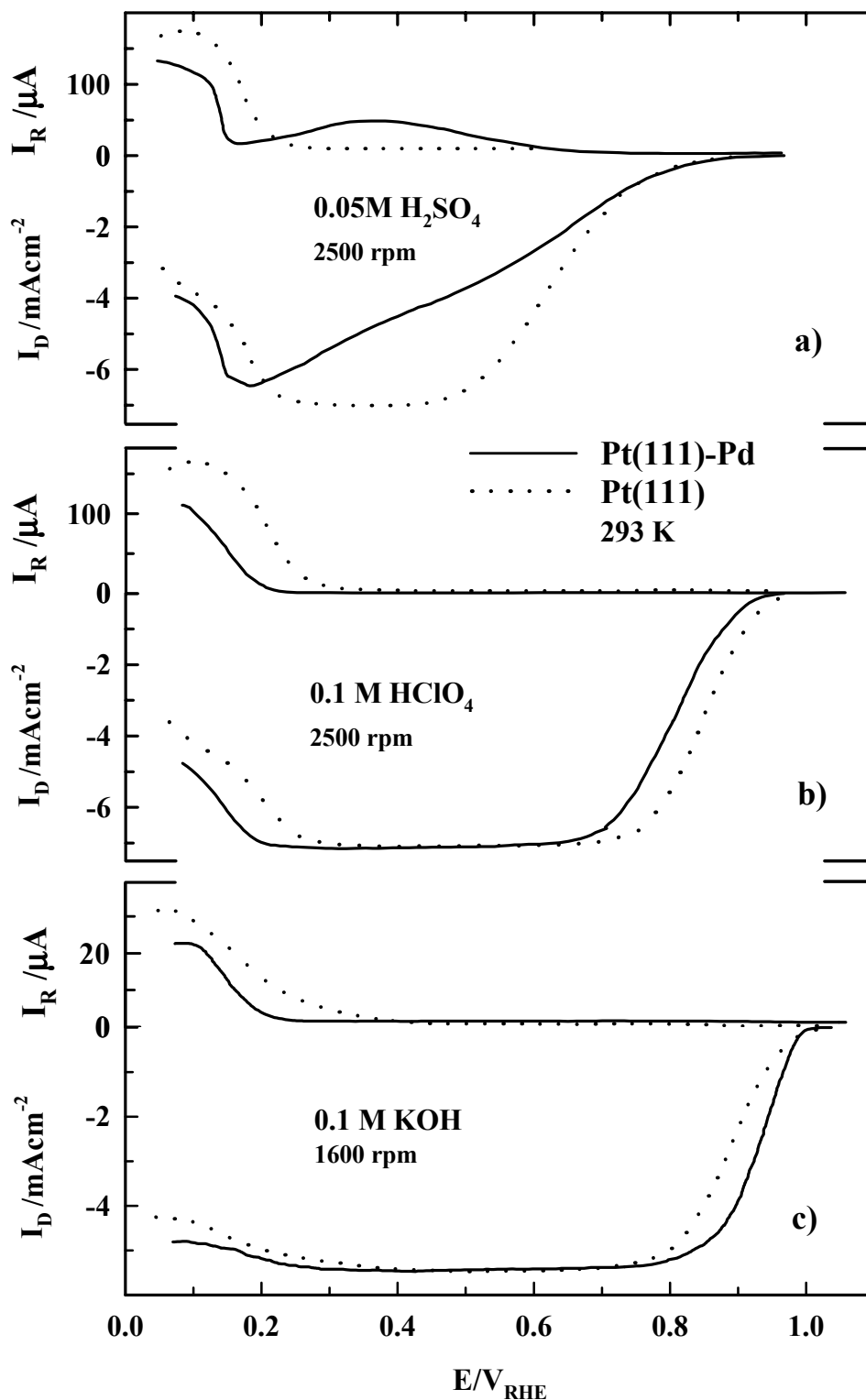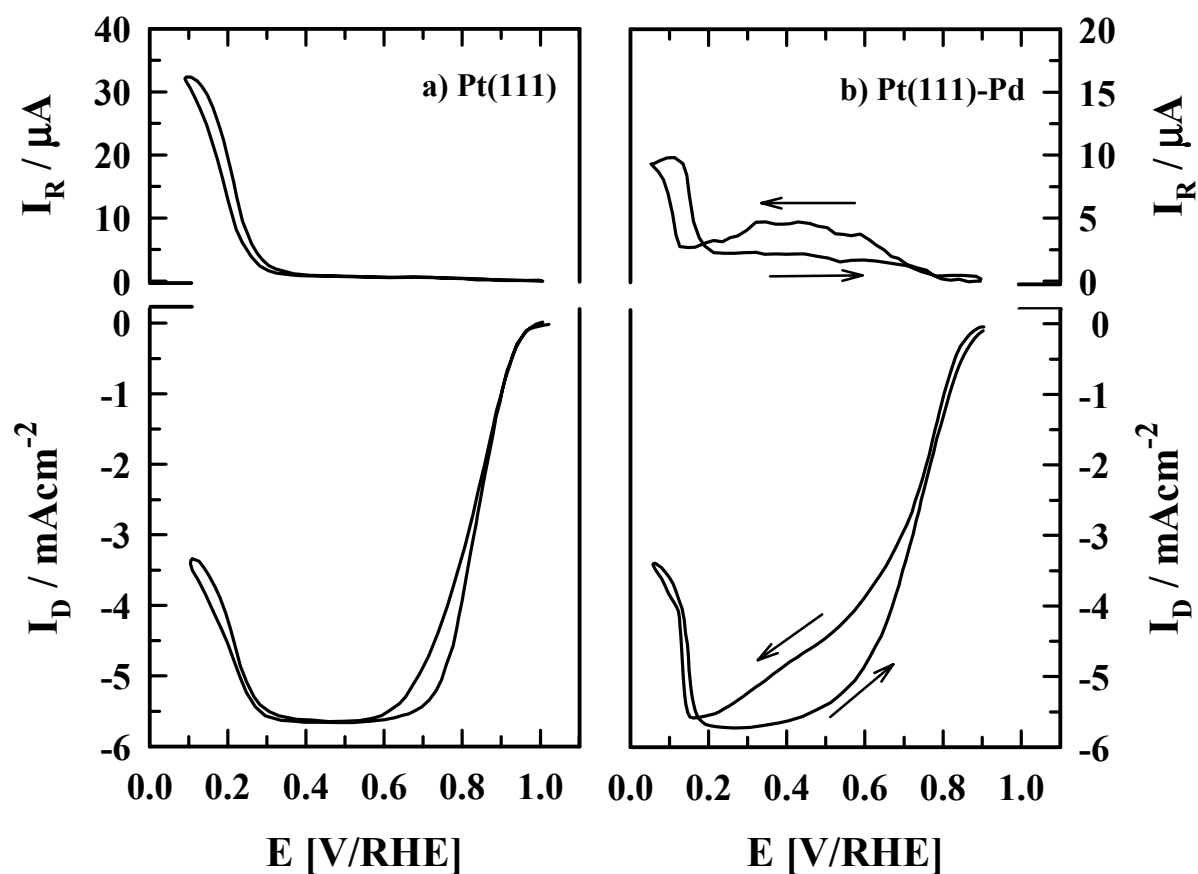

Figure 5.7: Polarization curve for the ORR on a Pt(111)-1ML Pd disk electrode and corresponding peroxide oxidation current on the ring electrode in 0.1 M HClO₄; the anodic and cathodic scan, respectively, are indicated by an arrow; 1600 rpm; 50 mV/s; 293 K;

The observed polarization curves are basically identical to those of reference [46], where the anodic potential sweep is shown. In contrast to Figure 5.6, however, here both the anodic and cathodic sweep of the polarization curve are shown. From Figure 5.7b it is obvious that on Pt(111)-Pd even in acid solution, where in the investigated potential region of 0.1 V < E < 0.9 V no oxide formation takes place (see voltammogram in Figure 4.6), the polarization curves of the anodic and cathodic potential sweep are remarkably different. It can be seen that the current densities in the cathodic sweep are considerably inhibited. This

inhibition is also reflected in the production of peroxide, detected on the ring electrode, in the potential region of mixed kinetic-diffusion control. By contrast, in the anodic scan peroxide formation virtually takes place only in the H_{upd} potential region. Although on bare Pt(111) a difference in the polarization curves between the anodic and cathodic sweep is observed as well (see Figure 5.7a), it is rather *small* compared to the difference observed on Pt(111)-Pd. Especially in the potential region of mixed kinetic-diffusion control on Pt(111) no ring currents can be observed in the anodic as well as in the cathodic potential sweep.
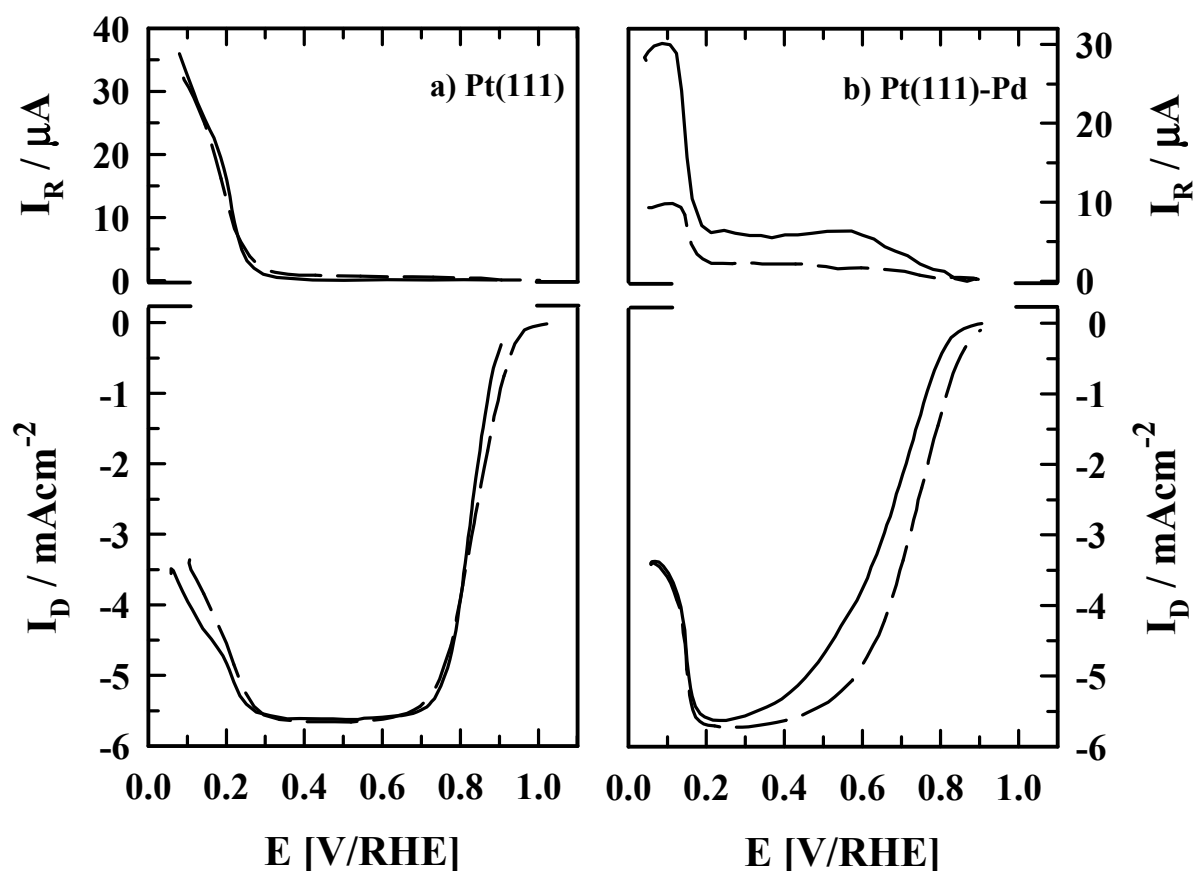

Figure 5.8: Polarization curves for the ORR on a Pt(111) (a) and Pt(111)-1ML Pd (b) disk electrode and corresponding peroxide oxidation current on the ring electrode in 0.1 M HClO$_4$ (dashed line) and 0.1 M HClO$_4$ + 10^{-6} M HCl (full line); 50 mV/s; 293 K;

From the previous discussion of the CO oxidation reaction on the Pt(111)-Pd electrodes introduced in chapter 4 it is reasonable to suggest that the increased anion adsorption on Pd inhibits the ORR on the Pt(111)-Pd surface in acid solution more strongly than on the bare Pt(111) electrode. Therefore, in order to resolve the difference in the ratio of the activity of the Pt(111)-Pd surface and the unmodified Pt(111) surface towards the ORR in the different solutions, additional measurements in perchloric acid solution are recorded. As

in the experiments introduced in chapter 4.3, in the following measurements very *small* amounts of chloride are intentionally added to the perchloric acid solution. The experimental procedure was the same as in alkaline solution and for the sake of simplicity only the polarization curves of the anodic potential sweep are shown. In Figure 5.8 the polarization curves of Pt(111)-Pd electrodes in O_2 saturated perchloric acid solution (at a rotation rate of 1600 rpm) are compared to those of bare Pt(111). The corresponding ring currents are included as well. The dashed line is recorded in "pure" perchloric acid solution, whereas the full line represents the measurements where 10^{-6} M HCl are added to the solution. In contrast to the findings where higher amounts of chloride (10^{-3} M HCl) [118] were added on Pt(111) the ORR is not affected by such very *small* amounts of chloride impurities in the solution. The disk as well as the ring currents observed in the two solutions are practically identical (see Figure 5.8a). On the pseudomorphic palladium film, however, the oxygen reduction in the mixed kinetic-diffusion control potential region is considerably inhibited by even extremely small amounts of chloride in the solution. In Figure 5.8b it is shown that in 0.1 M $HClO_4$ + 10^{-6} M HCl solution the diffusion limited current is only obtained in a narrow potential range at potentials positive of the H_{upd} region (0.2 V < E < 0.25 V). Concomitantly, at the ring electrode increased peroxide oxidation currents can be observed. Whereas in the "pure" perchloric acid solution peroxide is formed at the Pt(111)-Pd electrode only in the H_{upd} region, when small amounts of chloride are added to the solution peroxide formation can be observed almost in the whole potential region (0.05 V < E < 0.8 V).

These results are consolidated by the graph shown in Figure 5.9a where the kinetic currents for the ORR on Pt(111)-Pd in perchloric acid solution containing different amounts of chloride are calculated using equation (5.5). From these results a clear correlation between the concentration of strongly absorbing anions in the supporting electrolyte is evident. The kinetic currents at a fixed potential of 0.75 V are decreasing with a factor of two and four when 10^{-6} M HCl and 10^{-5} M HCl, respectively, are added to the perchloric acid solution. From the corresponding ring currents depicted in Figure 5.9b the correlation between the inhibition of the ORR and the amount of peroxide, as discussed for alkaline solution, is established. In the solution containing 10^{-5} M HCl large amounts of peroxide are produced in the potential region of mixed kinetic diffusion control (0.2 V < E < 0.8 V), whereas in pure perchloric acid solution only in the H_{upd} region considerable peroxide oxidation currents can be detected on the ring electrode. Interestingly, also in the H_{upd} potential region a correlation between the ring currents and the chloride concentration in the electrolyte is observed although identical disk currents are recorded (see Figure 5.8).
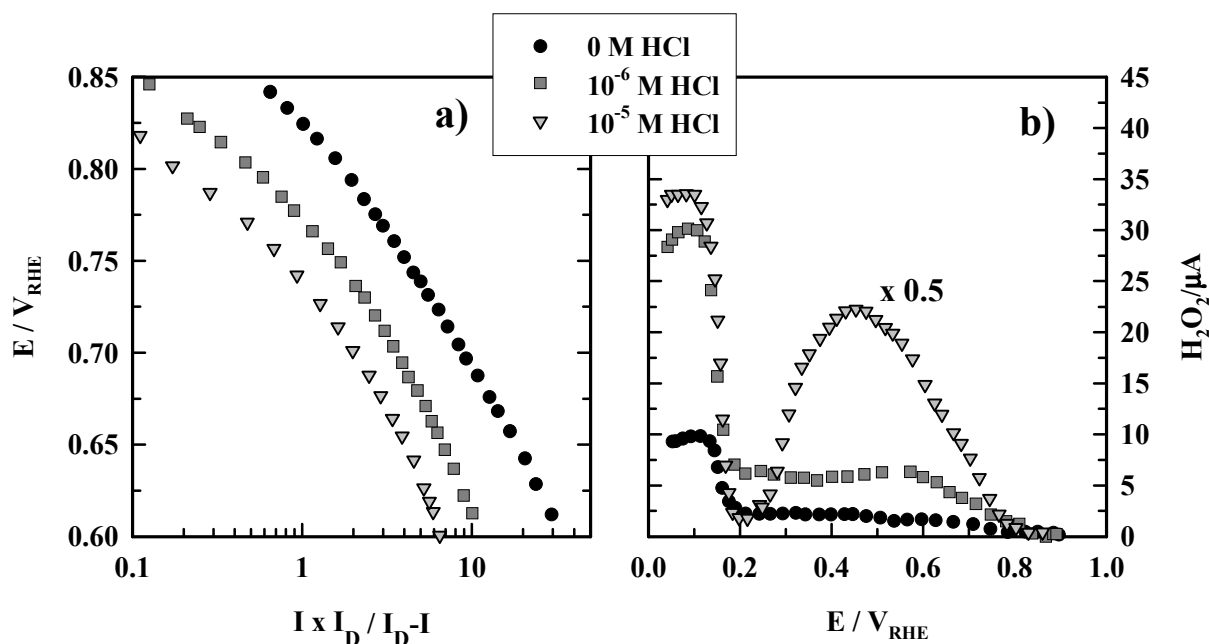
Figure 5.9: a) Kinetic currents of the ORR on a Pt(111)-Pd electrode in 0.1 M HClO$_4$ containing different amounts of chloride; b) corresponding ring currents

It is important to note, that as in the case of alkaline solution only current transients, are recorded. This has been already obvious from the measurements in pure perchloric acid solution where a difference in the current densities in the anodic and cathodic potential sweep was found (see Figure 5.7b). When introducing chloride into the solution this effect is even more pronounced. In perchloric acid solution after 1 minute steady state currents are observed. In contrast to the nonlinear behavior of the applied potential vs. the kinetic currents shown in Figure 5.9a in the steady state currents constant Tafel slopes of about (125 ± 10) mVdec^{-1}, are observed, independent of the amount of chloride added to the solution.

5.3.2 Discussion: ORR anion effect

The comparison of the polarization curves of Pt(111) and Pt(111)-Pd in the different solutions reveals that in acid solution specific anion adsorption plays a fundamental role in the electrocatalytic activity of a catalyst. The measurements presented in this section clearly document the high sensitivity of the Pt(111)-Pd surface to trace impurities. In fact Figure 5.6 suggests that the intrinsic electrocatalytic activity towards oxygen reduction of the Pt(111)-Pd surface is considerably higher than the one of the bare Pt(111) surface. However, since in acid solution even extremely small amounts of chloride contaminations inhibit the Pd atoms, this

increased catalytic activity is apparent only in alkaline solution. Figure 5.8 clearly reveals that Pt and Pd have a different affinity towards chloride contaminations. This fact is for example also reflected in the higher bond energy in PdCl than in PtCl compounds [129]. Following the line of the discussion of chapter 4, it is proposed here, that in "pure" perchloric acid solution chloride contaminations in the order of 10^{-7} M cause an inhibition of the Pt(111)-Pd surface, which otherwise would be more active towards the ORR than bare Pt(111). The inhibiting effect is directly correlated to the concentration of strongly adsorbing anions in the supporting electrolyte.

As discussed in the previous section based on equation 5.1, the kinetic current of the ORR is determined mainly by the availability of free adsorption sites, that is the $(1-\theta_{ad})^x$ term, and/or the change of Gibbs energy of adsorption of reaction intermediates with Θ_{OHad} or spectator species Θ_{anions} ($r_{ad}\Theta_{ad}$ term in equation 5.1). The chloride coverage independent Tafel slope at steady state conditions is a strong indication that the adsorption energy of the reaction intermediates is not affected by the specific adsorption of anions from the supporting electrolyte rather than a site blocking effect retards the reaction rate. For a discussion of the *mechanism* of the inhibiting effect, here, we closely follow the line given in previous investigations concerning of chloride and copper contaminations affecting the ORR on Pt(hkl) electrodes (note that considerably higher concentrations were used) [118, 130]. In contrast to specific chloride adsorption on Pt(111), on Pt(111)-Pd chloride adsorption clearly affects the reaction pathway, indicated by the chloride concentration dependent H_2O_2 oxidation currents. This difference in the inhibiting effect of chloride can be understood in terms of the stronger Pt(111)-Pd-Cl interaction compared to the Pt(111)-Cl interaction. The strong Pt(111)-Pd-Cl interaction inhibits the desorption of chloride in the potential region of $0.25 < E < 0.8$ V,. leading to a high anion coverage in the potential region of mixed kinetic-diffusion control. This effect can be nicely seen in Figure 5.9b in the solution containing 10^{-5} M HCl where, beginning at the negative potential limit, peroxide formation on the disk electrode follows at first the desorption of the H_{upd} layer and subsequently the adsorption and desorption of chloride. Consequently, the inhibition of the Pt(111)-Pd surface is assigned to a decrease in the number of pairs of adsorption sites required for adsorption of O_2 and the cleavage of the O-O bond ($(1-\theta_{ad})^x$ term in equation 5.1).

The chloride concentration dependent peroxide oxidation currents in the H_{upd} region suggest that chloride coadsorption on Pt(111)-Pd may take place in the H_{upd} potential region. For Pt(111) a similar effect is only found for the strongly adsorbing bromide anion (the Pt(111)-Br_{ad} interaction is stronger than the Pt(111)-Cl_{ad} interaction) [112], whereas on Pt(100), with a stronger Pt-Cl bond than on Pt(111), also chloride affects the reaction pathway [118].

Although these data are obtained in liquid electrolyte, similar effects can be expected in a solid-polymer electrolyte as present in a PEM fuel cell [105]. There chloride impurities on the level of a couple of ppm can be introduced, either due to incorporation into the MEA[12] during the preparation or due to a contamination of the humidified fuel cell feed. Therefore the sensitivity of a electrocatalyst to contaminations is not only of scientific interest but also of practical importance. However, from the obtained measurements final conclusions for a possible application of a Pt-Pd catalyst in a PEM fuel cell are difficult to draw since the adsorption conditions in the solid electrolyte of the PEMFC are not known. If extremely high purity conditions would be required for the MEA preparation and the humidified feed streams these catalyst were most likely unprofitable.

5.4 Summary: ORR

The oxygen reduction reaction on Pt(111)-xPd electrodes, with different amounts of palladium deposited, has been studied in alkaline as well as in perchloric acid solution.

Pt(111)-Pd turned out to be a very interesting model catalyst with exceptionally high activity towards the ORR. In alkaline solution a pseudomorphic monolayer of palladium considerably increases the activity of Pt(111), leading to the up to now most active surface towards the ORR. At submonolayer coverages, the increase in activity is correlated with the amount of palladium deposited, whereas the activity of the surface is rapidly decreasing when three dimensional growth sets in. It is still unclear, however, if the high catalytic activity of Pt(111)-Pd is a property of palladium itself, or if the platinum substrate is critically affecting the electrocatalytic properties.

On both surfaces, bare Pt(111) and Pt(111)-Pd, in the potential region of mixed kinetic-diffusion control, the oxygen reduction reaction proceeds mainly through a serial pathway. As a reason for the exceptional high catalytic activity of Pt(111)-Pd different hypothesis are discussed. The ability of the catalyst to reduce electrochemically peroxide further to water may be a cause for a high electrocatalytic activity. On the pseudomorphic palladium film the reduction of peroxide to water is significantly catalyzed by reversibly adsorbed Pd-OH layers.

---

[12] **M**embrane **E**lectrode **A**ssembly

Presumably at least equally important for its electrocatalytic activity towards the ORR is the tendency of a catalyst to become strongly (irreversibly) oxidized. In alkaline solution the formation of surface oxides inhibits the ORR by reducing the available adsorption sites for O_2 as well as by reducing the number of pairs of free sites, needed for breaking the O-O bond in the peroxide species. As steady state measurements reveal the tendency of Pt(111)-Pd to become irreversibly oxidized is (especially at high temperatures) lower than for bare Pt(111). Concomitantly, the tendency of surface roughening upon oxide formation is reduced on Pt(111)-Pd.

In acid solution specific anion adsorption results in a strong inhibition of the oxygen reduction on Pt(111)-Pd. Whereas in sulfuric acid solution sulfate adsorption is responsible for the inhibition, in perchloric acid solution small chloride contaminations, not the high concentration of perchlorate anions, are responsible for the difference in activity of the ORR on Pt(111)-Pd and on bare Pt(111). The high inhibiting effect of chloride impurities on the ORR can be assigned to the strong chloride interaction with palladium. On Pt(111)-Pd chloride is affecting the reaction pathway of the ORR due to a blocking of pairs of available sites for the cleavage of the O-O bond. In a PEMFC, where in principle no specific anion adsorption takes place from the polymer-electrolyte itself, Pd deposition may increase the activity of Pt. Special attention, however, would have to be paid to the cleanliness, when preparing the MEA with the Pd/Pt electrocatalyst. But the extreme demands in cleanliness most probably would be unprofitable.

Chapter 6

The hydrogen evolution/oxidation reaction

The hydrogen evolution reaction (HER) and the hydrogen oxidation reaction (HOR) are, together with the oxygen reduction reaction, among the most widely studied electrochemical processes. There are several reasons for the great importance of the hydrogen oxidation/reduction reaction. First of all, the mechanism of hydrogen evolution has been considered for a long time as a prototype for heterogeneous reaction kinetics and, hence, the reaction has been studied in order to obtain a systematic view on the catalytic properties of various metals [131, 132]. However, both reactions are also of great technological importance, the hydrogen *evolution* being strongly related to electrolytic hydrogenation of organic substances, corrosion and water electrolysis, e.g. for power backup systems on the basis of fuel cells. The hydrogen *oxidation* is the basic anode reaction in a fuel cell. Despite of the importance and the wealth of investigations, however, the key aspects of the reactions are still not understood sufficiently [133].

In this chapter the hydrogen oxidation/reduction reaction is studied on the Pt(111)-Pd surface in alkaline solution. Although there may be possible applications as a cathode catalyst in fuel cells, the focus of this chapter will be the use of the hydrogen reaction as a test reaction for characterizing the electrocatalytic and electronic properties of the Pt(111)-Pd surface. The investigations are motivated by the interesting catalytic properties of Pd observed in UHV, where it was found that transition metals, such as pure Pd, are good electron donors, and dissociation of H_2 on this surfaces occurs readily at room temperature. In contrast, no dissociation of H_2 has been claimed to occur on Re(0001)-Pd, which was attributed to the charge transfer from the Pd overlayer to the substrate [32, 134]. Therefore the hydrogen reaction may also serve in electrochemistry as a probe of the altering of the electronic properties of the Pd film by the Pt substrate.

The chapter is structured as follows. In the first section details on the hydrogen oxidation/reduction reaction are given. The mechanisms of the reactions are introduced and an overview of the most important results of previous work concerning the HOR/HER on platinum single crystal electrodes is given. Subsequently the experimental results of the HOR/HER on a Pt(111)-Pd electrode in alkaline are introduced. The discussion is held in the

light of previous results of Pt(111) obtained in both, alkaline and acid solution, and Pt(111)-Pd in acid solution. Finally, at the end of the chapter, a brief summary of the results is given.

6.1 Details: HER/HOR

6.1.1 Literature: HER/HOR

Historically, all the basic laws of electrode kinetics as well as the modern concepts in electrocatalysis were developed and verified by examining the hydrogen reaction [135],

$$H_2 \Leftrightarrow 2H^+ + 2e^-$$ (6.1)

The intrinsic kinetic rate of this reaction, expressed by the exchange current density, i_0, is defined as the rate at which the reaction proceeds at the equilibrium potential, that is the potential where the rate constants for the forward and backward reaction are the same, resulting in a zero net current. The exchange current density for the hydrogen reaction varies by 5-6 orders of magnitude depending on the electrode material. Attempts to correlate the exchange current density of the hydrogen reaction with the properties of the electrode substrate date back several decades. A breakthrough [136] with regards to the relationship between *log i_o* and physical properties of the electrode substrates was achieved when Conway and Bockris demonstrated a linear functionality between *log i_0* and the metal's work function, Φ, and attributed this to the relation between Φ and the metal-hydrogen interaction energy [137]. In the meantime, Parsons [138] and Gerischer [139] independently established from the classical transition state theory the correlation between *log i_0* and the Gibbs energy of adsorbed hydrogen (ΔG_{Had}^0), with the general form of this relation having a "volcano" shape. Two decades later, based on the relationship between *log i_0* and the M-H$_{ad}$ bond energy, Trasatti demonstrated that the "volcano" plot for the HER is valid for both metals and non-metals [96, 140].

Whereas the early kinetic studies of the HER/HOR were carried out on polycrystalline electrodes [135] or on platinum single crystals having a poorly defined surface structure [141], the first studies on well defined single crystal electrodes reported that the HER in acid solution is insensitive of the crystallographic surface structure [142-144]. This finding was somehow surprising, taking into account the differences in the work function at the different surface sites [145]. Recently, however, Markovic et al. [146, 147] as well as Conway and coworkers [148, 149] demonstrated that the HER/HOR is indeed a structure sensitive reaction. The structure sensitivity of the reaction is explained on the basis of structure-

sensitive heats of adsorption of the active intermediate, whose physical state, however, is still uncertain (see next section).

Summarizing, the main challenges of the HER/HOR, today, are the elucidation of the physical nature of the reaction intermediate and its relationship to underpotentially deposited hydrogen, H_{upd}. Furthermore the questions how the *absorption* of hydrogen effects the kinetics of the hydrogen reaction as well as why the rate of the HER/HOR is significantly lower in alkaline than in acid electrolytes are still not sufficiently explained [136].

6.1.2 Reaction mechanism and the determination of the kinetic parameters

Based on the comparison of the parameters derived from kinetic studies of the HER/HOR and the coverage of H_{upd} on the surfaces (calculated from cyclic voltammetry), it has been concluded that the reaction intermediate of the HER/HOR is adsorbed hydrogen, H_{ad}, which, however, is *different* in its catalytic properties than the underpotentially deposited H_{upd}. Following Conway's notation, in this thesis the reaction intermediate is called overpotentially deposited hydrogen, H_{opd}, in order to distinguish it from H_{upd}. Unfortunately, up to now very little is known about H_{opd} and it must be stressed that the physical nature of H_{opd} is still unclear and even its existence is a matter of conjecture [120]. However, it is beyond the scope of this work to discuss the nature of the reaction intermediate, and the catalytic activity of the Pt(111)-Pd towards the HER/HOR will merely be described using the above mentioned notation.

Using Conway's notation, the postulated mechanism of the hydrogen oxidation reaction in alkaline solution can then be expressed as follows [136]. The reaction is beginning with a slow Tafel step (Eq. 6.2):

$$H_2 + 2M \rightarrow MH_{opd} + MH_{opd} \tag{6.2}$$

and/or the Heyrovsky step (Eq. 6.3):

$$H_2 + OH^- + M \rightarrow MH_{opd} + H_2O + e^- \tag{6.3}$$
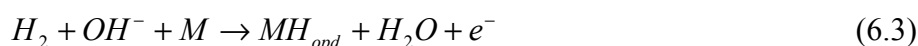
which is followed by a fast Volmer reaction (charge-transfer step (Eq. 6.4))

$$MH_{opd} + OH^- \leftrightarrow H_2O + M + e^- \tag{6.4}$$

Both, the Tafel-Volmer and the Heyrovski-Volmer sequences, require the cleavage of the H-H bond and the formation of adsorbed hydrogen. In order to emphasize the importance of the electrode material in determining the properties of the metal-hydrogen bond, the adsorbed hydrogen atoms are written together with the metal M. The energy of the free electron e^- is at the Fermi level of the metal.

Assuming that kinetic parameters (such as the activation energy) are the same for the HER and the HOR close to the hydrogen reversible potential, then, the mechanism of the HER would be the same as that above for the HOR, i.e., the fast charge-transfer step is followed by the Tafel and/or Heyrovski sequence. Finally, it should be noted, that the reaction mechanism of the HER/HOR in acid solution is similar to that in alkaline solution, except that hydrogen is formed from hydronium ions (H_3O^+) rather than from H_2O.

Based on this reaction scheme the observed "volcano" behavior, when comparing the exchange current density with the metal-hydrogen bond energy, can easily be rationalized. Discussing for example the HER, an increased metal-hydrogen bond energy is *increasing* the coverage of adsorbed hydrogen (eq. 6.4), whereas the recombination of two adsorbed hydrogen atoms (eq. 6.2) and/or the recombination of adsorbed hydrogen with water (eq. 6.3), respectively, to form H_2 is *decreasing*. Consequently, a maximum in the exchange current density is expected at intermediate values of the metal-hydrogen bond. However, the fact that the reaction intermediate is not H_{upd}, and there is no direct probe to distinguish between H_{opd} and H_{upd} is substantially complicating an elucidation of the HER/HOR on a atomistic level.

However, it is possible to derive the basic kinetic parameters, such as the exchange current density i_0 and the apparent activation energy $\Delta H^\#$ of the reaction. The basic equation for an kinetic analysis of a reaction proceeding on a surface is the Buttler-Volmer equation [7, 17]:

$$I = i_0 \left(\exp(\beta F \eta / RT) - \exp(-(1-\beta) F \eta / RT) \right), \qquad (6.5)$$

where η denotes the overpotential ($\eta = E - E_{rev}$) and β the symmetry factor. The exchange current density i_0, which characterises the intrinsic catalalytic activity of the catalyst, can be extracted by simplifying the Buttler-Volmer equation, either for the case of very high or for very low overpotentials. In this work, the exchange current density i_0 is calculated from the measured current densities in the polarization curves near the reversible potential, i.e. in the so-called micropolarisation region. Without going into details, the evalution is based on the fact that for small overpotentials (about $|\eta \leq 20mV|$) the general kinetic equation for the measured net current density I (eq. 6.5) can be simplified for the HER/HOR to [6, 7]:

$$I = i_0 \frac{\eta F}{RT} \qquad\qquad (6.6)$$

Consequently the exchange current density can be calculated from the slope of a graph where the current density is plotted versus the applied electrode potential at small overpotentials. Once the exchange current densities are obtained at different temperatures also the apparent activation energy $\Delta H^{\#}$ of the process can easily be calculated in an Arrhenius plot using the equation [17, 120]:

$$\frac{d \log i_0}{d(1/T)} = -\Delta H^{\#}/2.3R \qquad\qquad (6.7)$$

By evaluting these kinetic parameters the hydrogen reaction can be compared on the different surfaces and in different solutions.

6.2 Measurements in alkaline solution

The hydrogen reaction on platinum is one of the fastest known electrochemical reactions and it is experimentally very difficult to measure anything but diffusion polarization [150, 151]. Since the reaction is generally much slower in alkaline solution than in acid solution, the accurate measurement of the HER/HOR appears more tractable in alkaline solution and/or at low temperatures [120]. Therefore, in this work the HER/HOR is investigated in alkaline solution.

In Figure 6.1 a set of polarization curves of the HOR on a Pt(111)-Pd electrode in H_2 saturated 0.1 M KOH solution at room temperature is shown. As for the polarization curves of the ORR, introduced in the last chapter, three different potential regions can be distinguished. At low overpotentials a narrow potential region of mixed kinetic-diffusion control (ca. 0.0 V < E < 0.15 V) is followed by the potential region of diffusion limited currents (ca. 0.15 V < E < 0.95 V). The current densities are deviating from the diffusion limited value at electrode potentials E > 0.95 V. The very narrow potential region of mixed kinetic-diffusion controlled current densities, indicates the above mentioned fast kinetics of the hydrogen reaction. The equidistance of the current plateaus indicate diffusion limited current densities. This can be seen more clearly from the inset, where a Levich-Koutecky plot of the current densities at 0.4 V is shown. The intercept of the linear regression of the data is clearly at zero current density, and consequently the current densities are completely controlled by mass transport. As stated above, at potentials above ca. 0.95 V the current densities are decreasing. This decrease clearly points towards an inhibition of the reaction due to oxide formation of the surface.
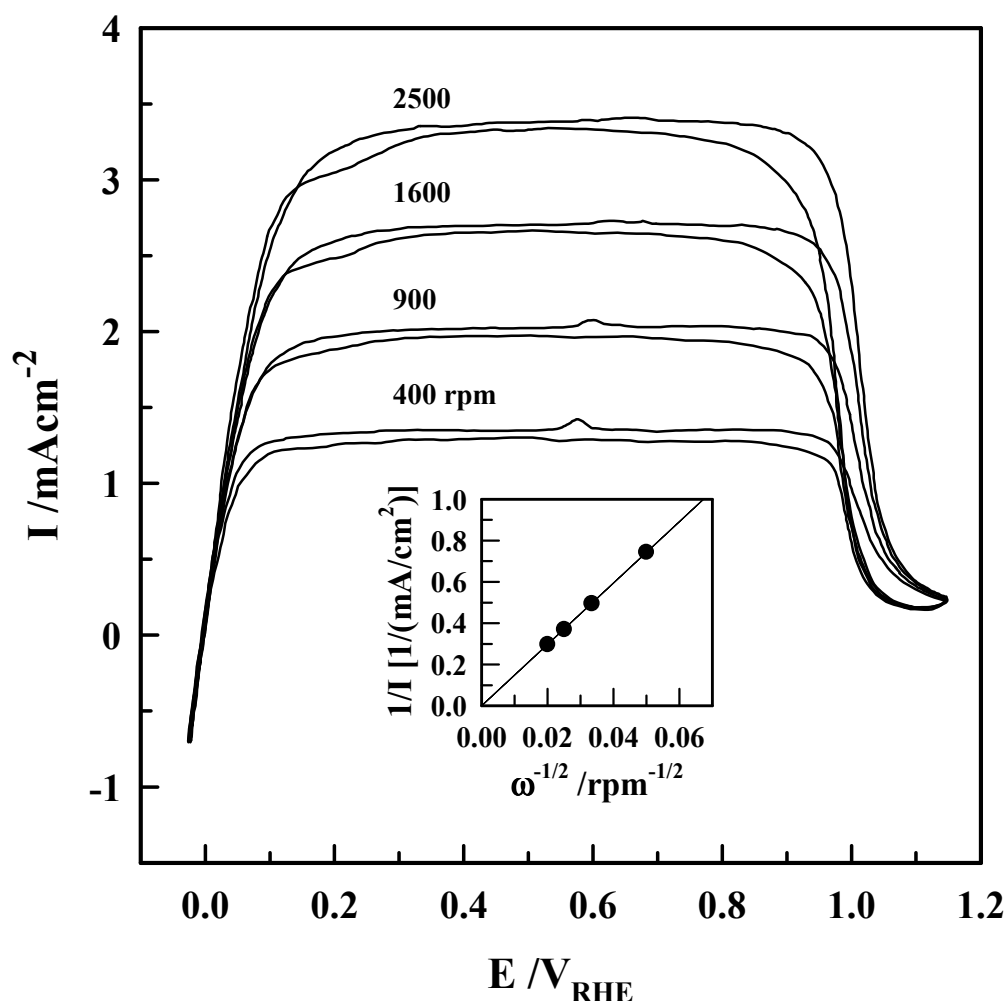
Figure 6.1:Set of polarization curves of the HER/HOR on Pt(111)-Pd in H_2 saturated 0.1 M KOH at 293 K; 50 mV/s; inset Levich-Koutecky plot of the current densities at 0.4 V

As mentioned in the previous section, the potential region of interest is at very low overpotentials, i.e. the micropolarization region. In Figure 6.2 the current densities of the HER/HOR in the micropolarization region are shown for two different temperatures 293 K and 333 K, respectively. (Note, that by definition the potential given by the reversible hydrogen electrode is in fact the overpotential of the HER/HOR). The rotation rate of both measurements was 2500 rpm. From the data, it is obvious that at both temperatures the current densities are symmetrical positive and negative from the reversible potential, indicating that there is a single exchange current density for the hydrogen electrode reaction applicable to both anodic and cathodic processes. Consequently, as already assumed in the previous chapter, both reactions can be discussed using the same reaction mechanism. Another point, which is obvious from Figure 6.2 is that higher current densities are obtained

at the elevated temperature. Consequently, it can be concluded, that the hydrogen reaction is an activated process. For an evaluation of the kinetic parameters of the HOR/HER on Pt(111)-Pd the polarization curves are fitted by straight lines, indicated in Figure 6.2.
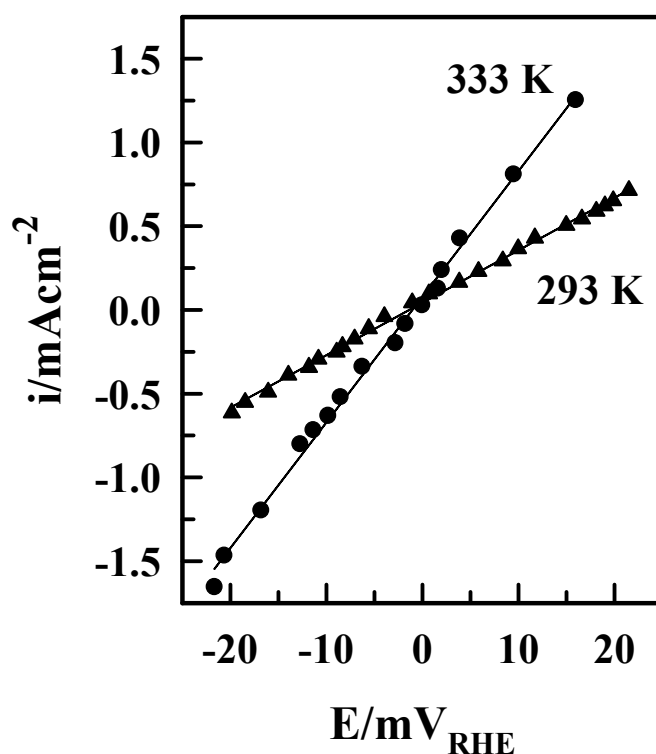

Figure 6.2: The current densities in the micropolarization region of the HER/HOR on Pt(111)-Pd recorded with 2500 rpm at 333 K and 293 K, respectively; the straight lines are linear fits of the data for the determination of the exchange current density

Based on the slopes of the straight lines the exchange current density i_0 can be evaluated using equation 6.6. The calculation is giving a value of $i_0 = 0.8$ *mA/cm^2* at 293 K, whereas at 333 K a value of $i_0 = 2.2$ *mA/cm^2* is obtained. Using these two points a rough estimation of the apparent activation energy of the process can be given by using equation 6.7. The Arrhenius plot of the two exchange current densities leads to a value of *$\Delta H^{\#} = 21$ KJ/mol*. Although, due to the limited data, this is only a rough estimation, it can still be used for a comparison of the catalytic activity of Pt(111)-Pd towards the hydrogen reaction with the results obtained in previous work for the bare Pt(111) surface.
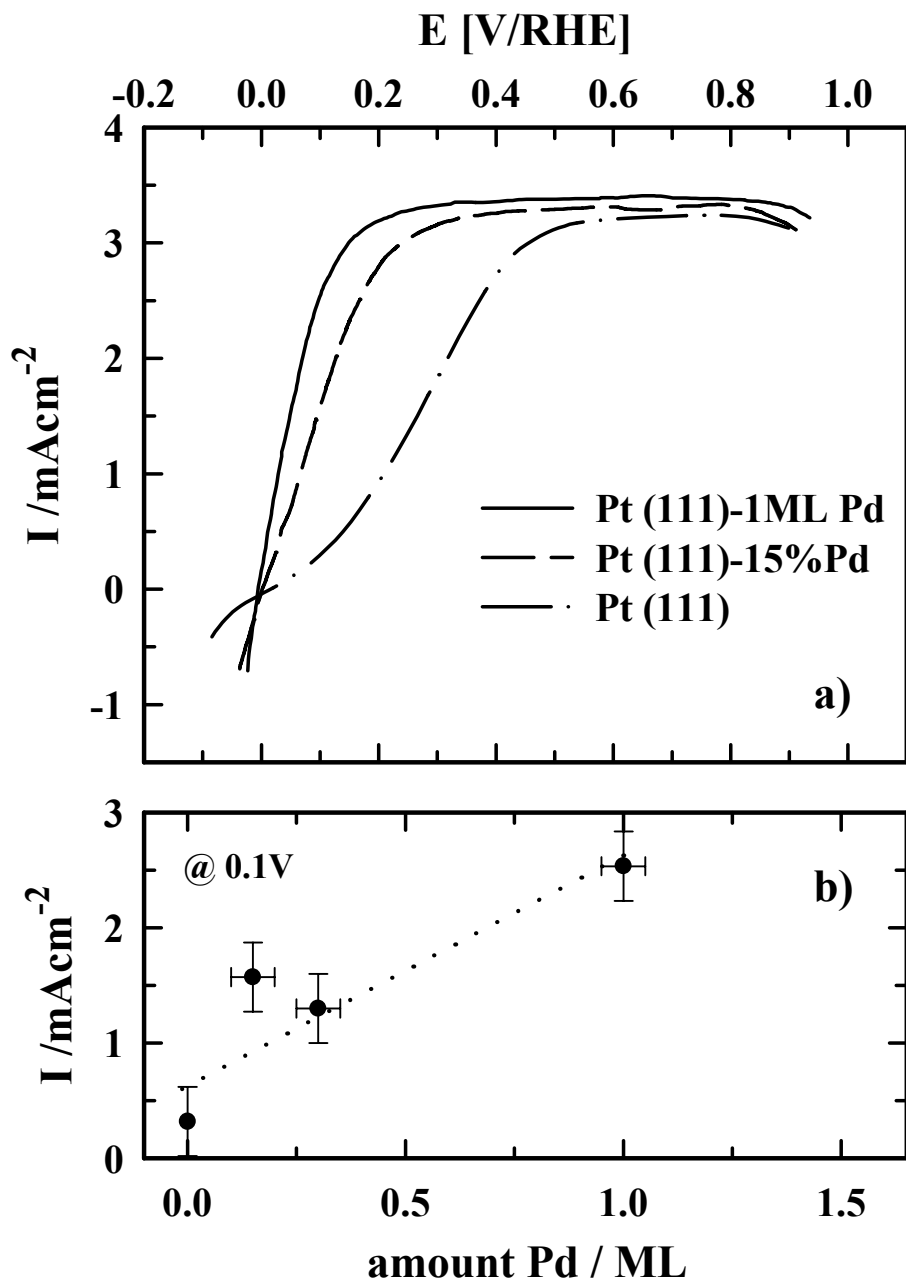
Figure 6.3: a) Polarization curves for the HOR on Pt(111)-x Pd disk electrodes (with 0 ≤ x ≤ 1) in 0.1 M KOH; 50 mV/s; 293 K; 2500 rpm b) corresponding currents at a fixed potential of 0.1 V

Another important point is the role of palladium in the enhancement of the electrocatalytic activity. As mentioned in the literature review (section 6.1.1), from measurements on Pt(hkl) it is well known that the HER/HOR is a structure sensitive process. During the palladium deposition, although a 2-dimensional growth mode has been established, an increase of steps and defect sites on the surface cannot be prevented.

That the catalytic activity of Pt(111)-Pd is indeed improved in comparison to bare Pt(111), can be seen in Figure 6.3a, where the polarization curves obtained for Pt(111)-xPd surfaces (with $0 \leq x \leq 1$) are compared in H_2 saturated 0.1 M KOH at room temperature. Whereas on bare Pt(111) a relative broad potential region of mixed kinetic-diffusion control is observed, the kinetic currents are measured in a considerably narrower potential region, even when only small amounts of palladium are deposited. This effect, however, can only be attributed to palladium since also steps and defect sites, introduced by the deposition, increase the electrocatalytic activity of the surface towards the HER/HOR.

Nevertheless, a comparison of the current densities at a fixed potential of 0.1 V for different amounts of palladium deposited is shown in Figure 6.3b. Again, a clear correlation of the palladium surface coverage and the electrocatalytic activity is obtained. However, the relative high uncertainty of the values points towards the difficulties in the determination of the kinetic parameters of the HER/HOR in alkaline solution. One reason may be a slightly different "qualities" in the obtained films during the deposition, i.e. different step/defect density. Another reason, however, may be that, similar to the ORR in alkaline solution, also for the hydrogen reaction a decrease of the current densities with time is observed in alkaline solution. In contrast to the ORR, this deactivation was almost completely irreversible in the potential limit $0 \leq E \leq 1$ V, indicating that the surface structure is massively altered. Although attempts have been made to classify the deactivation process, no clear reason is apparent. As a general rule it can be stated that the deactivation depends on the number of polarization curves recorded and results in a decrease of the current densities in the mixed diffusion region in the form that the diffusion limited current density is reached only at higher overpotentials.

Finally, it should be mentioned that very recent measurements performed in sulfuric acid solution have shown that for palladium coverages of more than one monolayer, a decrease of the electrocatalytic activity is obtained. This observation is summarized in Figure 6.4. The data are taken from reference [136].
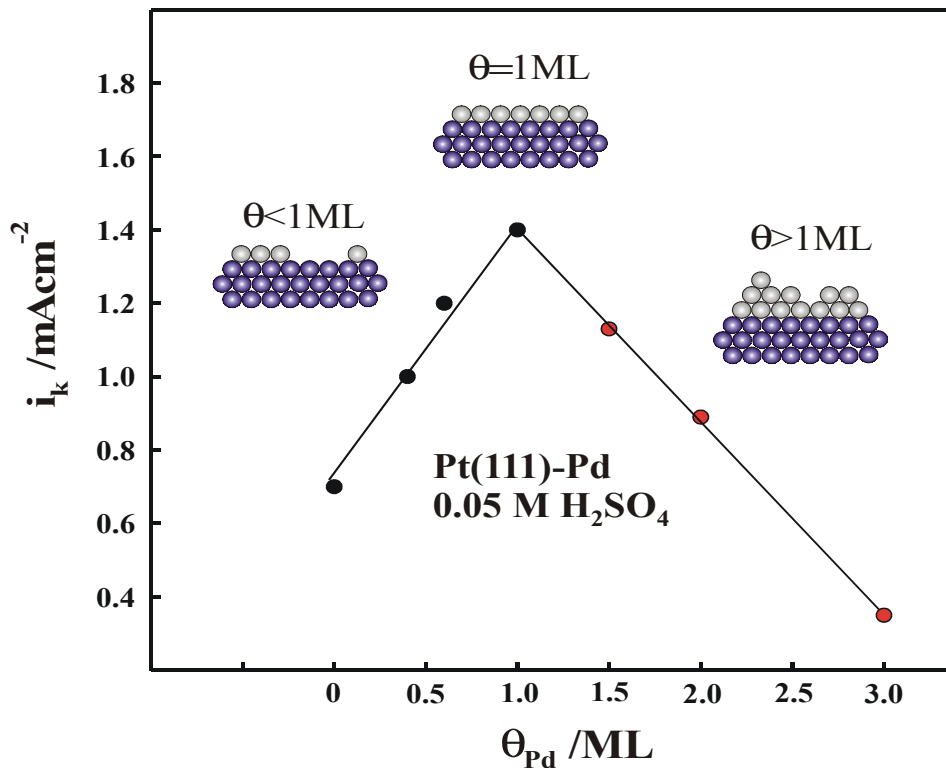
Figure 6.4: I_k vs. Θ_{Pd} relationship for the HOR in 0.05 M H2SO₄ at η = 0.25 mV; ideal models for pseudomorphic Pd (gray circles) layers on Pt(111) (dark circles), data taken from reference [136]

6.3 Discussion: Alkaline solution

The reaction rate of the hydrogen evolution/oxidation reaction in alkaline solution is substantially increased on Pt(111)-Pd compared to bare Pt(111). As already established for Pt(hkl) [120], the experimental results presented in this work reveal that also for Pt(111)-Pd the observed current densities in the micropolarization region are symmetrical, negative and positive of the reversible potential. Consequently, at potentials near the reversible potential the same kinetic parameters are obtained for the HER and the HOR. Therefore, for the sake of simplicity, in the following it is not distinguished between the two reactions.

One way to understand the hydrogen reaction on Pt(111)-Pd is by analyzing a simplified kinetic equation for the HER/HOR, which can be expressed as [152]:

$$i_0 \propto (1-\Theta_{ad})\exp(-\Delta H^{\#}/RT) \qquad (6.8)$$

with

$$\Theta_{ad} = \Theta_{H_{upd}} + \Theta_{H_{opd}} + \Theta_{OH_{ad}} + \Theta_{anions} \tag{6.9}$$

$$\Delta H^{\#} = \Delta H^{\#}_{\Theta_{H_{opd}}=0} - \gamma r \Theta_{H_{opd}} \tag{6.10}$$

The apparent activation energy in equation 6.10 is expressed in terms of the activation energy at zero coverage of the reaction intermediate ($\Theta_{Hopd} = 0$) and the correction term $\gamma r\Theta_{Hopd}$, indicating the decrease in the absolute value of the standard free energy of adsorption of the active intermediates with increasing Θ_{ad}.

Based on equation 6.8 two factors determine the exchange current density, the number of free sites ($1-\Theta_{ad}$) and the $\Delta H^{\#}$ term. The latter term has been evaluated by the kinetic analysis. The results, derived from Figure 6.2 are summarized in Table 2. The kinetic parameters of Pt(111), taken from the literature [136], are included as well. For Pt(111)-Pd an apparent activation energy for the hydrogen reaction of $\Delta H^{\#} = 21$ *KJ/mol* was obtained above. Within the uncertainty of the evaluation, this is about half of the value $\Delta H^{\#} = 46$ *KJ/mol* obtained for bare Pt(111) under the same conditions. The fact that the more active surface has also a lower activation energy is a "classic" result for electrocatalytic reactions and indicates that the energy of adsorption of the reactive intermediate plays an important role in the kinetics [120]. That, as for the oxygen reduction, the maximum in the electrocatalytic activity is obtained for a full monolayer of palladium points to the unique properties of this specific system.

0.1 M KOH solution	i_0 *[mA/cm^2]*				$\Delta H^{0\#}$ *[KJ/mol]*
	275 K	293 K	313 K	333 K	
Pt(111)	0.01	0.035	0.1	0.3	46
Pt(111)-Pd		0.8		2.2	21

Table 2: Kinetic parameters for the HER/HOR on Pt(111) (data taken from ref. [136]) and Pt(111)-Pd in 0.1 M KOH solution

Recently, Markovic et al. proposed that the key for resolving the different activities of the hydrogen reaction on Pt(hkl) is by understanding the nature of H_{upd}, i.e. strongly adsorbed hydrogen, and how this state affects the formation of H_{opd}, i.e. weakly adsorbed hydrogen, in eqs. 6.2 - 6.4. Following this line, it is important to recall that on Pt(111)-Pd at potentials near the reversible potential a full monolayer of H_{upd} is deposited, in contrast to bare Pt(111), where only 0.66 ML of H_{upd} are obtained. This finding was attributed to a stronger Pd-H_{upd} interaction compared to Pt-H_{upd}. Consequently the H_{upd} might sit "deeper" in the surface, e.g.

in three-fold hollow sites, being more *in* the surface than on the surface. In fact this is no new concept, and it has been proposed for some time with the concept of H_{opd} on polycrystalline platinum, that H_{upd} might be partially *absorbed* in the surface [7], leaving free sites for the adsorption and reaction of H_{opd}. This supposition for the adsorption of H_{upd}, being at least partially in a kind of subsurface state, would explain that the hydrogen reaction involving H_{opd} can occur on the geometrically homogeneous Pt(111)-Pd surface nominally covered completely by H_{upd}. The increased catalytic activity of the palladium film compared to the bare Pt(111) surface could be easily rationalized by the high ability of bulk Pd to absorb hydrogen. As long as only one monolayer of palladium is deposited, the hydrogen, however, can not be absorbed in the bulk but may be sitting, for example, underneath the Pd film at the Pd/Pt interface. If more than one monolayer of palladium is deposited the ability to absorb hydrogen in the bulk increases, and the surface becomes less active again. This conclusion is consistent with the latest experimental results, which show indeed a decrease in the electrocatalytic activity of the Pt(111)-Pd surface at palladium coverage higher than one monolayer.

However, the physical nature of such a partially absorbed state of H_{upd} is far from clear and hence, the difference of H_{upd} and H_{opd} can not be sufficiently explained. In the search of alternative explanations for the experimental findings another point has to be taken into account. In principle a transition of H_{upd} to H_{opd} may be possible. The difference of these two states of adsorbed H_{ad} is often described as weakly and strongly adsorbed, or reactive and unreactive hydrogen. From measurements performed in UHV it is well known that the interaction of molecules on a surface are affecting the binding energy. Consequently, a transition from unreactive H_{upd} to reactive H_{opd} might be facilitated on Pt(111)-Pd compared to bare Pt(111). One argument pointing into this direction is the anticipated smaller repulsion of H_{upd} on Pt(111)-Pd, which leads to the higher hydrogen coverage observed on this surface. However, as long as no direct probe for the physical nature of the H_{opd} state is at hand, a conclusive explanation for the hydrogen reaction remains elusive.

Another interesting point, which should be discussed, is the difference in the activation energies, measured in acid and in alkaline solution, i.e. the *pH effect* of the hydrogen reaction. In previous investigations of the hydrogen reaction on Pt(111)-Pd in sulfuric acid solution, an apparent activation energy of $\Delta H^{\#} = 9\ KJ/mol$ is reported [136], which is half of the value obtained in this work for alkaline solution. Interestingly, the *same* observation has been made for bare Pt(111), where the value of $\Delta H^{\#} = 46\ KJ/mol$ in alkaline solution, is also reduced roughly by half in acid solution ($\Delta H^{\#} = 18\ KJ/mol$) [146]. Furthermore, a similar pH effect has been reported some time ago for polycrystalline platinum [136, 153]. Therefore, it seems that a general mechanism, applicable for both surfaces is responsible for these observations. One difference in the formation of H_{opd} in acid and in alkaline solution, is that in the

Heyrovski step (eq 6.3) H_2 forms H_{opd} and H_3O^+ instead of H_{opd} and H_2O. For the Volmer step (eq. 6.4) the difference between alkaline and acid solution is similar. However, based on the fact, that for Pt(111)-Pd as well as for bare Pt(111) the H_{upd} coverages have been found to be independent of the pH of the solution, the net energy needed for the formation of H_{opd} should be the same in alkaline and acid solution, respectively. Therefore the differences in electrocatalytic activity depending on the pH of the solution seem to be due to another difference in alkaline and acid solution. One possible reason may be the coadsorption of OH_{ad}. In chapter 4 it has been shown, that in contrast to acid solution, in alkaline solution OH_{ad} is present even in the potential region of H_{upd}. This finding has been observed for Pt(111) as well as for Pt(111)-Pd. Taking into account equation 6.8 for the exchange current density, OH_{ad} affects the $(1-\Theta_{ad})$ term as well as the apparent activation energy $\Delta H^{\#}$ of the hydrogen reaction. In fact the same effect may even account for the slow deactivation process observed for Pt(111)-Pd. However, resolving the role of OH_{ad} more experiments, especially on the oxide formation process on platinum group metals in alkaline solution are necessary.

6.4 Summary: HER/HOR

In this chapter the electrocatalytic activity of a pseudomorphic palladium monolayer supported on Pt(111) towards the hydrogen evolution and the hydrogen oxidation reaction has been studied in alkaline solution.

The Pt(111)-Pd surface turned out to be more active than an unmodified Pt(111) surface. A maximum in its electrocatalytic activity is obtained if a complete monolayer is deposited, with no three dimensional growth yet. Based on an kinetic analysis in the micropolarization region, the hydrogen reaction is symmetrical, positive and negative of the reversible potential. The kinetic parameters indicate that the high catalytic activity is directly related to a lower apparent activation energy of the hydrogen reaction on Pt(111)-Pd compared to Pt(111). As for platinum, also for the palladium film a dependence of the apparent activation energy on the pH of the solution is found. As a rough estimation it can be stated that for both systems the activation energies are doubled in alkaline solution compared to acid solution.

A definitive explanation of the experimental findings is difficult since still no information of the physical state of the reactive intermediate of the hydrogen reaction exists. Therefore only assumptions can be made which explain best the findings of the present work and the results of previous investigations.

Two main hypothesis are discussed for the relation of the reactive intermediate H_{opd} and the more strongly adsorbed state of hydrogen, H_{upd}. The latter one being detectable by cyclic voltammetry. The first suggestion is, that, as on bare Pt(111), on Pt(111)-Pd H_{upd} is adsorbed at three-fold hollow sites. Due to the strong interaction of Pt(111)-Pd with H_{upd} the latter sits deeper in the potential well of the surface and is consequently more screened by the Pd atoms. In turn, the strongly adsorbed state of hydrogen does not affect the formation of the weakly adsorbed state, the actual reaction intermediate for the hydrogen reaction.

The alternative explanation is, that a transformation of H_{ad} from the strongly adsorbed state (unreactive) into the weakly adsorbed state (reactive) is possible. Such a transition from the unreactive into the reactive intermediate might be facilitated on the palladium film due the smaller repulsive interaction of hydrogen in the unreactive state.

The inhibition of the hydrogen reaction with higher OH^- concentration in the electrolyte seems to be a general property of platinum group electrodes. One possible explanation is the existence of OH_{ad} near the reversible potential, which has been proved for Pt(111)-Pd in this thesis by FTIR. The OH_{ad} affects both the number of free adsorption sites for the reactive intermediate as well as the apparent activation energy of the hydrogen reaction.

Chapter 7

The oxidation of small organic molecules

For almost all low-temperature fuel cell processes which use organic material as a fuel, poisoning of the catalyst is a serious problem. In this thesis the electrocatalytic activity of thin palladium films supported on Pt(111) is probed by the oxidation of two small organic molecules, formic acid and methanol, respectively. The oxidation of formic acid is only of minor technological importance and the main reason for investigating this reaction is its role as a model reaction for the poisoning of the catalyst due to the formation of CO_{ad} (see below). In contrast, the oxidation of methanol is of immediate technological interest due to its application in the direct methanol fuel cell.

In this thesis the electrooxidation of small organic molecules will only be treated shortly (particularly the methanol oxidation reaction) and there are still some measurements to be conducted in future investigations. However, there are two main reasons to discuss the experimental findings obtained so far. First, the role of the poisoning of an catalytically active electrode surface when oxidizing an organic fuel. As will be discussed in the literature review, the electrooxidation of HCOOH as well as CH_3OH to CO_2 proceeds via a so-called dual-path mechanism. In one path (see below) CO_{ad} is produced as a "poisoning intermediate", whereas the direct path is a fast reaction involving an "active" intermediate. For Pt(hkl) the activity of the respective surface is determined by the ability to oxidize the "poison" CO_{ad}. From a historic point of view in the elucidation of the poisoning intermediate as CO_{ad} and its influence on the activity of an electrode surface, the use of infrared spectroscopy was crucial [10, 154-156]. Therefore, it is interesting to compare the results of the electrooxidation of HCOOH (and CH_3OH) on Pt(111)-xPd with the FTIR investigations of the electrooxidation of CO described in chapter 4. Secondly, electrooxidation measurements are made with Pt(111)-xPd surfaces as well as with defined PtPd(111) bulk alloy beads. Consequently, based on these measurements, it is possible to compare the electrocatalytic properties *characteristic* for palladium *films* on Pt(111) with PtPd(111) alloys, where both sorts of metal atoms are randomly distributed over the surface.

The chapter is structured as follows. In the first section an overview over the most important results of previous work on formic acid as well as methanol oxidation on platinum

is given. In this section also the reaction pathway of both reactions is shortly discussed. In the next section the measurements performed in the course of this thesis are introduced. After shortly recalling the conclusions of the cyclic voltammetry in pure perchloric acid solution, at first the results of formic acid oxidation and then, shortly the results of methanol oxidation on the bimetallic surfaces are presented. After discussing the results of both systems a short summary is given.

7.1 Details

7.1.1 Formic acid oxidation on platinum surfaces

7.1.1.1 Literature

Although the electrochemical oxidation of formic acid is only of minor technological importance the investigation of this reaction on platinum and modified platinum electrodes has a long history. The reason for the wealth of investigations is that the reaction can be considered as a model reaction for understanding the mechanism of electrooxidation of organic molecules as well as the role of surface modifiers in enhancing the electrocatalytic activity [156, 157]. Since platinum is the catalyst of choice for low-temperature fuel cell application by far the most studies are performed on bare platinum and modified platinum surface. The sensitivity of formic acid oxidation to the surface structure of Pt(hkl) electrodes has been the subject of several papers, but there is still no consensus on the order of activity. This is, at least partially due to the fact that most of these activity assignments rely on cyclic voltammetry, which is, as will be demonstrated in the results section, only a qualitative measure of the reactivity. However, it is well established that the rate of the poisoning, i.e. the formation of CO_{ad} (see below) is a structure sensitive process with the inhibition being most severe on Pt(100). On Pt(100) the current due to formic acid oxidation drops to zero immediately after the reaction has started in a positive going potential scan. In contrast, Pt(111) is the least active surface initially, but the activity has a lower rate of decay than on the other surfaces.

Generally, the formic acid oxidation, detected by the formation of CO_{ad}, starts with the desorption of H_{upd} from the surface. Consequently, it has been proposed that the adsorption of organic molecules, and in particular of HCOOH is inhibited by H_{upd}. That is, H_{upd} has the same effect on the electrooxidation of formic acid as on the hydrogen oxydation and the oxygen reduction reaction, described in the previous chapters.

In the search of surface modifiers, which enhance the catalytic activity of Pt towards formic acid oxidation, numerous bimetallic systems were tested. A variety of examples (prior

to 1988) can be found in the review of Parsons and Vander-Noot [156]. The ideal role of the surface modifier, is to optimize the adsorption of HCOOH while oxidizing the poisoning species CO_{ad} with a minimum in the surface coverage of OH_{ad}. However, the positive effect of surface modifiers has often been overestimated, since only transients in the oxidation currents were recorded. As shown recently by Schmidt et al., one example is the enhancement in the catalytic activity by modifying the Pt(111) surface with irreversibly adsorbed bismuth [158]. The high catalytic activity of this surface is shown to be only transient in nature and at steady-state condition basically the same activity is found for bare Pt(111) and Pt(111) modified by bismuth. Consequently, when studying the electrooxidation of formic acid, it is important to elucidate the steady-state activity of the catalyst. Due to the difficulties in preparing palladium electrodes only very few studies on the electrocatalytic activity of palladium towards formic acid oxidation exist. However, in one interesting study by Kolb and coworkers an exceptionally high catalytic activity for the formic acid oxidation is reported on palladium films supported on gold and platinum single crystals, respectively [45]. These measurements are compared to the formic acid oxidation on well-defined Pd(hkl) surfaces.

7.1.1.2 Reaction pathway

As mentioned above, the mechanism of formic acid electrooxidation on Pt and selected Pt-group metal surfaces in acid solution proceeds via the so-called dual-pathway mechanism, originally suggested by Capon and Parsons [159]. A scheme of the reaction mechanism is shown in Figure 7.1. While numerous details remain uncertain, this scheme involves the adsorption of HCOOH (k_{ad}), followed by the dehydrogenation of HCOOH, and the formation of the chemisorbed "poison" (reaction 2, k_p) in competition with the direct dehydrogenation path via one or more reactive intermediates (reaction 1, k_d). The rate of the latter path is determined by the surface coverage of the poisoning species CO_{ad} as well as adsorbed anions and H_{upd}, indicated by reaction 5. Besides being a poison, CO_{ad} can also act as a reaction intermediate when some fraction of CO_{ad} is further oxidized to CO_2 (reaction 4, k_{ox}). The active surface oxidant is most likely adsorbed OH, as proposed in chapter 4. Following the reaction scheme for the oxidative removal of CO_{ad} the adsorption of oxygenated species is in strong competition with anion adsorption from the supporting electrolyte. In fact, different current densities are observed depending on the adsorption strength of the anions in the supporting electrolyte (for example sulfuric acid and perchloric acid solution) [156]. Consequently, the interdependence of the different reaction steps in reactions 1-4 and the competition for the adsorption sites of the reaction partners and intermediates usually leads to complex surface processes [160]. Under certain experimental conditions even non-linear reaction kinetics, leading to a variety of dynamic instabilities and oscillatory behavior, are observed. However, these phenomena are more frequently observed

on Pt(100) and Pt(110) surfaces (see for example ref. [161, 162]) and they play no role for the investigations introduced here.
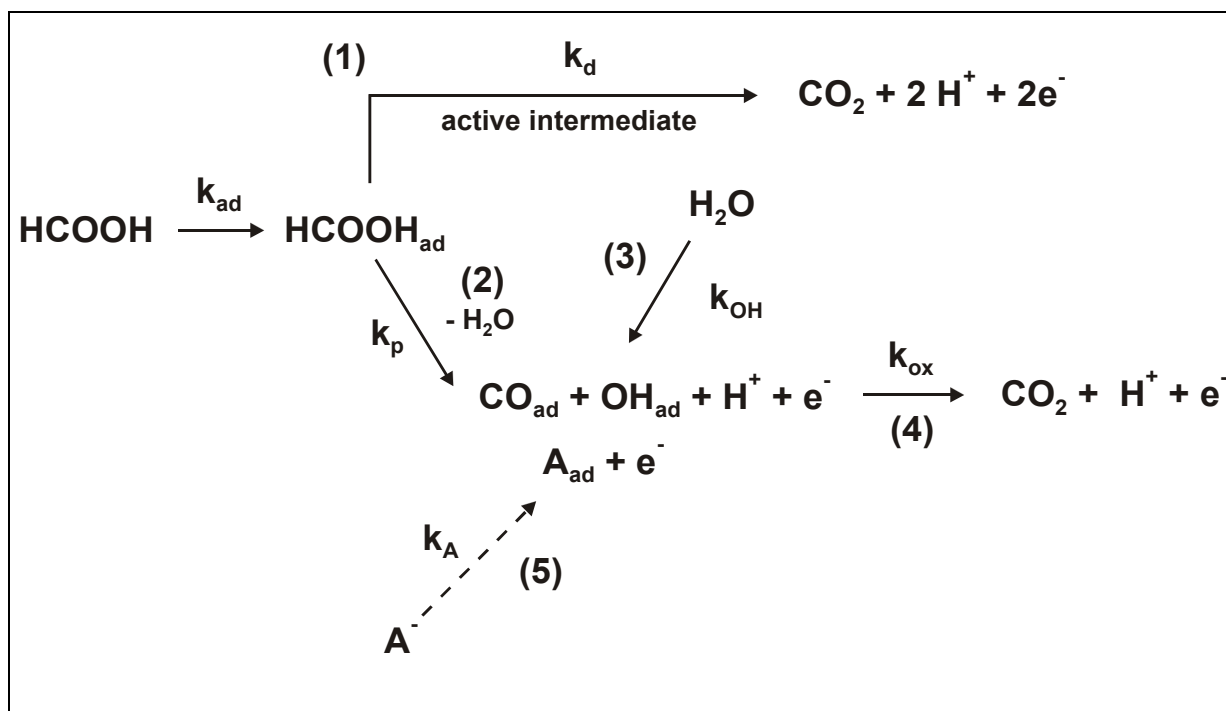

Figure 7.1: Reaction scheme of formic acid electrooxidation on Pt-group metals

7.1.2 Methanol oxidation on platinum surfaces

7.1.2.1 Literature

The electrooxidation of methanol is extensively studied because of its importance as a feedstock for fuel cell. Since this reaction is treated only shortly in this thesis no complete overview over the numerous results is given. Only some details are introduced, which are of importance for the discussion. For more details on the methanol oxidation reaction the reader is referred to ref. [69, 156].

On platinum at potentials below about 0.5 V the methanol oxidation is almost completely blocked by CO_{ad}. However, compared to the CO adlayer formed by dissolving CO into the solution (see chapter 4) smaller CO coverages are obtained. Additionally coadsorption of anions together with CO_{ad} can take place [69]. The anion adsorption from the supporting electrolyte has also a strong inhibiting effect on the electrocatalytic activity. The inhibiting effect is correlated with the adsorption strength of the anion, e.g. chloride has a stronger inhibiting effect than sulfate [82]. At potentials higher than 0.5 V CO_{ad} can react further to CO_2, and hence becomes a reaction intermediate. In order to enhance the

electrocatalytic activity of platinum various bimetallic surface have been studied, with Pt/Ru surfaces being at present the most active catalyst [82].

7.1.2.2 Reaction pathway

As for formic acid oxidation, for the oxidation of methanol an analogous dual-pathway with the formation of CO_{ad} as a spectator species, i.e. poison, has been frequently proposed (see for example ref. [69, 156, 157]). However, in the methanol oxidation reaction the dehydrogenation, rather than the dehydration (in the case of formic acid), is responsible for the formation of CO_{ad}. The reaction scheme shown in Figure 7.2 for the oxidation reaction of methanol is almost identical with the one proposed for the formic acid oxidation, again emphasizing the importance of the competition between the reactive intermediates and the spectator species. Much effort, particularly with in-situ IR spectroscopy and DEMS[13] (for reviews of this method see ref. [163, 164]), has been expended in trying to identify the unknown "direct" intermediate, but up to date a final conclusion is missing.
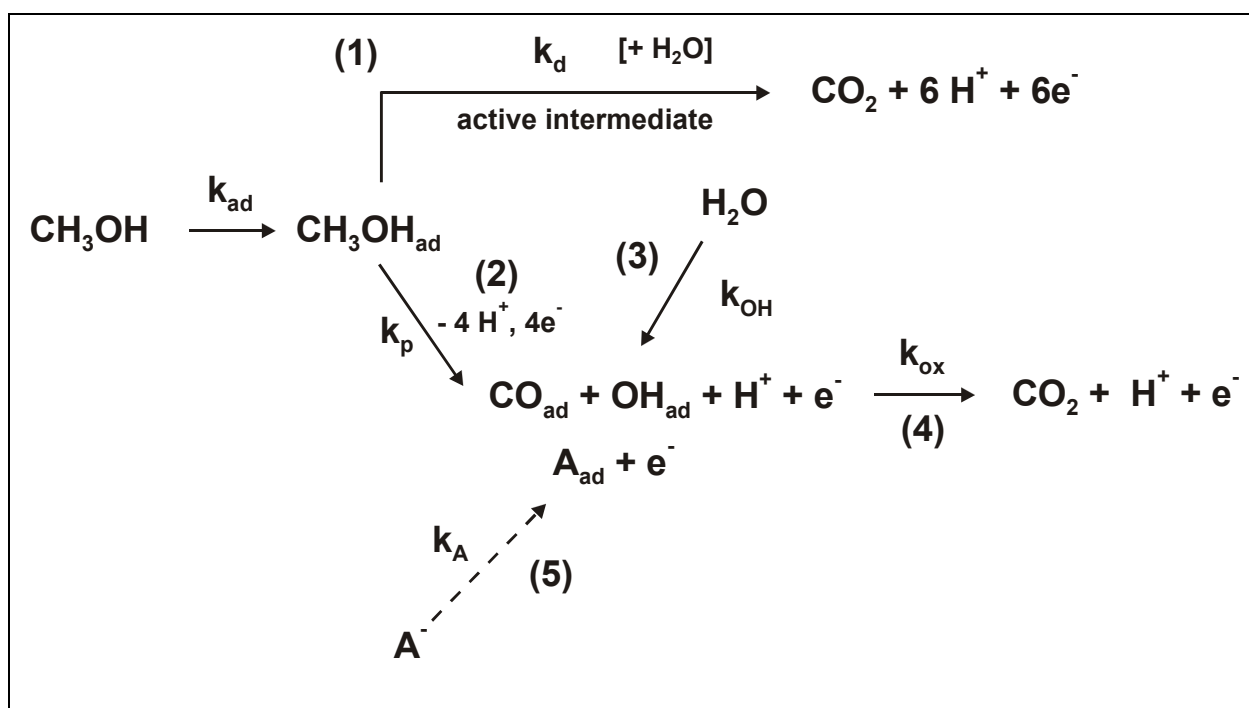

Figure 7.2: Reaction scheme of methanol electrooxidation on Pt-group metals

---

[13] **D**ifferential **E**lectrochemical **M**ass **S**pectroscopy

7.2 Measurements

All measurements of formic acid and methanol electrooxidation shown in this thesis are performed in 0.1 M HClO$_4$ + 50 mM HCOOH and 0.1 M HClO$_4$ + 50 mM CH$_3$OH solution, respectively. Perchloric acid was chosen as the supporting electrolyte in order to minimize the adsorption of anions from the supporting electrolyte without complicating the reaction by the formation of carbonate (in alkaline solution). Before coming to the results of the electrooxidation of small organic molecules, the cyclic voltammograms of the investigated surfaces in pure perchloric acid are shortly introduced.

7.2.1 Cyclic voltammetry in perchloric acid solution

In Figure 7.3 the cyclic voltammograms of two Pt(111)-xPd films (x = 0.2, x = 1) are compared to PdPt(111) bulk alloy surfaces in 0.1 M HClO$_4$ solution under the same conditions. The surface composition of the PdPt(111) single crystals was obtained by LEIS and a description of their properties will be published in reference [91]. For a discussion of the results presented in this thesis, only the surface composition and the fact that (in contrast to the palladium films) the palladium atoms are randomly distributed on the surface, are of importance.

Since the properties of the bulk alloys observed in the cyclic voltammograms are similar to the properties of the palladium films in perchloric acid, the results of chapter 4 are only shortly recapitulated. The palladium surface coverage affects the cyclic voltammetry in perchloric acid in three characteristic ways. With an increasing palladium coverage an increasing hydrogen coverage in H$_{upd}$ potential region is observed. Furthermore, at positive potentials the adsorption potential of OH$^-$ is shifted to more negative potentials, whereas the charge density of the butterfly peak is decreased with higher palladium surface coverages. From the cyclic voltammograms no clear influence of the surface morphology, i.e. if palladium is present in the form of islands or is randomly distributed on the surface, on the electrochemical properties can be observed.
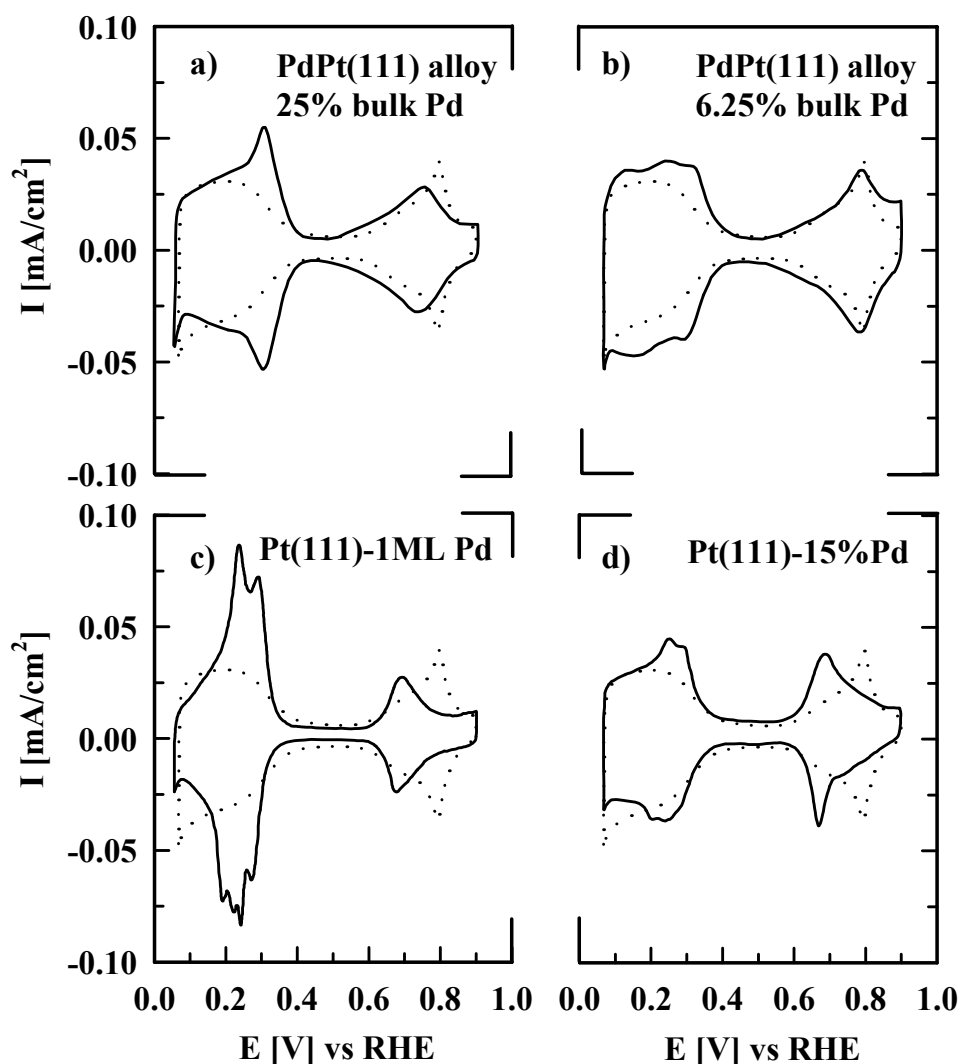
Figure 7.3:Cyclic voltammograms in 0.1M HClO₄ at 293K; 50mV/s on a) PdPt(111) bulk alloy with 25% Pd surface coverage; b) PdPt(111) bulk alloy with 25% Pd surface coverage; c) Pt(111)-1ML Pd; d) Pt(111)-20% Pd

7.2.2 Formic acid oxidation

In order to avoid effects of CO poisoning for recording the polarization curves of formic acid oxidation always the same procedure was applied. After equilibrating the temperature of the electrolyte the electrode is immersed at a potential of 0.05 V, and the start potential is applied for three minutes. Subsequently a polarization curve is recorded with 10 mV/s. The polarization curves *shown* in this thesis are always obtained in the *second* potential sweep recorded after the immersion, which is more characteristic than the first sweep.

In Figure 7.4 the polarization curves obtained for a palladium monolayer supported on Pt(111) is compared to the curve obtained for the PdPt(111) bulk alloy with low Pd coverage (6%) in 0.1 M HClO$_4$ + 50 mM HCOOH solution at 293 K. It can be seen that for both surfaces the maximum current densities observed in the forward and the backward scan, as indicated by the arrows, are different. Starting with the PdPt bulk alloy, this surface shows an almost identical behavior as reported in the literature for bare Pt (see for example ref. [162, 165-167]). In Figure 7.4a one recognizes the typical current-potential characteristics of a self-poisoning oxidation reaction of small organic molecules [156]. Starting at low potentials and scanning the potentials in positive direction, only small current densities are observed in the potential region of $0.05 \leq E \leq 0.5$ V. This inhibition of the reaction can clearly be assigned to the poisoning of the surface by CO$_{ad}$. The adsorption of OH$^-$ (see Figure 7.3) species at higher potentials $0.55 \leq E \leq 0.7$ V leads to an activation of the surface as a result of the oxidation of the poisoning species CO$_{ad}$, and consequently the current increases considerably. A further increase of the potential E >0.7 V deactivates the surface due to the higher coverage of oxygen species. In the reversed scan the surface gets reactivated as soon as the OH$^-$ species desorbs, showing almost the same form of the polarization curve as in the forward scan. However, in this reverse scan the maximum current density is increased by a factor of about two. This can be attributed to the fact that in the reverse scan the surface is almost free of poisoning species and the electrooxidation of formic acid can proceed in an unhindered manner.

Interestingly, the observed behavior of the Pt(111)-Pd surface is completely different. Scanning the potential from the negative limit in positive direction, the oxidation current is steeply increasing at a potential of about 0.2 V. High current densities are measured in the potential region of $0.25 \leq E \leq 0.4$ V. The maximum current density in the anodic scan is almost ten times higher than the one observed for the PdPt(111) bulk alloy. Increasing the potential to values where the adsorption of OH$^-$ species starts (E > 0.4V) leads to decreasing current densities. As for the bulk alloy, in the reverse scan the shape of the polarization curves is almost the same as in the anodic scan. For both scan directions a maximum of the activity is obtained at about 0.3 V, which is right after the desorption of H$_{upd}$, as shown in Figure 7.3. However, the maximum current density in the cathodic scan is decreased compared to the anodic scan. This behavior clearly contradicts a self-poisoning mechanism of the HCOOH electrooxidation on the palladium film. Consequently, its properties and the influence of the surface morphology are investigated more closely in further measurements.
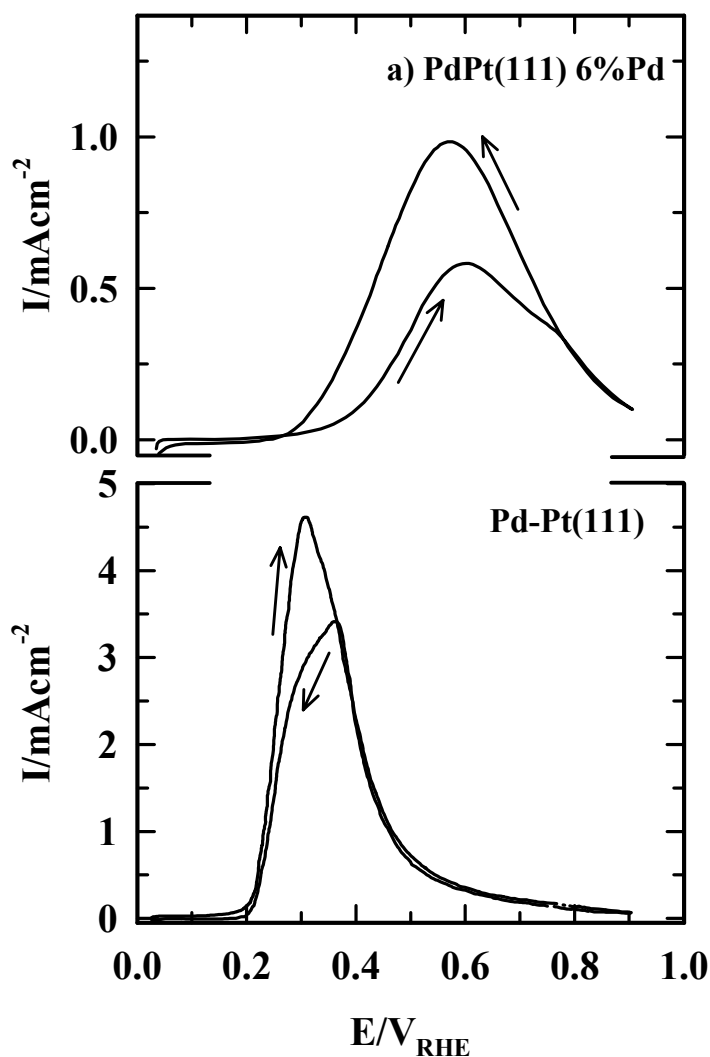
Figure 7.4: Polarization curves of a) PdPt(111) bulk alloy (6%Pd) and b) Pt(111)-1ML Pd in 0.1 M HClO$_4$ + 50 mM HCOOH at 293K; forward and backward scan are shown; v = 10mV/s;

In order to elucidate the influence of palladium and its distribution on the surface in Figure 7.5 the electrooxidation of formic acid is compared on two Pt(111)-xPd films (x = 0.2, x = 1) and two PdPt(111) bulk alloy surfaces (Pd surface coverage 6% and 25%, respectively). Polarization curves are recorded with two different scan rates 10 mV/s and 1 mV/s, respectively. It is obvious, that the measured current densities on all surfaces are dependent on the scan rate. Note that not only the value of the current densities is dependent on the scan rate, but also the shape of the polarization curves, i.e. the peak potential. For platinum and bimetallic platinum surfaces this observation is not new, and can be rationalized by the poisoning mechanism of the formic acid oxidation. In fact, the enhancement of the

reactivity by surface modifiers deposited on platinum electrodes is often misjudged in the way that only current transients of the formic acid oxidation are recorded [167, 168].

Beginning the description with Figure 7.5a, the formic acid oxidation current on the PdPt(111) bulk alloy with a palladium surface coverage of 25 % at a scan rate of 10 mV/s increases steeply at about 0.25 V and high current densities are measured in the potential region of $0.25 \leq E \leq 0.6$ V. The peak potential is located at about 0.45 V. Although the maximum current density is lower than on the complete palladium film, the surface is considerably more active than bare Pt(111). Moreover, high current densities are observed in a wide potential range compared to the palladium monolayer. In contrast, at a scan rate of only 1 mV/s, i.e. under quasi steady-state conditions, the current densities at low potentials are considerably decreased. A maximum in activity is obtained at a potential of about 0.7 V. This peak potential is about the same as on the bulk alloy with the low palladium surface coverage (6 %). Note also, that at low scan rates the peak of maximum current density shows a shoulder towards lower potentials. On the bulk alloy surface with low palladium concentration the form of the polarization curves is much less dependent on the scan rate. The current densities are decreased at the low scan rate, however, the observed shift in the peak potential towards higher values is smaller than on the surface with higher palladium content. This behavior of the bulk alloys clearly shows that the massive enhancement of the catalytic activity due to palladium on these type of bimetallic surfaces is only of transient nature.

In contrast, the properties of the palladium films are different in nature. As shown in Figure 7.5c on the complete palladium monolayer the shape of the polarization curves is almost *identical*, independently of the scan rate. Independent on the scan rate a maximum in the activity is obtained at about 0.3 V. As already concluded in the comparison of the anodic and cathodic scan, this behavior indicates no formation of a poisoning species (CO_{ad}) on the surface. Finally, the polarization curve of the palladium film with a surface coverage of 20 % is clearly a superposition of the properties of a bare Pt(111) surface and the complete palladium monolayer on Pt(111). At higher scan rates two peaks, located at 0.3 V and 0.55 V, respectively, can be observed in the polarization curves. By comparison with the polarization curves of the pseudomorphic palladium film and a bare Pt(111) surface (or the bulk alloy with low Pd surface coverage), the current densities observed at low potential can be attributed to formic acid oxidation on the palladium islands, whereas at higher potentials formic acid is oxidized mainly on the free platinum sites. On this surface, also no fundamental difference in the form of the polarization curve of the two scan rates can be observed, although the ratio of the current maxima of both peaks is affected by the scan rate. However, at the quasi steady-state the polarization curve shows an interesting additional feature. At the low scan rate, a third peak between the "palladium" and the "platinum" peak can be observed.
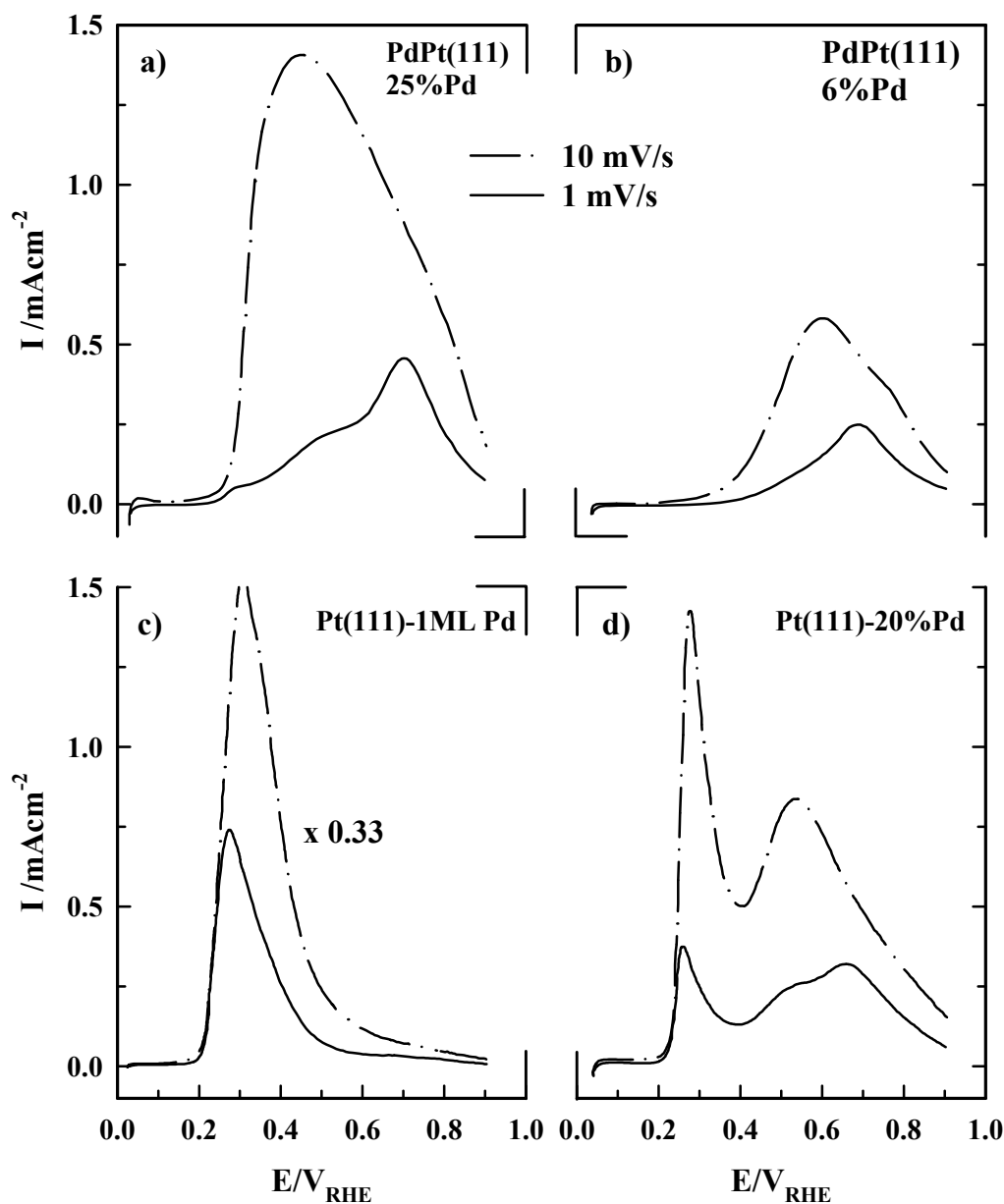
Figure 7.5: Polarization curves recorded with two different scan rates (as indicated) in 0.1 M HClO$_4$ + 50 mM HCOOH at 293K on a) PdPt(111) bulk alloy with 25% Pd surface coverage; b) PdPt(111) bulk alloy with 25% Pd surface coverage; c) Pt(111)-1ML Pd (current densities of both curves divided by 3); d) Pt(111)-20% Pd;

Summarizing, the observed behavior of the submonolayer of palladium on Pt(111), produced by electrodeposition, is completely different to the one of the PdPt(111) alloy, although the nominal surface composition is almost the same. Clearly, this is another proof for the palladium growth in form of islands on the Pt(111) surface. Another interesting consequence is, that due to the separated processes of the formic acid oxidation on Pt and Pd, the electrochemical properties of both surfaces, a pseudomorphic palladium monolayer

supported on Pt(111) and bare Pt(111), can be examined at the same time. In order to do so, in Figure 7.6 the polarization curves of formic acid oxidation on the Pt(111)-20% Pd surface are compared at two different temperatures, 283 V and 303 V, respectively.
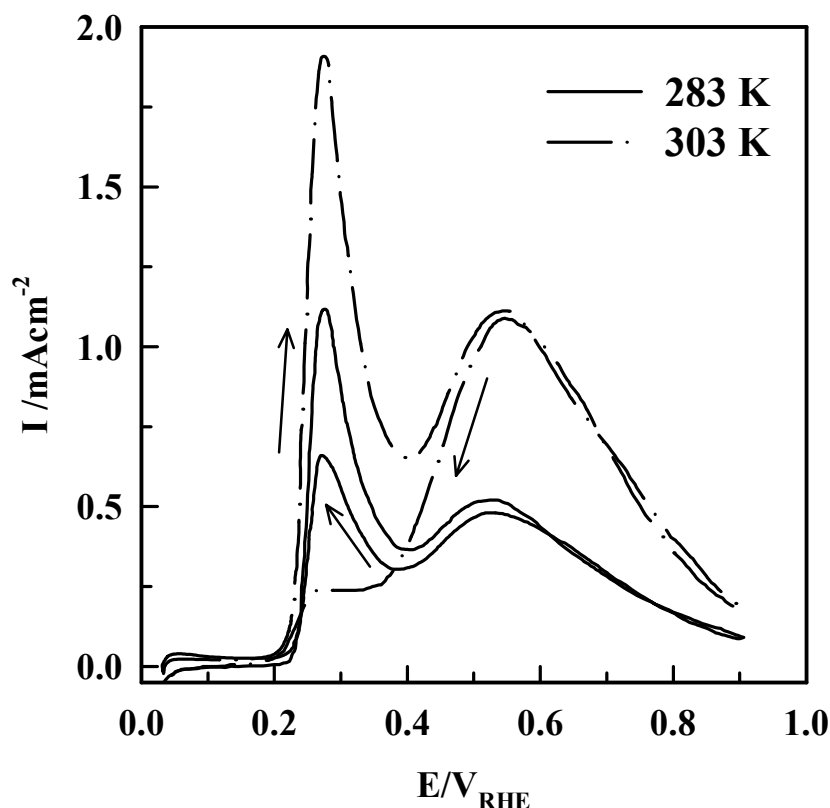

Figure 7.6: Polarization curves of Pt(111)-20% Pd in 0.1 M HClO₄ + 50 mM HCOOH recorded with 10mV/s; the electrolyte temperature is 283 K and 303 K, respectively

Beginning with the polaritzation curve recorded at 283 V, as discussed above, the observed oxidation currents can be separated in two peaks. For the sake of simplicity, it is assumed for the following discussion, that the peak at about 0.3 V is exclusively due to the oxidation of formic acid on Pd islands on Pt(111), whereas the peak at about 0.55 V is due to formic acid oxidation on bare Pt(111). In Figure 7.6 it can be seen that the ratio of the two peaks, the "palladium peak" and the "platinum peak" is different in the anodic and the cathodic scan. It seems that by cycling the potential to the anodic limit at 0.9 V the palladium gets deactivated. At a temperature of 303 K, this behavior is even more pronounced. Whereas for the free Pt(111) parts of the surface the same activity is observed in the anodic and the cathodic scan, the parts of the surface covered by the palladium film are almost completely inhibited in the backscan. Consequently, the influence of increasing the temperature has a completely different effect on Pt(111)-Pd and bare Pt(111).
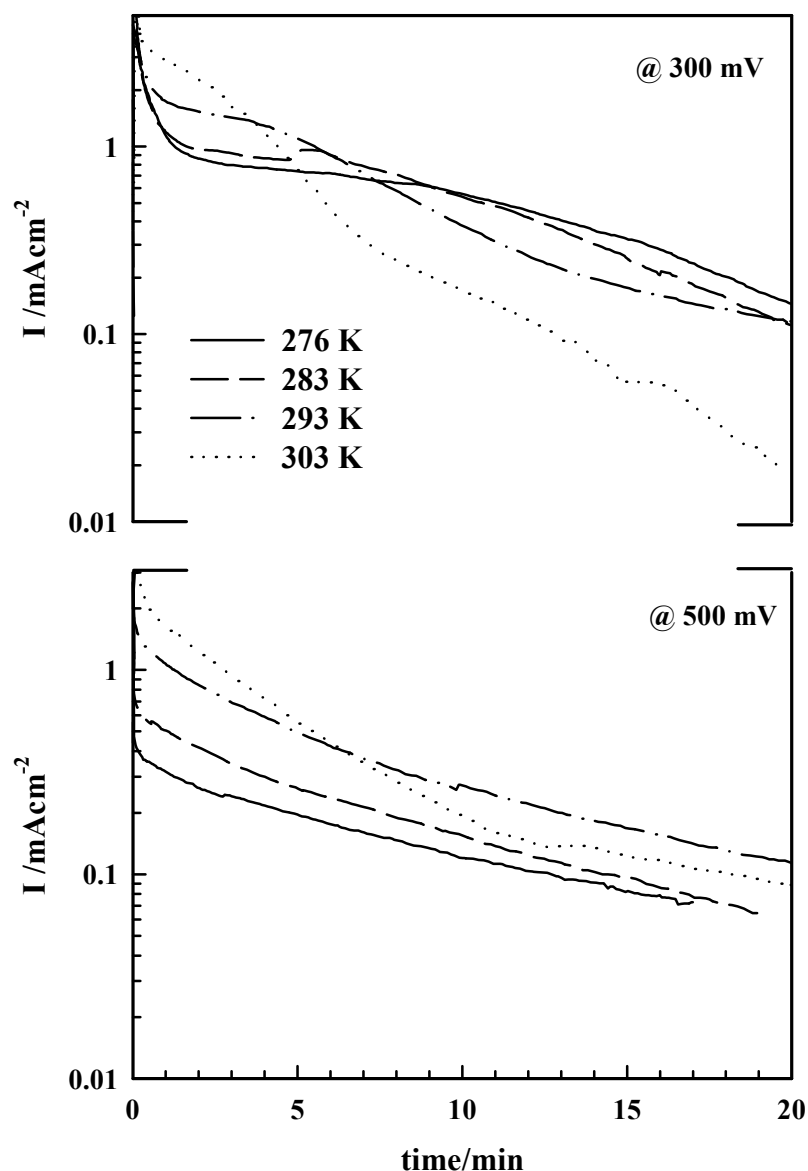
Figure 7.7: Potentiostatic oxidation of formic acid on Pt(111)-Pd at 276 K, 283 K, 293 K and 303 K, respectively, for two different potentials 0.3 V and 0.5 V;

For bare Pt(111) it is well known that the formic acid oxidation is an activated process, i.e. increasing the temperature increases the reaction rate, and an activation energy for the reaction has been calculated to be about $50 - 80$ *KJ/mol*, depending on the applied potential [168]. The calculation of activation energies is usually done by using data obtained under steady-state conditions. One suitable way to obtain these data, is by recording potentiostatic potential step experiments. In these kind of measurements the potentials is stepped from an potential where no reaction occurs to a potential where the reaction proceeds and the current densities are recorded as a function of time. Under these conditions transient effects can be

avoided. In Figure 7.7 the results of such potentiostatic stepping experiments for Pt(111)-Pd are shown. The experimental conditions are otherwise the same as in the polarization curves. For recording the potentiostatic current curves the surface was immersed at a potential of 0.05 V and subsequently stepped for 60 s to a potential of 0.9 V in order to oxidize all adsorbed CO. Then starting from 0.05 V the potential was stepped to the target potential and the current recorded as a function of time.

As a target potential the peak potential observed in the polarization curves, 0.3 V, and a value positive of the peak potential, 0.5 V, are taken. For the discussion, it is important to note that the current densities are shown in a logarithmic scale. Beginning with the *i-t* curves obtained at 0.3 V, after an initial quick deactivation of the surface observed in the first minute, the current densities are at first quite stable (at least for temperatures below 303 K). However, after a period of about 8 minutes another deactivation process, which proceeds slowly, becomes apparent. After 20 minutes only current densities decreased by a factor of 10 compared to the corresponding currents in the polarization curves, can be observed. Note also, that the slow deactivation process is clearly increased at higher temperatures. At 303 K the current densities are decreasing constantly. For all temperatures no clear steady-state current can be observed, even after 20 minutes.
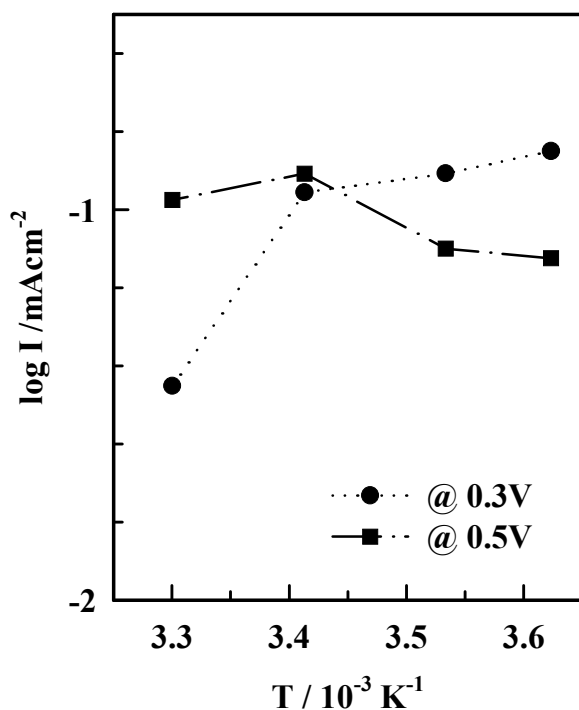

Figure 7.8: Arrhenius plots for the current densities of formic acid oxidation on Pt(111)-Pd after twenty minutes (data taken from Figure 7.7)

What is important to note, however, is that in the temperature range of 276 – 293 K in the time region of the first 10 minutes, higher current densities are measured than at a target

potential of 0.5 V under the same conditions. In other words the activity of the palladium film seems to have a maximum at potentials right after the desorption H_{upd}.

The constant deactivation process is more pronounced at a target potential of 0.5 V. The rate of deactivation is more or less constant in time at all temperatures and no different mechanisms are apparent. Note, that despite of the deactivation of the palladium film the current densities are always higher than the one obtained for the surface alloy with low palladium coverage under the same conditions.

This observed deactivation and its temperature dependence is pointing towards a complex interdependence of different mechanisms affecting the catalytic activity of Pt(111)-Pd towards the electrooxidation of formic acid. Consequently, it is not possible to determine any reliable activation energy for this process. This becomes obvious in the Arrhenius plot, shown in Figure 7.8, where the logarithm of the residual current densities after 20 minutes is plotted against the inverse of the temperature. For a target potential of 0.3 V, the reverse temperature effect of formic acid oxidation on Pt(111)-Pd compared to bare Pt(111), is observed. After 20 min with *increasing* temperature *decreasing* formic acid oxidation currents are observed. For a target potential of 0.5 V, at least for temperatures below 303 K, the "normal" behavior of increasing reaction rates with increasing the temperature can be observed. However, after 20 minutes at 303 K the surface is less active for formic acid oxidation than at 293 K.

7.2.3 Methanol oxidation

For recording the polarization curves for methanol acid oxidation the same procedure as for the oxidation of formic acid is applied. That is, after equilibrating the temperature of the electrolyte the electrode is immersed at a potential of 0.05 V, and the potential is applied for three minutes. Subsequently a polarization curve is recorded with 10 mV/s. The polarization curves shown in this thesis are always obtained in the *second* potential sweep recorded after the immersion.

In Figure 7.9 the polarization curves for methanol oxidation obtained in 0.1 M $HClO_4$ + 50 mM CH_3OH solution at 293 K are shown for two Pt(111)-xPd films (x = 0.2, x = 1) and the two PdPt(111) bulk alloys (Pd surface coverage 6% and 25%, respectively). Again, the polarization curves are recorded with two different scan rates 10 mV/s and 1 mV/s, respectively. From Figure 7.9 it is quite obvious that the order of activity of these four surfaces towards the methanol oxidation is *reversed* to the activity obtained for formic acid oxidation (see Figure 7.5). By far the most active surface is the PdPt(111) bulk alloy with low

palladium concentration, whereas the palladium monolayer is completely inactive towards the oxidation of methanol. The current densities at the methanol oxidation peak are in the same order than the current densities due to the desorption of H_{upd}.
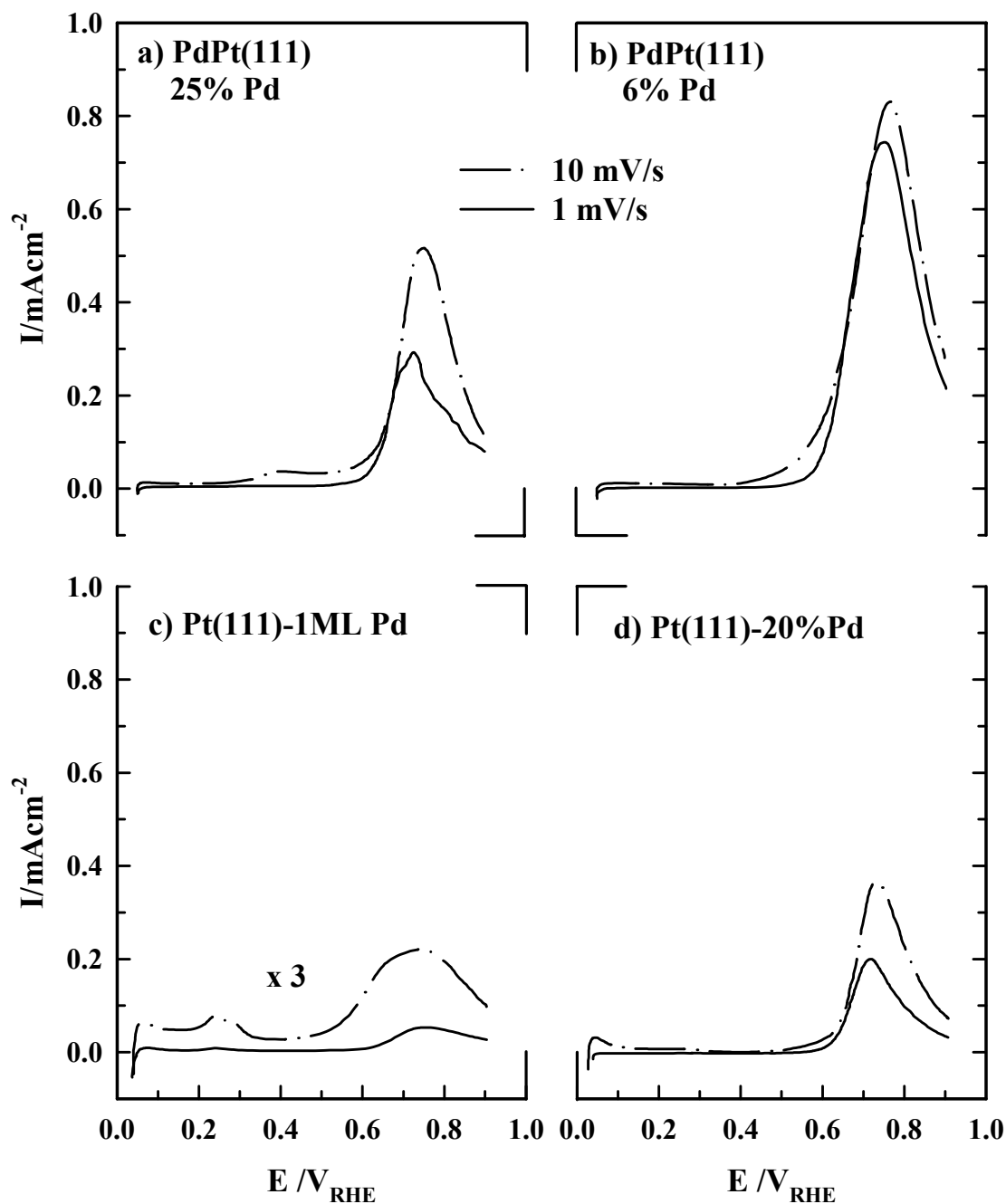

Figure 7.9: Polarization curves recorded with two different scan rates (as indicated) in 0.1 M $HClO_4$ + 50 mM CH_3OH at 293K on a) PdPt(111) bulk alloy with 25% Pd surface coverage; b) PdPt(111) bulk alloy with 25% Pd surface coverage; c) Pt(111)-1ML Pd (current densities in both curves are multiplied with 3); d) Pt(111)-20% Pd;

7.3 Discussion

Starting the discussion with the results of the electrooxidation of formic acid, the modification of the platinum surface with palladium clearly results in an increase in the electrocatalytic activity. In the cyclic voltammograms shown in Figure 7.4a it is obvious that the catalytic activity for platinum is different in the positive going vs. the negative going scan. This behavior for the (almost) bare platinum surface is typical for a self poisoning reaction, where increased current densities are detected when the reaction can proceed in an unhindered manner after oxidizing CO_{ad} at positive potentials. In contrast, the palladium monolayer supported on Pt(111) shows no indications of a poisoning reaction. Based on the experimental results it is therefore proposed that on the palladium film (at room temperature) the formic acid oxidation proceeds mainly via the direct path (k_d, in Figure 7.1) *without* the formation of the poisoning intermediate CO_{ad}.

This difference in the reaction mechanism results in an considerable increase in the electrocatalytic activity when modifying platinum with palladium, independently of the surface morphology. However, the enhancement on the PdPt(111) bulk alloys is mainly of transient nature. Several reasons may be responsible for this observation. One reason may be that on the bulk alloys CO formation takes place at the platinum sites (note, that most of the surface area is platinum) and the CO_{ad} can easily diffuse over the surface, inhibiting both palladium and platinum sites at low scan rates. Consequently, a random distribution of the palladium atoms is favoring the inhibition of the Pt as well as Pd sites in agreement with the experimental results. Based on the assumption that surface diffusion of CO_{ad} from platinum sites to palladium sites takes place, the observed behavior of the bulk alloy can be attributed to the lower mean distance between Pt and Pd sites on the bulk alloy. In contrast, the palladium film with nominally about the same surface coverage as the bulk alloy is less deactivated at low scan rates (see Figure 7.5).

However, also on this surface signs of a diffusion of CO from bare Pt sites to the palladium islands are indicated by the different ratio of the maximum current densities of the "palladium" and the "platinum" peak at the two scan rates in Figure 7.5c. But a possible deactivation of palladium by OH_{ad} and/or anions cannot be excluded. Interestingly, at both surfaces covered by about 25 % of palladium at low scan rates a shoulder in the main (platinum) oxidation peak towards lower potentials can be observed. A possible explanation for this behavior would be that this oxidation peak is due to oxidation at the boundary of Pt and Pd patches. Finally, the electronic properties of the bulk alloys versus the thin metal film should be different. However, up to date no studies about the electronic structure of the thin

palladium film exist. Consequently the difference in the electronic properties of a random distribution of the palladium and platinum atoms versus a thin palladium film remains elusive.

Although being far from a detailed understanding of the formic acid oxidation on the Pt(111)-Pd surface, very recent in-situ FTIR investigations of formic acid oxidation on Pt(111)-xPd surfaces are indeed supporting the supposition of different (main) reaction paths on bare Pt and on Pt(111)-Pd [169]. Reviewing shortly the preliminary results of these measurements, it has been found that, whereas on bare Pt(111) the formation of CO_{ad} begins immediately after the desorption of H_{upd}, on Pt(111)-nPd (n $\geq$ 1) no formation of CO_{ad} can be observed in the whole potential range. In contrast, the production of CO_2 increases linearly with the palladium coverage, strongly suggesting that on the palladium film the oxidation of formic acid proceeds in the direct path k_d, without the formation of the poisoning intermediate CO_{ad}. However, no clear Pd-CO_{ad} band could be observed so far from a Pt(111)-0.5 ML Pd film. The reason for this is not clear since even on Pt on-top sites only very low CO coverage are obtained and further measurements are necessary to clarify the role of CO_{ad} surface diffusion.

The results of the measurements presented here, can be compared with previous results of Kolb et al., which are, however obtained under different experimental conditions (a different palladium deposition procedure was applied as well as higher formic acid concentration in sulfuric acid as supporting electrolyte were used) [45]. To our knowledge this is the only work so far, in which the formic acid oxidation is investigated on Pd films and the experiments are pioneering work on the properties of thin palladium films in electrochemistry. Furthermore, the results are also compared to the oxidation on Pd(hkl) single crystals.

However, some small differences are apparent in both investigations. First of all, in the study of Kolb et al. the peak which is assigned here as "Pt-peak" is still seen at a nominally full monolayer of palladium and vanishes only if two palladium monolayers are deposited. In agreement with the FTIR results introduced in chapter 4 we address this to a more complete monolayer obtained when using the palladium deposition method described in chapter 3, i.e. depositing palladium from solutions containing very small amounts of palladium. Furthermore the assignment of the palladium coverage solely on the basis of integrated charges applied in ref. [45] seems to have some drawbacks.

Discussing the steady state measurements, at room temperature (or below) on the complete palladium monolayer in this thesis, the current densities measured ten minutes after a potential step to 0.3 V are much less deactivated, compared to the measurement presented in ref. [45]. Based on a comparison of the results of Kolb et al. and the measurements presented

here, it seems that a coverage assigned in reference [45] as 2 ML is in fact only about one monolayer. Based on this hypothesis of an inaccurate coverage determination in ref. [45] at steady-state conditions the activity of the monolayer towards formic acid oxidation is shown to be indeed superior to films with palladium coverages assigned as 5 and 10 ML [45]. Therefore it is concluded here, that the electrocatalytic activity of the pseudomorphic palladium film is most probably higher than the activity of Pt(111)-nPd (n > 2) as well as Pd(111) (see reference [45]). However, due to the onset of 3-dimensional growth when more than one monolayer is deposited it is not clear if the reported decrease in the steady-state activity with $\theta_{Pd} > 2$ (1) ML is to be assigned due to changes in the surface structure. Finally, this discussion shows the importance of a well established method in determining the surface coverage of a bimetallic surface and, at least in some cases, reverting to the use of UHV methods (LEIS) seems to be appropriate.

A rather puzzling result is, at first sight, the observed complex temperature dependence of the electrocatalytic activity. Due to the limited data the observations cannot conclusively be discussed. However, based on the results obtained so far, there may be one main reason accountable for the deactivation. The author proposes that presumably the most important reason for the deactivation with increasing the temperature is that the reaction pathway of formic acid oxidation is indeed *temperature* dependent on the palladium film. That is, whereas at low temperatures (up to room temperature) the reaction proceeds mainly via the *fast* direct oxidation pathway (k_d in Figure 7.1), at higher temperatures the formation of the poisoning intermediate CO_{ad} (k_p), and hence the *slow* pathway becomes more predominant resulting in a decrease of the activity of the palladium film. In other words the ratio k_d/k_p is a function of temperature. Another aspect is that the ratio of the rate constants k_d and k_p (and of course k_{ox}) in Figure 7.1 are most likely also *potential* dependent. This would explain the fact that a completely different behavior is observed at the two target potentials in the Arrhenius plot shown in Figure 7.8. Based on these conclusions, the definition of a unique activation energy for the formic oxid oxidation on the palladium is unclear. Anyway, a determination with an Arrhenius plot, as shown in Figure 7.8, is *not* suitable. For a further investigation of the pathway temperature-dependent FTIR measurements would be helpful.

Another aspect which should be taken into account is the inhibiting effect of anion adsorption on the electrocatalytic activity of the palladium film. In perchloric acid solution chloride adsorption (see chapter 4 and 5) as well as OH_{ad} may inhibit the electrocatalytic activity of the palladium film. An inhibiting effect of OH_{ad} may seem at first sight surprising due its role on bare Pt sites. However, since at low temperature the reaction mechanism proceeds mainly via the direct pathway, OH_{ad} has no function as an "oxidizer" of the poison

CO_{ad} as for example on bare platinum. Therefore its role should be basically the one of a site blocking species. The role of chloride as a site blocking species has been reported in the literature for bare Pt [156]. Based on the previous results described in chapter 4 and 5 the inhibiting effect should be even increased on palladium. Note also, that the purity grade of formic acid is lower than the ultrapure acids used as supporting electrolyte. Finally, at higher temperatures the adsorption of chloride impurities might be enhanced leading to a further deactivation of the surface.

Without giving a final conclusion of all aspects, as an important result it can be stated that the formic acid oxidation on a thin palladium film supported on Pt(111) shows a complex interdependence of several factors affecting its catalytic activity.

Due to the very limited data for the methanol oxidation no discussion of this reaction can be given. It can only be stated that a possible blocking of reaction sites may also be partially accountable for the complete inhibition of the palladium film for the electrooxidation of methanol since this reaction needs more adsorption sites than the oxidation of formic acid. However, most likely further influences are responsible for the low catalytic activity of the palladium towards methanol.

7.4 Summary: Oxidation of small organic molecules

The results of formic acid as well as methanol oxidation on Pt(111)-Pd electrodes confirm that by using the described deposition method a complete palladium monolayer can be obtained. This pseudomorphic monolayer supported on Pt(111) has a considerably improved electrocatalytic activity towards formic acid oxidation compared to bare Pt(111). The enhancement in the reaction rate is confirmed by transient measurements as well as by quasi steady-state measurements.

The high catalytic activity of the palladium film is attributed to a reaction mechanism which proceeds at room temperature (and below) mainly via a fast direct oxidation path. In contrast, on bare Pt(111) a slow pathway is operative via the formation of CO_{ad} as a poisoning intermediate. On the palladium film the reaction pathway is both temperature as well as potential dependent leading to a complex behavior. No activation energy for the process can be determined using an Arrhenius approach.

Under steady state conditions the highest catalytic activity is observed at a potential of about 0.3 V and at temperatures below room temperature, where the direct pathway is favored. However, an ongoing deactivation with time can be observed. The reason for this observation is still not clear, but site blocking effects due to chloride and/or OH^- species may be accountable.

The palladium film is completely inactive towards methanol electrooxidation. One assumption is that also site blocking effects due to anion adsorption may be the reason for this low catalytic activity. The more adsorption sites are needed in the reaction mechanism the higher becomes this influence on the catalytic activity.

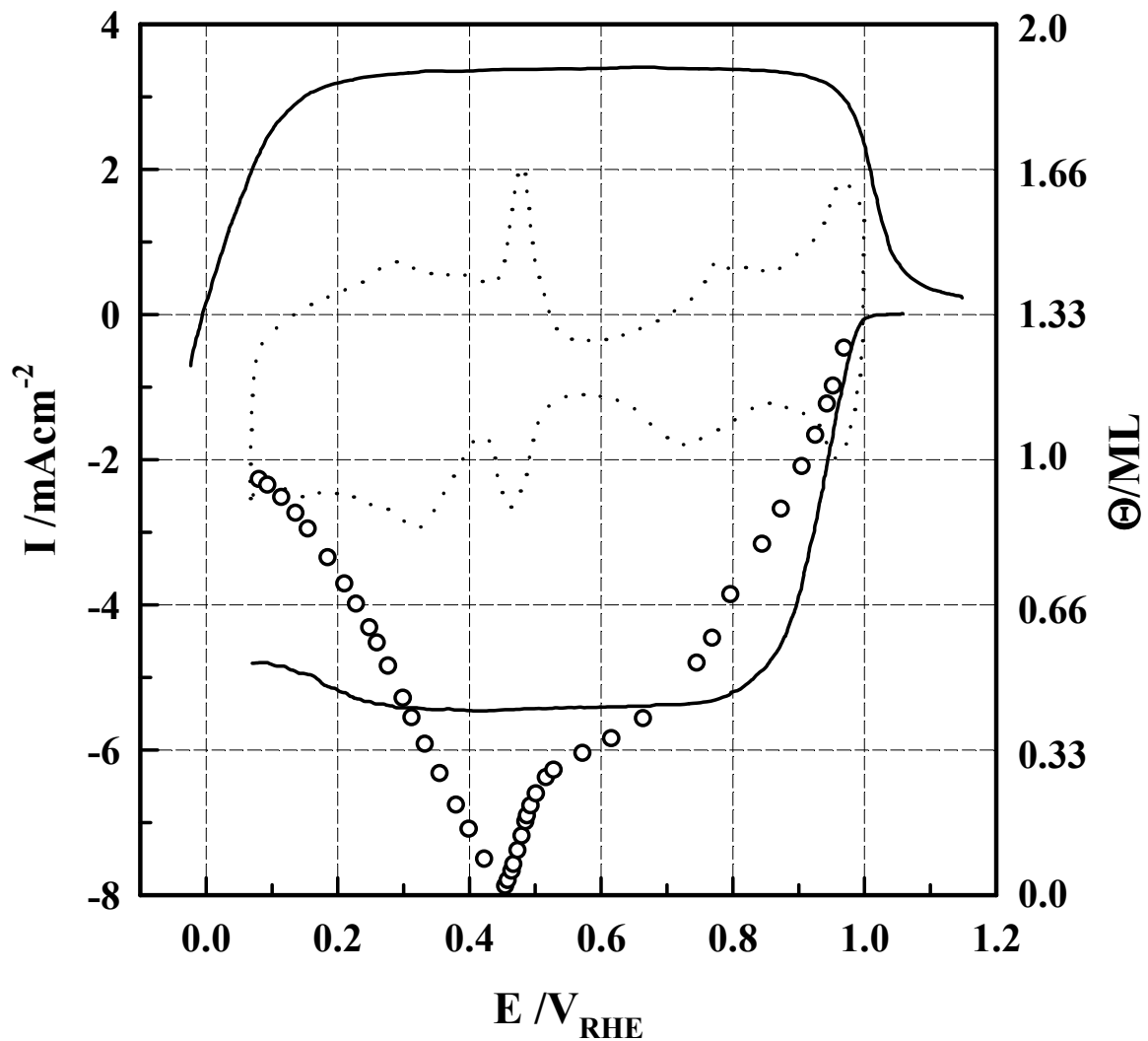# Chapter 8

Conclusions

8.1 Concluding discussion

Figure 8.1: Summary of the polarization curves of oxygen reduction and hydrogen oxidation on Pt(111)-Pd; the base voltammogram in argon saturated electrolyte is included as well; 0.1 M KOH at 293 K; scan rate is 50 mV/s; the integrated charges of H_{upd} and OH_{ad} are shown as open circles

Conclusively, the results of the investigation of a pseudomorphic palladium monolayer supported on Pt(111) can be summarized by reviewing the basic fuel cell reactions, the HOR and the ORR in alkaline solution (see Figure 8.1). As it has been pointed out in the course of this thesis the surface coverage of anions has an important influence on the rate of a reaction. Therefore, additionally to the polarization curves of the HOR and ORR, in Figure 8.1, the cyclic voltammogram and the integrated charges of H_{upd} and OH_{ad} are included as well.

The most important aspect which becomes apparent when analyzing Figure 8.1 is, that the activation and deactivation of both processes, the HOR and the ORR are *correlated* to each other. When scanning the potential from the current plateau region of diffusion limited control in negative direction, the deactivation of the hydrogen oxidation occurs concomitantly with the deactivation of the ORR. In fact only slight differences are observed in the deactivation process, which can be rationalized by the different kinetic rates of the two reactions. For the hydrogen reaction exchange current densities of about 10^{-3} A/cm^2 are determined, whereas for the oxygen reaction typical values are by a factor of 1000 lower. Consequently the potential region of diffusion limited current densities (plateau) is broader for the HOR compared to the ORR. At low potentials for example, the diffusion limited current density of the HOR is obtained slightly before the diffusion limited potential region of the ORR is reached. (Note, that the HOR and the ORR are recorded by starting from the negative potential limit and scanning in positive direction).

The same correlation of the deactivation of both processes can be observed at positive potentials. Based on the comparison with the cyclic voltammogram in Figure 8.1, the effect of OH_{ad} can be summarized. The formation of the reversible form of OH_{ad} seems not to block the active sites for both reactions. In turn, at high potentials the decrease of the current densities of both reactions is concomitant with the formation of irreversible adsorbed OH. In the cyclic voltammogram the formation of surface oxides is indicated by the peak at 0.95 V. Once the surface is covered by an oxide layer the adsorption sites for the reactants are totally blocked. In other words, coming from positive potentials, the oxygen reduction starts with the reduction of surface oxides.

At low potentials, H_{upd} plays the same role as a site blocking species as the oxide formation at high potentials. The fact that H_{upd} affects the ORR on Pt(111)-Pd less than on Pt(111), indicates that H_{upd} is adsorbed in deeper potential wells of the first layer. Consequently, also the HOR is more active on Pt(111)-Pd than on Pt(111) since more reaction sites for H_{opd} are available.

If more than one palladium monolayer is deposited on Pt(111), the film (growth) seems to have the same effect for the electrocatalytic activity of the HOR and the ORR. This

may indicate that the different surface structure affects the absorption of hydrogen at negative potentials in the same way as it does affect the formation of surface oxides at high potentials.

8.2 Summary

In this work the electrocatalytic properties of pseudomorphic palladium films supported on a Pt(111) electrode are investigated. Instead of examining one reaction extensively, the concept of this thesis is to probe the activity of the surface towards a *variety* of reactions and to gain insight into the *general* aspects which affect the catalytic properties of the catalyst by comparing the different results. The selection of the reactions which are investigated has been undertaken on the basis that all reactions are related to low-temperature fuel cell applications. The reactions investigated are the carbon monoxide oxidation reaction, the oxygen reduction reaction, the hydrogen evolution as well as the hydrogen oxidation reaction, and the oxidation of small organic molecules.

In the following the most important results are summarized. In catalysis, when doing basic research, working with reproducible, well-defined surfaces is crucial. Therefore, after giving in chapter 2 the theoretical and experimental details, in chapter 3 the thin palladium film is characterized. From previous work it was known that palladium deposition on Pt(111) in sulfuric acid solution yields to pseudomorphic growth and a complete monolayer can be obtained before 3-dimensional growth sets in. In this work the morphology of the thus prepared palladium films is investigated with FTIR by using CO_{ad} as a probe molecule. It is verified, that in fact palladium grows in large islands of monoatomic height on the Pt(111) surface. By transfer experiments, where UHV prepared palladium films are transferred to an electrochemical cell, a calibration curve is developed which allows the determination of the palladium coverage of *electrochemically* deposited films on Pt(111). This procedure has the advantage that in the following investigations electrochemically deposited palladium films of a known surface coverage can be used and no further transfer experiments are necessary.

The first reaction probed on the well-characterized Pt(111)-xPd surface is the electrooxidation reaction of adsorbed carbon monoxide (chapter 4). The main analytical tool for these experiments is the in-situ FTIR spectroscopy.

In alkaline solution it is shown that the onset potential of the CO oxidation reaction is about the same on Pt(111)-Pd and on bare Pt(111), respectively. The reaction rate, however, is

considerably lower on Pt(111)-Pd than on Pt(111). This observation is attributed to a stronger interaction of OH⁻ with the Pt(111)-Pd surface, than with the bare Pt(111) surface.

In perchloric acid solution another factor which affects the oxidation rate on Pt(111)-Pd is specific anion adsorption from the supporting electrolyte. It is shown, that chloride impurities contained in perchloric acid solution effectively block the adsorption sites for OH_{ad} formation, and thus, inhibit the CO oxidation reaction.

In chapter 5 the oxygen reduction reaction is investigated by applying the RRDE technique. In alkaline solution an exceptionally high catalytic activity is found for Pt(111)-1ML Pd, this surface being the most active catalyst for the ORR in alkaline solution. The ultimate reason for this high catalytic activity is still unclear. However, some suppositions are given in the discussion. The most important finding is, that in alkaline solution the catalytic activity of a surface can be directly linked to its tendency to become strongly oxidized.

The discussion of the results obtained in perchloric acid solution is more straightforward. The comparison of the measurements of the ORR on Pt(111)-Pd in acid and in alkaline solution demonstrate the influence of the supporting electrolyte on the catalytic activity of a catalyst. The lower catalytic acticity in perchloric acid solution can clearly be ascribed to the site blocking effect of specifically adsorbed chloride from the supporting electrolyte. Even small amounts of these "spectator" anions, which are not involved in the reaction, influence the reactivity of the catalyst simply by reducing the number of active sites for the reaction to proceed. Consequently, by complementing these results with investigations of the adsorption behavior of anions, especially chloride, conclusions about the reactive sites of the catalyst should be possible. Since the adsorption conditions in the solid electrolyte of a low temperature PEM fuel cell are *not* known, it is important to investigate model catalysts in different supporting electrolytes and to see in which environment the catalyst works best.

In chapter 6 the hydrogen reactions (HER/HOR) are investigated on Pt(111)-Pd. As for the ORR, the RRDE technique is the main analytical tool. It is shown, that also for the hydrogen reactions Pt(111)-Pd has a high catalytic activity. The exchange current density of the hydrogen reactions is determined and a correlation between the apparent activation energy and the reaction rate is established. This correlation shows, as generally expected, higher reaction rates with lower activation energies. As for the ORR, the reason for the high activity is difficult to determine. However, it is proposed that the adsorption behavior of H_{upd} on Pt(111)-Pd is one of the main keys for understanding the reactivity.

In chapter 7 the oxidation of small organic molecules, i.e. formic acid and methanol is investigated. Whereas the Pt(111)-Pd surface is completely inactive for methanol oxidation, it is highly active for formic acid oxidation. For formic acid oxidation it is shown that at room temperature, in contrast to bare Pt(111), on Pt(111)-Pd a direct oxidation pathway is active. The fast direct oxidation pathway results in a high catalytic activity of the Pt(111)-Pd surface. However, at higher temperatures the reaction mechanism changes to a serial pathway with the formation of the site blocking species CO_{ad}. It is suggested that the pseudomorphic palladium monolayer supported on Pt(111) has special properties compared to the surfaces of bulk alloys and bulk Pd(111).

The low catalytic activity towards methanol oxidation may be, at least partially, due to the strong anion adsorption and therefore a consequence of a blocking of the adsorption sites.

As an outlook, it can be emphasized that for a complete *interpretation* of the electrocatalytic properties of Pt(111)-Pd established in this work, atomic level studies (by STM) of the process of oxide formation in alkaline solution as well as the adsorption behavior of anions in acid solution, and the investigation of the electronic structure of the thin palladium film are necessary.

8.3 Zusammenfassung in deutscher Sprache

Die vorliegende Arbeit handelt von der Untersuchung der elektrokatalytischen Eigenschaften von pseudomorphen Palladium-Filmen, die auf einer Pt(111) abgeschieden wurden. Anstatt eine einzelne Reaktion sehr ausführlich zu untersuchen, werden durch die Untersuchung einer Vielzahl verschiedener Reaktionen *generelle* Aspekte, die die katalytischen Eigenschaften von Katalysatoren beeinflussen, herausgearbeitet. Die Auswahl der untersuchten Reaktionen wurde nach dem Kriterium getroffen, dass alle Reaktionen einen Bezug zu Niedertemperatur-Brennstoffzellen haben. Die Reaktionen sind im Einzelnen die CO-Oxidation, die Sauerstoffreduktionsreaktion, die Wasserstoffoxidationsreaktion und die Oxidation kleiner organischer Moleküle.

Im Folgenden werden die wichtigsten Ergebnisse noch einmal zusammenfassend dargestellt. Die Arbeit beginnt nach einer kurzen Einführung (Kapitel 1) mit der Erläuterung der angewandten Untersuchungsmethoden und der zugrundeliegenden Theorie. Zudem werden die experimentellen Details der Untersuchungen angegeben (Kapitel 2). Da es für Untersuchungen grundsätzlicher Art eine wesentliche Voraussetzung ist mit reproduzierbaren,

eingehend charakterisierten Oberfläche zu arbeiten, beginnt der Ergebnisteil der Arbeit mit der Charakterisierung der verwendeten Oberfläche (Kapitel 3). Die Palladiumfilme werden elektrochemisch durch Zykeln in Schwefelsäure mit geringen Mengen an Palladiumoxid auf eine Pt(111)-Elektrode aufgebracht. Aufbauend auf den Ergebnissen vorhergehender Untersuchungen wird zunächst die Morphologie des pseudomorphen Palladiumfilms mittels FTIR Spektroskopie von adsorbiertem CO untersucht. CO dient dabei als Sondenmolekül. Durch einen Vergleich der Spektren der freien Pt(111) Oberfläche und eines kompletten Palladiumfilms mit denen einer Submonolage Palladium auf Pt(111) wird darauf geschlossen, dass Palladium unter den gewählten Parametern in Inseln von monoatomarer Höhe auf Pt(111) aufwächst. Weiterhin werden mittels Transferexperimente die zyklischen Voltammogramme von im UHV präparierten Pt(111)-xPd Oberflächen mit denen von elektrochemisch hergestellten Pt(111)-xPd Oberflächen verglichen. Es zeigt sich, dass die Voltammogramme der auf beide Weisen hergestellten Filme im wesentlichen identisch sind. Dies ermöglicht es, eine Eichkurve zu erstellen, die die im UHV bestimmte Oberflächenzusammensetzung der Probe mit dem elektrochemischen Verhalten in Schwefelsäure vergleicht. Auf diese Weise ist es möglich auf elektrochemischen Wege Palladiumfilme mit bekannter Bedeckung herzustellen, und es kann im folgenden auf die aufwendigen Transferexperimente verzichtet werden.

Die erste katalytische Oberflächenreaktion, die in der vorliegenden Arbeit untersucht wird, ist die Elektrooxidation von adsorbiertem Kohlenmonoxid (Kapitel 4). Die Haupt-untersuchungsmethode ist hierbei die in-situ FTIR Spektroskopie.

Zunächst wird die Reaktion in *alkalischer* Lösung untersucht. Es zeigt sich, dass die Oxidation von adsorbiertem CO auf der freien Pt(111) und der Pt(111)-Pd Oberfläche in etwa bei dem gleichen Potential beginnt. Jedoch ist die Reaktionsrate der CO-Oxidation auf beiden Oberflächen unterschiedlich. Es wird beobachtet, dass die Reaktionsrate auf dem Palladiumfilm geringer ist als auf der freien Pt(111) Oberfläche. Diese Inhibition der Oxidation auf dem Palladiumfilm wird auf eine stärkere Pt(111)-Pd-OH$_{ad}$ Wechselwirkung zurückgeführt.

In Perchlorsäure wird ein weiterer Faktor, der die Reaktion beeinflusst, deutlich. Es wird gezeigt, dass in der Säure Anionenadsorption die Reaktionsplätze für die CO-Oxidation blockiert. Zu niedrigen Potentialen hin wird die OH$^-$ Adsorption durch adsorbiertes Chlorid verhindert. Daher kommt es zu einer Konkurrenz bei der Koadsorption zwischen OH$^-$ und Chlorid Anionen. Es wird gezeigt, dass je höher die Konzentration von stark adsorbierenden Anionen im Elektrolyten ist, desto höher ist das Potential bei dem die CO-Oxidation einsetzt. Zusammenfassend kann also gesagt werden, dass in *Perchlorsäure* die starke

Wechselwirkung von Palladium mit Anionen dazu führt, dass, im Vergleich zur freien Pt(111) Oberfläche, auf dem Palladiumfilm die Oxidation von CO erst bei höheren Potentialen einsetzt.

In Kapitel 5 wird die Sauerstoffreduktionsreaktion mittels der Methode der rotierenden Ring-Scheiben-Elektrode untersucht. Die Ergebnisse zeigen, dass ein pseudomorpher Palladiumfilm abgeschieden auf Pt(111) eine außerordentlich hohe katalytische Aktivität bezüglich der Sauerstoffreduktion in alkalischer Lösung besitzt. Es kann die Aktivität von der reinen Pt(111) Oberfläche, dem bis dato aktivsten Katalysator in alkalischer Lösung, erheblich gesteigert werden. Eine abschließende Erklärung für die hohe Aktivität des Palladiumfilms kann noch nicht gegeben werden. Es werden jedoch verschiedene Lösungsansätze diskutiert. Dabei wird gezeigt, dass in alkalischer Lösung die katalytische Aktivität von (bimetallischen) Oberflächen der Platingruppe direkt mit der Tendenz, irreversibel oxidiert zu werden, zusammenhängt.

In Perchlorsäure sind die Ergebnisse eindeutiger zu interpretieren. Ein Vergleich der Messungen an Pt(111)-Pd in Säure und in alkalischer Lösung zeigt deutlich den Einfluss des Grundelektrolyten auf die Aktivität des Katalysators. In Perchlorsäure kann, im Vergleich zu Pt(111), eine erhöhte Chloridadsorption auf dem Palladiumfilm nachgewiesen werden. Das Chlorid stammt von geringsten Verunreinigungen, die selbst in Perchlorsäure mit maximal erhältlicher Reinheit noch vorhanden sind. Dies führt dazu, dass aufgrund von erhöhter Anionenadsorption, die Anzahl der freien Reaktionsplätze auf der Oberfläche der Pt(111)-Pd Elektrode (und somit ihre Aktivität) in Perchlorsäure geringer ist als auf der freien Pt(111) Oberfläche. Die schwache Wechselwirkung der Oberfläche mit Perchloratanionen beeinflusst hingegen die Reaktion nicht. Daher ist für weiterführende Untersuchungen ein Studium des Adsorptionsverhaltens von Anionen auf der Pt(111)-Pd Oberfläche, z.B. mittels STM, interessant. Dies könnte, unter anderem, Hinweise auf die aktiven Reaktionsplätze der Oberfläche geben.

Da die genauen Adsorptionsbedingungen in einer realen Niedertemperatur-Brennstoffzelle nicht bekannt sind, muss folglich bei einem Studium von Elektrokatalysatoren immer der Einfluss des Grundelektrolyten beachtet werden.

In Kapitel 6 wird die Wasserstoffentwicklungs- und -oxidationsreaktion untersucht. Wie schon in den Untersuchungen der Sauerstoffreduktion wird im wesentlichen die Methode der rotierenden Scheiben Elektrode angewandt. Für die Wasserstoffentwicklungs- und -oxidationsreaktion wird ebenfalls eine hohe katalytische Aktivität der Pt(111)-Pd Oberfläche gefunden. Dabei kann eine Korrelation zwischen der Reaktionsrate und der

Aktivierungsenergie der Reaktion nachgewiesen werden. Es zeigt sich, dass (wie erwartet) eine geringere Aktivierungsenergie eine höhere Reaktionsrate zur Folge hat. Für die Pt(111)-Pd Oberfläche wird aufgrund der hohen katalytische Aktivität bezüglich der Wasserstoffoxidations-Reaktion darauf geschlossen, dass bei Unterpotential abgeschiedener Wasserstoff, H_{upd}, nicht auf der Oberfläche sitzt, sondern teilweise in der ersten Lage absorbiert ist.

In Kapitel 7 wird das Verhalten des auf Pt(111) abgeschiedenen, pseudomorphen Palladiumfilms bezüglich der Oxidation kleiner organischer Moleküle untersucht. Hierzu wurde Ameisensäure und Methanol ausgewählt. Es zeigt sich, dass der Palladiumfilm komplett inaktiv gegenüber der Oxidation von Methanol ist, jedoch bei Raumtemperatur eine sehr hohe Aktivität bezüglich der Oxidation von Ameisensäure besitzt. Diese hohe Aktivität kann auf eine Oxidation der Ameisensäure über einen direkten Oxidationspfad, ohne die Bildung von CO_{ad}, zurückgeführt werden. Bei einer Temperatur von 303 K kommt es zu einer Verringerung der Reaktionsrate, was auf einen Wechsel im Reaktionspfad zurückgeführt wird. In Gegensatz hierzu, wird bei der Oxidation von Ameisensäure auf Platinelektroden im gesamten Temperaturbereich CO_{ad}, gebildet, welches die Adsorptionsplätze der Ameisensäure blockiert.

Bezüglich der Methanoloxidation liegen für die Pt(111)-Pd Oberfläche nur begrenzte Erkenntnisse vor. Ein Ansatz, um die geringe Reaktionsrate zu erklären, ist die Blockade von Adsorptionsplätzen für Methanol durch Anionenadsorption.

Als ein Ausblick bleibt zu erwähnen, dass die wichtigsten Details, die für ein komplettes Verständnis der katalytischen Aktivität der Pt(111)-Pd Oberfläche fehlen, die elektronische Struktur des Palladiumfilms, ein Einblick in den Prozess der Oxidbildung in alkalischer Lösung, sowie das Adsorptionsverhalten von Anionen in einem sauren Elektrolyten sind.

Chapter 9
References

[1]   Berzelius, J.J., Jahresberichte aus der Chemie, 1836. **15**: p. 237.

[2]   Grove, W.R., Philos. Mag., 1839. **14**: p. 127.

[3]   Carrette, L., K.A. Friedrich, and U. Stimming, ChemPhysChem, 2000. **1**(4): p. 162-193.

[4]   Markovic, N.M. and P.N. Ross, CatTech, 2000. **4**(2): p. 110-126.

[5]   Ertl, G. and J. Kuppers, *Low energy electrons and surface chemistry*. 1985, Weinheim: VCH.

[6]   Greef, R., R. Peat, L.M. Peter, D. Pletcher, J. Robinson, and S.e. group), *Instrumental methods in electrochemistry*, ed. T.J. Kemp. 1990: Ellis Horwood.

[7]   Gileadi, E., *Electrode kinetics for chemists, chemical engineers, and materials scientists*. 1993: Wiley-VCH.

[8]   Nicholson, R.S. and I. Shain, Analytical Chemistry, 1964. **36**(4): p. 706-23.

[9]   Nicholson, R.S., Analytical Chemistry, 1965. **37**(11): p. 1351-5.

[10]   Beden, B. and C. Lamy, *Infrared Reflectance Spectroscopy*, in *Spectroelectrochemistry-theory and practice*, R.J. Gale, Editor. 1988, Plenum Press.

[11]   Bewick, A. and K. Kunimatsu, Surface Science, 1980. **101**(1-3): p. 131-8.

[12]   Bishop, D.M., Journal of Chemical Physics, 1993. **98**(4): p. 3179-3184.

[13]   Lambert, D.K., Electrochimica Acta, 1996. **41**(5): p. 623-630.

[14]   Bockris, J.O.M. and A.K.N. Reddy, *Modern Electrochemistry*. Vol. 2. 1970, New York: Plenum Press.

[15]   Iwasita, T. and F.C. Nart, Progress in Surface Science, 1997. **55**(4): p. 271-340.

[16]   Nichols, R., *IR spectroscopy of molecules at the solid-solution interface*, in *Adsorption of molecules at metal electrodes*, J. Lipkowski and P.N. Ross, Editors. 1992, VCH Weinheim.

[17]   Bard, A.J. and L.R. Faulkner, *Electrochemical methods: fundamentals and applications*. 1980: John Wiley & Sons.

[18]   Albery, W.J. and M.L. Hitchman, *Ring-Disk Electrodes*. 1971, Oxford: Clarendon Press.

[19]   Plsekov, Y.V. and V.Y. Filinovskij, *The rotating disc electrode*. 1976, New York: Consultant Bureau.

[20]   Levich, V.G., *Physicochemical Hydrodynamics*. 1962, Englewood Cliffs, NJ: Prentice Hall.

[21]   Ross, P.N., *The science of electrocatalysis on bimetallic surfaces*, in *Electrocatalysis*, J. Lipkowski and P.N. Ross, Editors. 1998, Wiley-VCH.

[22]   Niemantsverdriet, J.W., *Spectroscopy in Catalysis*. 1993: VCH.

[23]   Niehus, H., W. Heiland, and E. Taglauer, Surface Science Reports, 1993. **17**: p. 213-303.

[24]   Markovic, N.M., H.A. Gasteiger, and P.N. Ross, Journal of Physical Chemistry, 1995. **99**(11): p. 3411-3415.

[25]   Clavilier, J., D. Armand, S.G. Sun, and M. Petit, Journal of Electroanalytical Chemistry, 1986. **205**: p. 267-277.

[26]   Markovic, N.M., M. Hanson, G. McDougall, and E. Yeager, Journal of Electroanalytical Chemistry, 1986. **214**: p. 555-566.

[27]   Stuhlmann, C., H. Hoffschulz, and K. Wandelt, *Properties of bimetallic electrodes: spectroscopic characterization and electrocatalysis*, in *Interfacial electrochemistry*, A. Wieckowski, Editor. 1999, Marcel Dekker, Inc.: New York.

[28]   Somorjai, G.A., *Introduction to Surface Chemistry and Catalysis*. 1993, New York: John Wiley & Sons.

[29]   Henzler, M. and W. Göpel, *Oberflächenphysik des Festkörpers*. 1991, Stuttgart: B.G. Teubner.

[30]   Kilian, U. and C. Weber, *Lexikon der Physik*. Vol. 4. 2000, Heidelberg: Spektrum Akademischer Verlag.

[31]   Rodriguez, J.A. and D.W. Goodman, Science, 1992. **257**(5072): p. 897-903.

[32]   Campbell, R.A., J.A. Rodriguez, and D.W. Goodman, Physical Review B-Condensed Matter, 1992. **46**(11): p. 7077-87.

[33]   Han, M., P. Mrozek, and A. Wieckowski, Physical Review B-Condensed Matter, 1993. **48**(11): p. 8329-8335.

[34]   Sellidj, A. and B.E. Koel, Surface Science, 1993. **284**(1-2): p. 139-153.

[35]   Sellidj, A. and B.E. Koel, Physical Review B, 1994. **49**(12): p. 8367-8376.

[36]   Poulston, S., M. Tikhov, and R.M. Lambert, Catalysis Letters, 1996. **42**(3-4): p. 167-172.

[37]   Rodriguez, J.A., Surface Science Reports, 1996. **24**: p. 223-287.

[38]   Hammer, B., Y. Morikawa, and J.K. Norskov, Physical Review Letters, 1996. **76**(12): p. 2141-2144.

[39]   Mavrikakis, M., B. Hammer, and J.K. Norskov, Physical Review Letters, 1998. **81**(13): p. 2819-2822.

[40]   Pallassana, V., M. Neurock, L.B. Hansen, B. Hammer, and J.K. Norskov, Physical Review B, 1999. **60**(8): p. 6146-6154.

[41]   Koschel, H., U. Birkenheuer, G. Held, and H.P. Steinruck, Surface Science, 2001. **477**(2-3): p. 113-125.

[42]   Attard, G. and A. Bannister, Journal of Electroanalytical Chemistry, 1991. **300**: p. 467.

[43]   Llorca, M.J., J.M. Feliu, A. Aldaz, and J. Clavilier, Journal of Electroanalytical Chemistry, 1993. **351**(1-2): p. 299-319.

[44]   Attard, G.A., R. Price, and A. Alakl, Electrochimica Acta, 1994. **39**(11-12): p. 1525-1530.

[45]   Baldauf, M. and D.M. Kolb, Journal of Physical Chemistry, 1996. **100**(27): p. 11375-11381.

[46]   Climent, V., N.M. Markovic, and P.N. Ross, Journal of Physical Chemistry B, 2000. **104**(14): p. 3116-3120.

[47]   Inukai, J. and M. Ito, Journal of Electroanalytical Chemistry, 1993. **358**(1-2): p. 307-315.

[48]   Alvarez, B., V. Climent, A. Rodes, and J.M. Feliu, Journal of Electroanalytical Chemistry, 2001. **497**(1-2): p. 125-138.

[49]   Markovic, N.M., C.A. Lucas, V. Climent, V. Stamenkovic, and P.N. Ross, Surface Science, 2000. **465**(1-2): p. 103-114.

[50]   Kibler, L.A., M. Kleinert, R. Randler, and D.M. Kolb, Surface Science, 1999. **443**(1-2): p. 19-30.

[51]   Naohara, H., S. Ye, and K. Uosaki, Electrochimica Acta, 2000. **45**(20): p. 3305-3309.

[52]   Naohara, H., S. Ye, and K. Uosaki, Journal of Physical Chemistry B, 1998. **102**(22): p. 4366-4373.

[53]   Naohara, H., S. Ye, and K. Uosaki, Journal of Electroanalytical Chemistry, 1999. **473**(1-2): p. 2-9.

[54]   Baldauf, M. and D.M. Kolb, Electrochimica Acta, 1993. **38**(15): p. 2145-2153.

[55]   Kibler, L.A., PhD. thesis, University of Ulm, 2000.

[56]   Gomez, R., A. Rodes, J.M. Perez, J.M. Feliu, and A. Aldaz, Surface Science, 1995. **344**(1-2): p. 85-97.

[57]   Gomez, R., A. Rodes, J.M. Perez, J.M. Feliu, and A. Aldaz, Surface Science, 1995. **327**(3): p. 202-215.

[58]   Clavilier, J., M.J. Llorca, J.M. Feliu, and A. Aldaz, Journal of Electroanalytical Chemistry, 1991. **310**: p. 429.

[59]   Clavilier, J., J.M. Feliu, A. Fernandez-Vega, and A. Aldaz, Journal of Electroanalytical Chemistry, 1989. **269**: p. 175.

[60]   Llorca, M.J., J.M. Feliu, A. Aldaz, and J. Clavilier, Journal of Electroanalytical Chemistry, 1994. **376**(1-2): p. 151-160.

[61]   Koper, M.T.M. and J.J. Lukkien, Journal of Electroanalytical Chemistry, 2000. **485**(2): p. 161-165.

[62]   Funtikov, A.M., U. Linke, U. Stimming, and R. Vogel, Surface Science, 1995. **324**(1): p. L343-L348.

[63]   Friedrich, K.A., K.P. Geyzers, U. Linke, U. Stimming, and J. Stumper, Journal of Electroanalytical Chemistry, 1996. **402**(1-2): p. 123-128.

[64]   Kitamura, F., M. Takahashi, and M. Ito, Surface Science, 1989. **223**: p. 493.

[65]   Physical-Electronics, *Handbook of auger electron spectroscopy*. 3. Edition ed. 1995, Eden Prairie.

[66]   Gil, A., A. Clotet, J.M. Ricart, F. Illas, B. Alvarez, A. Rodes, and J.M. Feliu, Journal of Physical Chemistry B, 2001. **105**(30): p. 7263-7271.

[67]   Engel, W. and G. Ertl, in *The Chemical Physics of Solid Surfaces and Heterogeneous Catalysis*, D.P. Woodruff and D.A. King, Editors. 1982, Elsevier: New York. p. 73.

[68]   Lamy, C. and J.M. Leger, *Advanced electrode materials for the direct methanol fuel cell*, in *Interfacial Electrochemistry*, A. Wieckowski, Editor. 1999, Marcel Dekker, Inc.: New York.

[69]   Hamnet, A., *Mechanism of Methanol Electro-Oxidation*, in *Interfacial Electrochemistry*, A. Wieckowski, Editor. 1999, Marcel Dekker, Inc.: New York.

[70]   Markovic, N.M. and P.N. Ross, Electrochimica Acta, 2000. **45**(25-26): p. 4101-4115.

[71]   Wasberg, M., L. Palaikis, S. Wallen, M. Kamrath, and A. Wieckowski, Journal of Electroanalytical Chemistry, 1988. **256**: p. 51.

[72]   Zurawski, D., M. Wasberg, and A. Wieckowski, Journal of Physical Chemistry, 1990. **94**: p. 2076.

[73]   Villegas, I. and M.J. Weaver, Journal of Chemical Physics, 1994. **101**(2): p. 1648-1660.

[74]   Villegas, I., X.P. Gao, and M.J. Weaver, Electrochimica Acta, 1995. **40**(10): p. 1267-1275.

[75]   Lucas, C.A., N.M. Markovic, and P.N. Ross, Surface Science, 1999. **425**(1): p. L381-L386.

[76]   Akemann, W., K.A. Friedrich, and U. Stimming, Journal of Chemical Physics, 2000. **113**(16): p. 6864-6874.

[77]   Markovic, N.M., B.N. Grgur, C.A. Lucas, and P.N. Ross, Journal of Physical Chemistry B, 1999. **103**(3): p. 487-495.

[78]   Akemann, W., K.A. Friedrich, U. Linke, and U. Stimming, Surface Science, 1998. **404**(1-3): p. 571-575.

[79]   Lebedeva, N.P., M.T.M. Koper, E. Herrero, J.M. Feliu, and R.A. van Santen, Journal of Electroanalytical Chemistry, 2000. **487**(1): p. 37-44.

[80]   Markovic, N.M., C.A. Lucas, A. Rodes, V. Stamenkovic, and P.N. Ross, Surface Science, 2002. **499**: p. L149-L158.

[81]   Zou, S.Z., R. Gomez, and M.J. Weaver, Journal of Electroanalytical Chemistry, 1999. **474**(2): p. 155-166.

[82]   Markovic, N.M. and P.N. Ross, Surface Science Reports, 2002(in print).

[83]   Bergelin, M., J.M. Feliu, and M. Wasberg, Electrochimica Acta, 1998. **44**(6-7): p. 1069-1075.

[84]   Bergelin, M., E. Herrero, J.M. Feliu, and M. Wasberg, Journal of Electroanalytical Chemistry, 1999. **467**(1-2): p. 74-84.

[85]   Schmidt, T.J., P.N. Ross, and N.M. Markovic, Journal of Physical Chemistry B, 2001. **105**(48): p. 12082-12086.

[86]   Beden, B. and C. Lamy, Electrochimica Acta, 1990. **35**: p. 691.

[87]   Wagner, F.T. and P.N. Ross, Journal of Electroanalytical Chemistry, 1988. **250**: p. 301.

[88]   Markovic, N.M., T.J. Schmidt, B.N. Grgur, H.A. Gasteiger, R.J. Behm, and P.N. Ross, Journal of Physical Chemistry B, 1999. **103**(40): p. 8568-8577.

[89]   Chang, S.C. and M.J. Weaver, Surface Science, 1990. **238**: p. 42.

[90]   Wasileski, S.A., M.T.M. Koper, and M.J. Weaver, Journal of Physical Chemistry B, 2001. **105**(17): p. 3518-3530.

[91]   Schmidt, T.J., N.M. Markovic, V. Stamenkovic, P.N. Ross, G. Attard, and D. Watson, submitted to Langmuir, 2002.

[92]   Lebedeva, N.P., M.T.M. Koper, J.M. Feliu, and R.A. van Santen, Electrochemistry Communications, 2000. **2**(7): p. 487-490.

[93]   Lebedeva, N.P., M.T.M. Koper, J. Feliu, and R.A. v. Santen, submitted to J. Phys. Chem. B., 2002.

[94]   Lebedeva, N.P., M.T.M. Koper, J. Feliu, and R.A. v. Santen, Journal of Electroanalytical Chemistry (in press), 2002.

[95]   Markovic, N.M., C.A. Lucas, B.N. Grgur, and P.N. Ross, Journal of Physical Chemistry B, 1999. **103**(44): p. 9616-9623.

[96]   Trasatti, S., Journal of Electroanalytical Chemistry, 1972. **39**: p. 163.

[97]   Markovic, N.M. and P.N. Ross, Journal of Electroanalytical Chemistry, 1992. **330**: p. 499.

[98]   Sawatari, Y., J. Inukai, and M. Ito, Journal of Electron Spectroscopy & Related Phenomena, 1993. **64-65**: p. 515.

[99]   Arenz, M., V. Stamenkovic, T.J. Schmidt, K. Wandelt, P.N. Ross, and N.M. Markovic, Surface Science (in press), 2002.

[100]   Tarasevich, B.J., D.A. Rand, and R. Woods, Journal of Electroanalytical Chemistry, 1973. **44**: p. 83.

[101]   Tarasevich, M.R., A. Sadkowski, and E. Yeager, *Oxygen Electrochemistry*, in *Comprehensive Treatise in Electrochemistry*, B.E. Conway, et al., Editors. 1983, Plenum Press: New York.

[102] Markovic, N., H. Gasteiger, and P.N. Ross, Journal of the Electrochemical Society, 1997. **144**(5): p. 1591-1597.

[103] Adzic, R.R., *Recent advances in the kinetics of oxygen reduction*, in *Electrocatalysis*, J. Lipkowski and P.N. Ross, Editors. 1998, Wiley-VCH: New York.

[104] Gottesfeld, S. and T.A. Zawodzinski, *Chapter 4*, in *Advances in Electrochemical Science and Engineering*, R.C. Alkire and D.M. Kolb, Editors. 1997, Wiley-VCH: Weinheim.

[105] Markovic, N.M., T.J. Schmidt, V. Stamenkovic, and P.N. Ross, Fuel Cells, 2001. **1**(2): p. 117-131.

[106] Appleby, A.J., *Electrocatalysis*, in *Comprehensive Treatise of Electrochemistry*, B.E. Conway, et al., Editors. 1983, Plenum Press: New York.

[107] Appleby, A.J., Catalysis Reviews, 1970. **4**: p. 221.

[108] Appleby, A.J., Surface Science, 1971. **27**: p. 225.

[109] El Kadiri, F., R. Faure, and R. Durand, Journal of Electroanalytical Chemistry, 1991. **301**: p. 177.

[110] Markovic, N.M., R.R. Adzic, B.D. Cahan, and E.B. Yeager, Journal of Electroanalytical Chemistry, 1994. **377**(1-2): p. 249-259.

[111] Markovic, N.M., H.A. Gasteiger, and P.N. Ross, Journal of Physical Chemistry, 1996. **100**(16): p. 6715-6721.

[112] Markovic, N.M., H.A. Gasteiger, B.N. Grgur, and P.N. Ross, Journal of Electroanalytical Chemistry, 1999. **467**(1-2): p. 157-163.

[113] Kinoshita, K., *Electrochemical Oxygen Technology*. 1992, New York: John Wiley & Sons.

[114] Bagotskii, V.S., M.R. Tarasevich, and Filinovskij, Élektrokhimiya, 1969. **5**: p. 1218.

[115] Wroblowa, H., Y.C. Pan, and J. Razumney, Journal of Electroanalytical Chemistry, 1976. **69**: p. 195.

[116] Schmidt, T.J., V. Stamenkovic, M. Arenz, N.M. Markovic, and P.N. Ross, submitted to Electrochimica Acta, 2002.

[117] Grgur, B.N., N.M. Markovic, and P.N. Ross, Canadian Journal of Chemistry-Revue Canadienne De Chimie, 1997. **75**(11): p. 1465-1471.

[118] Stamenkovic, V., N.M. Markovic, and P.N. Ross, Journal of Electroanalytical Chemistry, 2001. **500**(1-2): p. 44-51.

[119] Uribe, F., M.S. Wilson, T. Springer, and S. Gottesfeld. in *Proceedings of the Workshop on Structural Effects in Electrocatalysis and Oxygen Electrochemistry*. 1992. Pennington, NJ: Electrochemical Society.

[120] Markovic, N.M. and P.N. Ross, *Electrocatalysis at well-defined surfaces: kinetics of oxygen reduction and hydrogen oxidation/evolution on Pt(hkl) electrodes*, in *Interfacial Electrochemisty*, A. Wieckowski, Editor. 1999, Marcel Dekker, Inc.: New York.

[121] Clavilier, J., *Flame -annealing and cleaning technique*, in *Interfacial Electrochemisty*, A. Wieckowski, Editor. 1999, Marcel Dekker, Inc.: New York.

[122] Markovic, N.M., personal communication, 2002.

[123] Davis, R.E., G.L. Horvath, and C.W. Tobias, Electrochimica Acta, 1967. **12**: p. 287.

[124] *CRC Handbook of Chemistry and Physics*. 66th ed, ed. R.C. Weast. 1986, Boca Raton, FL: CRC Press.

[125] Rodriguez, J.A. and D.W. Goodman, Journal of Physical Chemistry, 1991. **95**: p. 4196-4206.

[126] Kinoshita, K., K. Routsis, and J.A.S. Bett, Thermochimica Acta, 1974. **10**: p. 109.

[127] Auer, E., A. Freund, T. Lehmann, K.-A. Starz, R. Schwarz, and U. Stenke, *German Patent No. DE 19721437 A1*. 1998.

[128] Stonehart, P., *United States Patent No. US 5.593.934*. 1998.

[129] Weast, R.C., and M.J. Astle, Editors, *CRC Handbook of Chemistry and Physics* 1983, Boca Raton, Florida: CRC Press, Inc.

[130] Stamenkovic, V. and N.M. Markovic, Langmuir, 2001. **17**(8): p. 2388-2394.

[131] Enyo, M., *Hydrogen electrode reaction on electrocatalytically active metals*, in *Comprehensive Treatise of Electrochemistry*, B.E. Conway, et al., Editors. 1983, Plenum Press: New York.

[132] Conway, B.E., *Electrochemical processes involving H adsorbed at metal electrode surfaces*, in *Interfacial Electrochemisty*, A. Wieckowski, Editor. 1999, Marcel Dekker, Inc.: New York.

[133] Schmickler, W., *Grundlagen der Elektrochemie*. 1996, Braunschweig: Vieweg.

[134] Hammer, B. and J.K. Norskov, in *Chemisorption and reactivity on supported clusters and thin films*, R.M. Lambert and G. Pacchioni, Editors. 1997, Kluwer Academic Publisher. p. 285.

[135] Vetter, K.J., *Electrochemical kinetics*. 1967, New York: Academic Press.

[136] Markovic, N.M., *The hydrogen electrode reaction and the electrooxidation of CO and H2/CO mixtures on well-characterized Pt and Pt-bimetallic surfaces*, in *Handbook of Fuel Cell Technology*, W. Vielstich, A. Lamm, and H. Gasteiger, Editors. 2002, John Wiley & Sons Ltd.: New York.

[137] Conway, B.E. and J.O.M. Bockris, Journal of Chemical Physics, 1957. **26**: p. 532.

[138] Parsons, R., Transaction of the Faraday Society, 1958. **54**: p. 1053.

[139] Gerischer, H., Bulletin Des Societes Chimiques Belges, 1958. **67**: p. 506.

[140] Trasatti, S., Surface Science, 1995. **335**: p. 1.

[141] Schuldiner, S., M. Rosen, and D.R. Flinn, Journal of the Electrochemical Society, 1970. **117**: p. 1251.

[142] Seto, K., A. Iannelli, B. Love, and J. Lipkowski, Journal of Electroanalytical Chemistry, 1987. **226**: p. 351.

[143] Kita, H., S. Ye, and y. Gao, Journal of Electroanalytical Chemistry, 1992. **334**: p. 351.

[144] Gomez, R., A. Fernandezvega, J.M. Feliu, and A. Aldaz, Journal of Physical Chemistry, 1993. **97**(18): p. 4769-4776.

[145] Wandelt, K., Applied Surface Science, 1997. **111**: p. 1-10.

[146] Markovic, N.M., B.N. Grgur, and P.N. Ross, Journal of Physical Chemistry B, 1997. **101**(27): p. 5405-5413.

[147] Markovic, N.M., S.T. Sarraf, H.A. Gasteiger, and P.N. Ross, Journal of the Chemical Society-Faraday Transactions, 1996. **92**(20): p. 3719-3725.

[148] Barber, J., S. Morin, and B.E. Conway, Journal of Electroanalytical Chemistry, 1998. **446**(1-2): p. 125-138.

[149] Barber, J.H. and B.E. Conway, Journal of Electroanalytical Chemistry, 1999. **461**(1-2): p. 80-89.

[150] Breiter, M. and R. Clamroth, Zeitschrift für Elektrochemie, 1954.

[151] Bagotskii, V.S. and V. Osetrova, Journal of Electroanalytical Chemistry, 1973. **43**: p. 233-249.

[152] Schmidt, T.J., N.M. Markovic, and P.N. Ross, Journal of Electroanalytical Chemistry, 2002. **in press**.

[153] Osetrova, V. and V.S. Bagotskii, Elektrokhimiya, 1973. **9**: p. 1527.

[154] Beden, B., A. Bewick, and C. Lamy, Journal of Electroanalytical Chemistry, 1983. **148**: p. 147.

[155] Kunimatsu, K., Journal of Electroanalytical Chemistry, 1986. **213**: p. 149.

[156] Parsons, R. and T. VanderNoot, Journal of Electroanalytical Chemistry, 1988. **257**: p. 9.

[157] Jarvi, T.D. and E.M. Stuve, *Fundamental aspects of vacuum and electrocatalytic reactions of methanol and formic acid on platinum surfaces*, in *Frontiers in Electrochemistry*, J. Lipkowski and P.N. Ross, Editors. 1998, Wiley-VCH: New York.

[158] Schmidt, T.J., B.N. Grgur, R.J. Behm, N.M. Markovic, and P.N. Ross, Physical Chemistry Chemical Physics, 2000. **2**(19): p. 4379-4386.

[159] Capon, A. and R. Parsons, Journal of Electroanalytical Chemistry, 1973. **45**: p. 205.

[160] Schmidt, T.J., B.N. Grgur, N.M. Markovic, and P.N. Ross, Journal of Electroanalytical Chemistry, 2001. **500**(1-2): p. 36-43.

[161] Strasser, P., M. Eiswirth, and G. Ertl, Journal of Chemical Physics, 1997. **107**(3): p. 991-1003.

[162] Strasser, P., M. Eiswirth, and G. Ertl, Journal of Chemical Physics, 1997. **107**(3): p. 991-1003.

[163] Bittins-Cattaneo, B., E. Cattaneo, P. Königshoven, and W. Vielstich, *New developments in electrochemical mass spectroscopy*, in *Electroanalytical Chemistry - A series of advances*, A.J. Bard, Editor. 1991, Marcel Dekker, Inc.: New York.

[164] Baltruschat, H., *Differential electrochemical mass spectroscopy as a tool for interfacial studies*, in *Interfacial Electrochemistry*, A. Wieckowski, Editor. 1999, Marcel Dekker, Inc.: New York.

[165] Lamy, C., J.M. Leger, J. Clavilier, and R. Parsons, Journal of Electroanalytical Chemistry, 1983. **150**: p. 71.

[166] Iwasita, T., X.H. Xia, E. Herrero, and H.D. Liess, Langmuir, 1996. **12**(17): p. 4260-4265.

[167] Schmidt, T.J., R.J. Behm, B.N. Grgur, N.M. Markovic, and P.N. Ross, Langmuir, 2000. **16**(21): p. 8159-8166.

[168] Schmidt, T.J., *Electrocatalysis of low-temperature fuel cell reactions*. 2000, PhD. thesis, University of Ulm.

[169] Stamenkovic, V. and N.M. Markovic, personal communication, 2002.

Acknowledgement – Danksagung

Meinen Eltern möchte ich herzlich für ihre, nicht nur finanzielle, Unterstützung während meines Studiums danken.

Zum Schluss möchte ich mich ganz besonders bei meiner Frau Gabriele bedanken für ihre große Geduld und ihre Unterstützung in den nicht immer einfachen Phasen des Zusammenschreibens dieser Arbeit.